2016

Synthesis and Properties of Acrylated Epoxidized Soybean Oil Copolymers and Their Composites with Natural Fillers

Andrew Jacob Fox
Bucknell University, ajf025@bucknell.edu

SYNTHESIS AND PROPERTIES OF ACRYLATED EPOXIDIZED SOYBEAN OIL COPOLYMERS AND THEIR COMPOSITES WITH NATURAL FILLERS

by

Andrew J. Fox

A Thesis Submitted to the Honors Council

For Honors in Chemical Engineering

May 11, 2016

Approved by:

Adviser: Dr. Jeffrey Csernica

Department Chairperson: Dr. Timothy Raymond

ACKNOWLEDGEMENTS

I'd like to start out by thanking my adviser, Dr. Jeffrey Csernica. Without out his guidance and direction, I would have never been able to accomplish anything close to what I have done here. His advice and recommendations helped drive me through nearly two full years of experimentation and research that went into this project. Most importantly, without his encouragement, this thesis might never have been written. None of this would have been possible without him.

I would also like to thank Bucknell University and its Chemical Engineering Department. The materials and equipment I was able to access were beyond helpful and allowed me to complete all the work that went into this thesis and more.

I'd like to thank all of my family for their continuing reassurance throughout this process and my education in general. Their confidence in me inspired me throughout this project and, and their belief in me inspired me to become the man I am today.

I need to thank all my of my friends who put up with me throughout this project for helping me to stay relaxed and maintain my sanity.

To all of you and more, from the bottom of my heart, thank you for helping me through this wonderful and amazing process. I couldn't have done it without you.

-Andrew

TABLE OF CONTENTS

Acknowledgements i

Table of Contents ii

List of Tables v

List of Figures vii

Abstract xiv

1. Introduction 1

2. Materials and Methods 5

2.1. Sample Synthesis 5

2.1.1. Sample Components 5

2.1.1.1. Copolymer Components 5

2.1.1.2. Fillers 7

2.1.2. Sample Preparation 8

2.1.2.1. Blend Composition 8

2.1.2.2. Sample Development 10

2.2. Experimental Procedures 11

2.2.1. Scanning Electron Microscopy 11

2.2.2. Three Point Flexural Testing 13

2.2.3. Dynamic Mechanical Analysis 16

2.2.4. Impact Testing 20

2.2.5. Durometer Measurements 21

3. Acrylated Epoxidized Soybean Oil Copolymers 24

3.1. Scanning Electron Microscopy 24

3.2. Three Point Flexural Testing 26

3.3. Dynamic Mechanical Analysis 29

3.4. Impact Testing 34

3.5. Durometer Measurements 35

4. Summary of Filled Composites 38

5. Composite with Bulk Fillers 45

5.1. Benefits of Bulk Fillers 45

5.2. Pecan Nut Shell Flour Filler 45

5.2.1. Scanning Electron Microscopy 45

5.2.2. Three Point Flexural Testing 50

5.2.3. Dynamic Mechanical Analysis 54

5.2.4. Impact Testing 58

5.2.5. Durometer Measurements 60

5.3. Egg Shell Calcium Filler 61

5.3.1. Scanning Electron Microscopy 61

5.3.2. Three Point Flexural Testing 66

5.3.3. Dynamic Mechanical Analysis 69

5.3.4. Impact Testing 72

5.3.5. Durometer Measurements 74

6. Composites with Nanofillers 76

6.1. Benefits of Nanofillers 76

6.2. Organically Modified Clay Filler 76

6.2.1. Scanning Electron Microscopy 76

6.2.2. Three Point Flexural Testing 81

6.2.3. Dynamic Mechanical Analysis 85

6.2.4. Impact Testing 89

6.2.5. Durometer Measurements 90

7. Conclusions 92

8. Recommendations 96

9. Bibliography 98

Appendix A: Three Point Flexural Testing Data A-1

Appendix B: Impact Testing Data B-1

Appendix C: Durometer Measurement Data C-1

Appendix D: Dynamic Mechanical Analysis Data D-1

Appendix E: Scanning Electron Microscopy Images E-1

LIST OF TABLES

Table 1: Comparison of Polystyrene and 36 vol% ESC Filled Composite A-1

Table 2: Three Point Flexural Data of AESO/Styrene Copolymers A-1

Table 3: Three Point Flexural Data of PNSF Filled Composites..... A-1

Table 4: Three Point Flexural Data of ESC Filled Composites..... A-1

Table 5: Three Point Flexural Data of OMC Filled Composites..... A-2

Table 6: Impact Testing Data of AESO/Styrene Copolymers B-1

Table 7: Impact Testing Data of PNSF Filled Composites..... B-1

Table 8: Impact Testing Data of ESC Filled Composites..... B-1

Table 9: Impact Testing Data of OMC Filled Composites..... B-2

Table 10: Durometer Measurement Data of AESO/Styrene Copolymers C-1

Table 11: Durometer Measurement Data of PNSF Filled Composites..... C-1

Table 12: Durometer Measurement Data of ESC Filled Composites..... C-1

Table 13: Durometer Measurement Data of OMC Filled Composites..... C-2

Table 14: DMA Data of AESO/Styrene Copolymers..... D-1

Table 15: 30 °C Storage Modulus Data of AESO/Styrene Copolymers D-2

Table 16: Measured and Predicted T_g Data of AESO/Styrene Copolymers..... D-2

Table 17: Storage Modulus and $\bar{M}c$ Data of AESO/Styrene Copolymers..... D-3

Table 18: DMA Data of PNSF Filled Composites D-4

Table 19: 30 °C Storage Modulus Data of PNSF Filled Composites..... D-5

Table 20: Glass Transition Temperature Data of PNSF Filled Composites..... D-5

Table 21: DMA Data of ESC Filled Composites..... D-6

Table 22: 30 °C Storage Modulus Data of ESC Filled Composites……..... D-7

Table 23: Glass Transition Temperature Data of ESC Filled Composites….. D-7

Table 24: DMA Data of OMC Filled Composites……..…..... D-8

Table 25: 30 °C Storage Modulus Data of OMC Filled Composites…….. D-9

Table 26: Glass Transition Temperature Data of OMC Filled Composites….... D-9

LIST OF FIGURES

Figure 1: Acrylated Epoxidized Soybean Oil with Acrylated Groups Circled.....5

Figure 2: JSM-6390LV Scanning Electron Microscope.....12

Figure 3: Example of a Stress-Strain Curve 15

Figure 4: Tinius Olsen Universal Testing Machine.....16

Figure 5: Example of an Output of a Dynamic Mechanical Analysis 18

Figure 6: RSA3 Rheometrics System Analyzer.....19

Figure 7: Tinius Olsen Model 92T Impact Tester 21

Figure 8: PTC Model 409 Type D Durometer.....22

Figure 9: SEM Image of Styrene Polymer Fracture Site 25

Figure 10: SEM Image of AESO Polymer Fracture Site.....25

Figure 11: SEM Image of 50:50 AESO/Styrene Copolymer.....26

Figure 12: Average Flexural Stress of AESO/Styrene Copolymers.....27

Figure 13: Average Flexural Strain of AESO/Styrene Copolymers.....27

Figure 14: Average Flexural Modulus of AESO/Styrene Copolymers 28

Figure 15: Figure 15: 30 °C Storage Modulus of AESO/Styrene Copolymers.....30

Figure 16: 30-100 °C Storage Modulus of AESO/Styrene Copolymers 31

Figure 17: Measured and Predicted Tg of AESO/Styrene Copolymers 32

Figure 18: $\bar{M}c$ of AESO/Styrene Copolymers.....33

Figure 19: Average Breaking Energy of AESO/Styrene Copolymers.....35

Figure 20: Average Durometer Hardness of AESO/Styrene Copolymers.....36

Figure 21: Breaking Stress of Filled Composites and Polystyrene.....39

Figure 22: Breaking Strain of Filled Composites and Polystyrene.....40

Figure 23: Flexural Modulus of Filled Composites and Polystyrene 40

Figure 24: Storage Modulus of Filled Composites and Polystyrene 41

Figure 25: Tg of Filled Composites and Polystyrene 42

Figure 26: Breaking Energy of Filled Composites and Polystyrene.....43

Figure 27: Hardness of Filled Composites and Polystyrene.....44

Figure 28: Low Mag SEM Image of 7 vol% PNSF Filled Composite 46

Figure 29: Low Mag SEM Image of 15 vol% PNSF Filled Composite 47

Figure 30: Low Mag SEM Image of 23 vol% PNSF Filled Composite 48

Figure 31: High Mag SEM Image of 7 vol% PNSF Filled Composite 48

Figure 32: High Mag SEM Image of 15 vol% PNSF Filled Composite 49

Figure 33: High Mag SEM Image of 23 vol% PNSF Filled Composite 50

Figure 34: Average Flexural Breaking Stress of PNSF Filled Composites.....51

Figure 35: Average Flexural Breaking Strain of PNSF Filled Composites.....52

Figure 36: Average Flexural Modulus of PNSF Filled Composites.....53

Figure 37: 30 °C Storage Modulus of PNSF Filled Composites 55

Figure 38: 30 -100 °C Storage Modulus of PNSF Filled Composites.....56

Figure 39: Glass Transition Temperature of PNSF Filled Composites 57

Figure 40: Average Breaking Energy of PNSF Filled Composites 59

Figure 41: Average Durometer Hardness of PNSF Filled Composites 60

Figure 42: Low Mag SEM Image of 20 vol% ESC Filled Composite 62

Figure 43: Low Mag SEM Image of 27 vol% ESC Filled Composite 63

Figure 44: Low Mag SEM Image of 36 vol% ESC Filled Composite 63

Figure 45: High Mag SEM Image of 20 vol% ESC Filled Composite.....64

Figure 46: High Mag SEM Image of 27 vol% ESC Filled Composite.....65

Figure 47: High Mag SEM Image of 36 vol% ESC Filled Composite.....65

Figure 48: Average Flexural Breaking Stress of ESC Filled Composites.....66

Figure 49: Average Flexural Breaking Strain of ESC Filled Composites.....67

Figure 50: Average Flexural Modulus of ESC Filled Composites.....68

Figure 51: 30 °C Storage Modulus of ESC Filled Composites 70

Figure 52: 30-100 °C Storage Modulus of ESC Filled Composites.....71

Figure 53: Glass Transition Temperature of ESC Filled Composites 72

Figure 54: Average Breaking Energy of ESC Filled Composites 73

Figure 55: Average Durometer Hardness of ESC Filled Composites 75

Figure 56: Low Mag SEM Image of 1 vol% OMC Filled Composite.....77

Figure 57: Low Mag SEM Image of 2 vol% OMC Filled Composite.....77

Figure 58: Low Mag SEM Image of 4 vol% OMC Filled Composite.....78

Figure 59: High Mag SEM Image of 1 vol% OMC Filled Composite.....79

Figure 60: High Mag SEM Image of 2 vol% OMC Filled Composite.....80

Figure 61: High Mag SEM Image of 4 vol% OMC Filled Composite.....81

Figure 62: Average Flexural Breaking Stress of OMC Filled Composites 82

Figure 63: Average Flexural Breaking Strain of OMC Filled Composites 83

Figure 64: Average Flexural Modulus of OMC Filled Composites 84

Figure 65: 30 °C Storage Modulus of OMC Filled Composites.....86

Figure 66: 30-100 °C Storage Modulus of OMC Filled Composites 87

Figure 67: Glass Transition Temperature of OMC Filled Composites.....88

Figure 68: Average Breaking Energy of OMC Filled Composites.....89

Figure 69: Average Durometer Hardness of OMC Filled Composites.....91

Figure 70: 22x Mag SEM Image of Styrene Polymer Fracture Site.....E-1

Figure 71: 75x Mag SEM Image of AESO Polymer Fracture Site..... E-1

Figure 72: 70x Mag SEM Image of 50:50 AESO/Styrene Copolymer E-2

Figure 73: 75x Mag SEM Image of 50:50 AESO/Styrene Copolymer E-2

Figure 74: 500x Mag SEM Image of 50:50 AESO/Styrene Copolymer E-3

Figure 75: 33x Mag SEM Image of 7 vol% PNSF Filled Composite E-.3

Figure 76: 35x Mag SEM Image of 7 vol% PNSF Filled Composite E-4

Figure 77: 55x Mag SEM Image of 7 vol% PNSF Filled Composite E-4

Figure 78: 100x Mag SEM Image of 7 vol% PNSF Filled Composite E-5

Figure 79: 150x Mag SEM Image of 7 vol% PNSF Filled Composite E-5

Figure 80: 400x Mag SEM Image of 7 vol% PNSF Filled Composite E-6

Figure 81: 700x Mag SEM Image of 7 vol% PNSF Filled Composite E-6

Figure 82: 30x Mag SEM Image of 15 vol% PNSF Filled Composite E-7

Figure 83: 35x Mag SEM Image of 15 vol% PNSF Filled Composite E-7

Figure 84: 100x Mag SEM Image of 15 vol% PNSF Filled Composite E-8

Figure 85: 250x Mag SEM Image of 15 vol% PNSF Filled Composite E-8

Figure 86: 500x Mag SEM Image of 15 vol% PNSF Filled Composite E-9

Figure 87: 1000x Mag SEM Image of 15 vol% PNSF Filled Composite E-9

Figure 88: 30x Mag SEM Image of 23 vol% PNSF Filled Composite E-10

Figure 89: 35x Mag SEM Image of 23 vol% PNSF Filled Composite E-10

Figure 90: 100x Mag SEM Image of 23 vol% PNSF Filled Composite E-11

Figure 91: 250x Mag SEM Image of 23 vol% PNSF Filled Composite E-11

Figure 92: 500x Mag SEM Image of 23 vol% PNSF Filled Composite E-12

Figure 93: 30x Mag SEM Image of 20 vol% ESC Filled Composite..... E-12

Figure 94: 30x Mag SEM Image of 20 vol% ESC Filled Composite..... E-13

Figure 95: 100x Mag SEM Image of 20 vol% ESC Filled Composite..... E-13

Figure 96: 250x Mag SEM Image of 20 vol% ESC Filled Composite..... E-14

Figure 97: 500x Mag SEM Image of 20 vol% ESC Filled Composite..... E-14

Figure 98: 1000x Mag SEM Image of 20 vol% ESC Filled Composite..... E-15

Figure 99: 27x Mag SEM Image of 27 vol% ESC Filled Composite..... E-15

Figure 100: 35x Mag SEM Image of 27 vol% ESC Filled Composite..... E-16

Figure 101: 100x Mag SEM Image of 27 vol% ESC Filled Composite..... E-16

Figure 102: 250x Mag SEM Image of 27 vol% ESC Filled Composite..... E-17

Figure 103: 500x Mag SEM Image of 27 vol% ESC Filled Composite..... E-17

Figure 104: 1000x Mag SEM Image of 27 vol% ESC Filled Composite..... E-18

Figure 105: 27x Mag SEM Image of 36 vol% ESC Filled Composite..... E-18

Figure 106: 35x Mag SEM Image of 36 vol% ESC Filled Composite..... E-19

Figure 107: 100x Mag SEM Image of 36 vol% ESC Filled Composite..... E-19

Figure 108: 250x Mag SEM Image of 36 vol% ESC Filled Composite..... E-20

Figure 109: 500x Mag SEM Image of 36 vol% ESC Filled Composite..... E-20

Figure 110: 500x Mag SEM Image of 36 vol% ESC Filled Composite..... E-21

Figure 111: 33x Mag SEM Image of 1 vol% OMC Filled Composite..... E-21

Figure 112: 33x Mag SEM Image of 1 vol% OMC Filled Composite..... E-22

Figure 113: 100x Mag SEM Image of 1 vol% OMC Filled Composite.....E-22

Figure 114: 250x Mag SEM Image of 1 vol% OMC Filled Composite..... E-23

Figure 115: 500x Mag SEM Image of 1 vol% OMC Filled Composite..... E-23

Figure 116: 1000x Mag SEM Image of 1 vol% OMC Filled Composite..... E-24

Figure 117: 30x Mag SEM Image of 2 vol% OMC Filled Composite..... E-24

Figure 118: 35x Mag SEM Image of 2 vol% OMC Filled Composite..... E-25

Figure 119: 100x Mag SEM Image of 2 vol% OMC Filled Composite..... E-25

Figure 120: 250x Mag SEM Image of 2 vol% OMC Filled Composite..... E-26

Figure 121: 500x Mag SEM Image of 2 vol% OMC Filled Composite..... E-26

Figure 122: 1000x Mag SEM Image of 2 vol% OMC Filled Composite..... E-27

Figure 123: 30x Mag SEM Image of 4 vol% OMC Filled Composite..... E-27

Figure 124: 35x Mag SEM Image of 4 vol% OMC Filled Composite..... E-28

Figure 125: 100x Mag SEM Image of 4 vol% OMC Filled Composite..... E-28

Figure 126: 250x Mag SEM Image of 4 vol% OMC Filled Composite..... E-29

Figure 127: 500x Mag SEM Image of 4 vol% OMC Filled Composite..... E-29

Figure 128: 1000x Mag SEM Image of 4 vol% OMC Filled Composite..... E-30

Figure 129: 4000x Mag SEM Image of 4 vol% OMC Filled Composite..... E-30

ABSTRACT

As the global supply of petrochemicals diminishes, the polymer industry will need to incorporate renewable resources into the production process. Acrylated expoxidized soybean oil, a modified plant oil, is one possible candidate for use as a monomer in plastics. When polymerized alone, AESO creates a fairly unusable polymer, with poor physical and material properties. To improve the properties, the monomer can be copolymerized with styrene and other additives and can be incorporated into a composite to further increase the usability. By using biorenewable fillers, the overall use of nonrenewable materials in the composite can be further decreased. In this research, composites consisting of a 50:50 AESO:styrene copolymer matrix and either pecan nut shell flour (PNSF), egg shell calcium (ESC), or organically modified clay (OMC) were created and their physical properties analyzed.

AESO and styrene were successfully polymerized into a cohesive copolymer, with greater amounts of AESO producing copolymers that were softer and more rubbery. Higher amounts of AESO generally led to a decrease in stiffness, strength, and hardness, while increasing the flexibility. The brittleness of the material decreased as the amount of AESO increased. Thermal analysis revealed that higher AESO contents resulted in lower thermal stability and glass transition temperatures, but increased the amount of crosslinking within the copolymer.

The addition of the fillers generally improved the properties of the composite. The stiffness and hardness both improved as filler content increased; however, the brittleness, strength, and flexibility all worsened. All of the fillers achieved good dispersion within the composite and maintained low particle sizes at high loadings. The fillers did not improve the thermal stability of the composite, nor did they degrade it any further. Of the fillers tested, egg shell calcium (ESC) produced the greatest improvement to the mechanical properties and could achieve the highest loadings. Future work should continue to analyze the effect of blend composition on copolymer, as well as investigate the use of bonding agents to improve filler-matrix cohesion.

1. INTRODUCTION

In the present day, the plastics industry is completely and understandably dominated by the use of petrochemicals. [1] While the use of these raw materials is currently the most effective and efficient, they have a fatal flaw; the world's supply of petrochemicals is rapidly diminishing and will soon become unreasonably expensive. [2] In addition, new uses for polymers and polymeric materials continue to arise, creating new demand as supply decreases. [3] To deal with these rising concerns, as well as growing economic and environmental issues surrounding the use of oil, a surge toward renewable resources as polymer feedstock has developed. [4-11]

One particularly promising alternative to petroleum as the source of polymer precursors is plant-based oils. [12-16] Derived from various vegetables and vegetation, plant oils offer the distinction of both having the double bonds within their chemical structure desirable for polymer precursors and being completely biorenewable. Unfortunately, due to the diminished reactivity of the double bonds, vegetable oils behave in a different fashion than petroleum in polymers. [17,18] This loss of reactivity can be overcome by the functionalization of the molecules, creating a chemical structure that is more available to polymerization. [13,19,20,49]

Interest has already been shown in the usage of plant oils within preexisting polymeric systems and materials. Functionalized plant oils have been

added to polymers for property modification, including use as a toughening agent, a plasticizer, and to reduce the amount of petroleum comonomer content. [25-28] Several studies have also been conducted looking into both modified and unmodified vegetable oils as comonomers for various copolymers. [21-24] Styrene monomer, a relatively easy chemical to polymerize, has often been used as a comonomer with which to polymerize plant oils. [38-40] With its derivation from petrochemicals, it detracts somewhat from the goal of reducing the polymer industry's petroleum dependency. [41] Substantial incorporation of plant oils into the polymer still reduces the overall petroleum based content and helps move the industry away from total dependence.

When copolymerized with other comonomers, plant oil based polymers often produce a rubberlike final product. [28] To combat this and improve overall mechanical properties, fillers have been added to the polymers to create composite materials. These fillers, both natural and artificial, have been found to help control the properties of the final polymer and allow for a wider range of uses of the polymer. [42-44] Proper use of these fillers can help to better create composites with real world applications and can expedite the progress of biorenewable materials into the market.

Soybean oil is an especially interesting plant oil that seems to be a potential petroleum replacement in polymers. Like many other plant-based oils, natural soybean oil does not create polymers when polymerized using free

radicals. [29] To achieve polymerization, the triglyceride molecule within the chemical structure must be functionalized using various chemical processes. [15,29-31] Notably, the epoxidation of soybean oil, followed by acrylation, seems to be particularly effective in creating a polymer precursor. [32-37] This process creates acrylated epoxidized soybean oil (AESO), containing acrylated functional groups that are particularly conducive to polymerization.

AESO has been studied as a comonomer in polymeric systems, with usages ranging from biomedical applications to polymer surface modification. [28,41-47] These studies, however, have been fairly limited in the scope of their investigation, often focusing more on the actual production of AESO or on a narrow range of AESO content. There has also been very little study done on AESO copolymerized with styrene [48] and what has been done has only investigated a very specific blend of AESO and styrene. Studies have been conducted on incorporating fillers into an AESO polymer, but, again, only with a specific blend of AESO. [47]

Composites composed of AESO and styrene will likely have inferior properties to polystyrene. Previous studies have shown that the addition of AESO causes a decrease in the strength of the material and a reduction in the glass transition temperature. [48] Additional studies have investigated the effect of AESO content on modulus, hardness, and brittleness, but have been unable to identify significant trends. [50] The addition of fillers to the copolymer could result

in a number of different changes to the properties of the material. The strength has been seen to increase [51,55] or decrease [53,54], while the modulus has increase [51, 53, 54, 55] unless no trend exists at all. [42] Both the flexibility and the brittleness of the material have been seen to worsen as filler is added. [53,54,55] The glass transition temperature of the composite has been found to increase [51] and decrease [54] as filler content is increased.

In my project, I intend to expand on the growing body of knowledge surrounding polymerized AESO through a systematic study of an AESO-based system. Using styrene as a comonomer, I will investigate the physical and mechanical properties of AESO/styrene copolymers. I will explore the relationships between these properties and the AESO content of the copolymers, and will use this to draw conclusions as to the feasibility of polymerized AESO for widespread usage. I intend to investigate additional natural fillers with the goal of improved and controllable mechanical properties and reduced petroleum based content in polymer composites. I will attempt to use these fillers to create a composite with similar or improved properties to that of polystyrene.

2. MATERIALS AND METHODS

2.1. SAMPLE SYNTHESIS

2.1.1. SAMPLE COMPONENTS

2.1.1.1. Copolymer components

The copolymers tested were comprised primarily of polymerized acrylated epoxidized soybean oil (AESO) and styrene. AESO, shown in Figure 1 below, is plant oil derived from the seeds of the soybean plant (*Glycine mac*) and functionalized through acrylation and epoxidation. The base molecule is a saturated triglyceride that, lacking double bonded carbons, cannot be polymerized using free radical polymerization. The process of acrylation creates a series of acrylated functional groups, denoted in Figure 1 by the circles. The newly functionalized molecule, containing double bonded carbons, can undergo free radical polymerization and can create polymers. The process of adding these functional groups has been extensively studied and, having already been implemented as an industrial process, will not be investigated in this study.

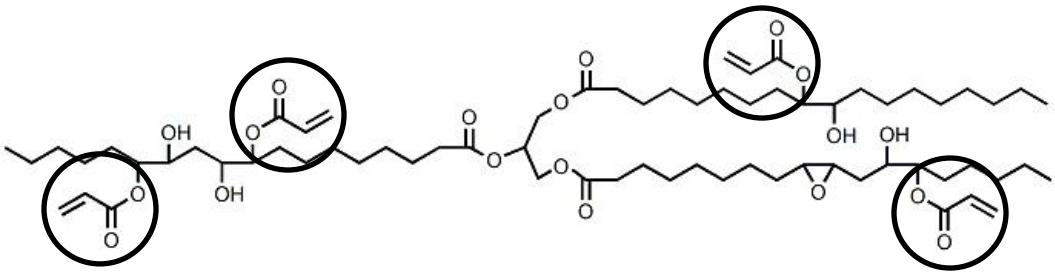

Figure 1: Acrylated Epoxidized Soybean Oil with Acrylated Groups Circled

Through initial experimentation, it was determined that AESO could be polymerized with several comonomers, including styrene and isobutyl methacrylate. Every attempted comonomer was able to be successfully copolymerized with AESO, allowing for freedom in the selection of the scope of this study. For this project, styrene was selected as the comonomer to be copolymerized with AESO. The rationalization of this selection is three fold. Styrene, as a monomer, polymerizes very easily due to the presence of a resonance stabilized vinyl group. In experimentation, this allows for increased consistency and predictability in the production of styrene based polymers. Additionally, the properties of polymerized styrene greatly differ from those of polymerized AESO. The properties of copolymers created from these monomers would therefore potentially have properties that exist in a wider range and would produce more easily discernable results. Finally, styrene as a monomer and comonomer is frequently used in the polymer industry. The incorporation of styrene in future copolymers would require little adaptation in industrial settings, allowing the implementation of these copolymers to progress more rapidly.

To improve polymerization and crosslinking of the polymer, divinylbenzene (DVB) was added in small amounts to the comonomer blend. Divinylbenzene contains multiple vinyl groups, allowing it to promote crosslinking throughout the copolymer. Additionally, the DVB allowed for

increased viscosity control of the comonomer blend; AESO, by itself, is quite viscous and cannot be easily manipulated in a laboratory setting. The addition of DVB to the mixture decreased the viscosity and allowed for the material to be easily handled. The exact amount of divinylbenzene used was based off of a literature review and was not varied in this experimentation.

In order to encourage polymerization of the comonomer blend, azobisisobutyronitrile (AIBN) was added. Azobisisobutyronitrile is a radical initiator that forms free radicals when exposed to high temperatures. These free radicals initiate polymerization by breaking double bonded carbons and binding them together in a chain. The exact amount of AIBN used was based off of a literature review and was not varied in the course of this experimentation.

2.1.1.2. Fillers

Three fillers were considered throughout this study. The fillers were selected due to their renewability and likelihood to be successfully integrated into composites with an AESO/Styrene copolymer. The fillers were also expected to be stiffer and stronger than the copolymer, improving the material properties of the composites. Pecan nut shell flour (PNSF) and egg shell calcium (ESC) were selected as bulk fillers for this experimentation. These fillers were composed of macroscopic particles that were produced from the pulverization of renewable products, namely pecan shells and egg shells, and contained particles between 10

and 50 μm. The PNSF (E = 25,000 MPa) [57] was produced by the Georgia Southern Pecan Company and is composed primarily of cellulose fibers [$(C_6H_{10}O_5)_n$]. The ESC (E = 79,600 MPa) [56] was sourced from Pet's Friend Eggshellent Calcium and is composed primarily of calcium carbonate [$CaCO_3$]. Organically Modified Clay (OMC) was used as a nanofiller in AESO based composites. The OMC (E = 50,000 MPa) [53] was produced from nanoscale clay particles, modified with an undisclosed organic molecule to promote adhesion to polymers, and was produced by Nanocor. The fillers were selected due to increased moduli and hardness compared to the base copolymers and their ability to be successfully polymerized around.

Several alternative fillers were initially considered, but ruled out. Glass and fly ash were found to be too dense to be used in this composite fabrication process. The dense fillers did not remain suspended in the polymer and did not create a uniform material. Ground flax was also considered, however the flax did not mix uniformly with the comonomer blend. The resulting polymer contained sporadic clusters of flax dense regions.

2.1.2. SAMPLE PREPARATION

2.1.2.1. Blend Composition

Prior to polymerizing monomers in various copolymer blends, an appropriate mixture of the two monomers was created. The two monomers,

AESO and styrene, were combined at different blend ratios, ranging from 100 wt% styrene and 0 wt% AESO to 100 wt% AESO and 0 wt% styrene. In addition, 5 wt% of the blend mass in divinylbenzene (DVB) was added as an additive to assist in polymerization and 0.2 wt% of azobisisobutyronitrile (AIBN) was added to initiate the polymerization reaction under the presence of heat. A goal of a final mass of approximately 50 grams of each mixture was targeted in creating each blend. The amounts of both DVB and AIBN used were based off of previously completed studies and were not investigated or altered throughout the course of the experiment. While multiple blend ratios were used in the basic copolymer study and the properties of the produced copolymers were investigated. For the addition of fillers to the copolymers to create composites, however, only one blend ratio 50:50 AESO:Styrene was used. The blend ratio was selected as it contained at least half renewable chemicals and was viscous enough to suspend the filler during polymerization, yet was easily mixable. Alternative mixes with higher AESO contents were ruled out due to inferior initial properties.

The addition of the filler to the comonomer blend created viscous, syrup-like suspensions that became increasingly viscous at higher filler amounts. Every filler was independently blended and the workable range of added filler was determined. The bulk fillers PNSF and ESC became unusably viscous above 50 and 75 wt%, respectively. Additionally, the suspension was not viscous enough to keep the filler suspended below 5 and 30 wt%, respectively. To create samples for

experimentation, PNSF was blended at 10, 20, and 30 wt% (7, 15, and 23 vol%) and, ESC was blended at 40, 50, and 60 wt% (20, 27, and 26 vol%). The nanofiller OMC was found to become unusable viscous above 15 wt%, but remained suspended at all blend compositions below this threshold. For this experimentation, OMC was blended at 2, 5, and 10 wt% (1, 2, and 4 vol%). The experimental blend compositions created feasible suspensions that created visually uniform, rigid polymers.

2.1.2.2. Sample Development

After creating each mixture, samples were polymerized using a water bath set to 70 °C. The mixtures were first placed in cylindrical glass test tubes of either approximately 8 mm and 10 mm in diameter and the tops of each tube covered with foil. The test tubes were then place within the aforementioned water bath and left to polymerize for eighteen hours; longer polymerization times were tested, but determined to have no effect on the measured properties of the final polymerized product. After the samples had finished polymerizing, they were removed from the test tubes via percussive shattering of the glass.

The neat copolymers were able to fully polymerize throughout the composition range, regardless of the percentage of AESO in the blend mixture. The materials created were smooth in texture, with the color ranging from almost completely clear, to increasingly yellow with increased AESO content. The

samples were completely solid, with increased AESO content causing the samples to become increasingly flexible and rubbery in nature. The entirely AESO based polymer was found to be extremely delicate, often breaking in the process of production.

The addition of the fillers created noticeably stiffer materials that changed in color depending on the type and amount of filler contained. The ESC caused the polymer to take on a pinkish tone that deepened as the filler content increased. The PNSF produced a brown composite that also became darker as the amount of PNSF increased. The OMC produced a brownish-gray composite; however, the color remained fairly constant regardless of the amount of filler added.

2.2. EXPERIMENTAL PROCEDURES

2.2.1. SCANNING ELECTRON MICROSCOPY

Scanning electron microscopy, or SEM, is a three dimesnional technique for producing high magnification images of a material. Unlike standard light microscopy, SEM uses a focused beam of electrons to visualize a material. The electrons interact with the surface of the material, scattering off of the topmost atoms. The scattering of the electrons is measured and used to produce images depicting the topography of the material's surface. In polymeric samples, this method can provide a depiction of the polymer's physical shape, showing the planes which form in the polymer. In composites, this techniques can be used to

demonstrate the uniformity of dispersion of a filler and its particle size. Low magnification images can show how widespread the filler is over the surface, with high dispersion correlating with a lack of high visual density areas. High magnification images can provided measurements of the size of particles, which can be used to determine if particle growth occurs at higher loadings. Particle growth indicates an inefficient use of filler, as improved properties are caused by higher surface area of contact.

Figure 2: JSM-6390LV Scanning Electron Microscope

To produce high magnification images of the material and to investigate the properties of the composites, scanning electron microscopy was perform using a JSM-6390LV Scanning Electron Microscope shown in Figure 2. Samples were created by cutting a small piece of material that exposed a fracture site from impact testing and affixing it to a brass disk. The sample was then coated in gold using a Denton Vacuum Desk IV Cold Sputter/Etch Unit. The gold coating prevents charge build-up on the sample surface and produces higher quality images. Samples were then place inside the vacuum chamber of the SEM and were analyzed using 10 kV electron beam.

2.2.2. THREE POINT FLEXURAL TESTING

Three point flexural testing is a method of determining various mechanical properties of a material subject to a bending-type load. A cylindrical sample of the material is loaded upon a testing base consisting of two fixed points a set distance apart. A testing head, consisting of a third point, is lowered down on the top of the material sample at a given loading displacement rate. The force required to achieve this deflection is recorded perioidically, producing a force-displacement curve. Using Equations 1 and 2, the stress and strain at each point can be calculated and used to produce a stress-strain curve, an example of which can be seen below in Figure 3. The peak value of this curve gives the flexural breaking stress and the flexural braking strain. The flexural breaking stress is a measure of

the strength of a material before it breaks under an external pressure. The flexural breaking strain is a measure of the deformation that a material can incur before failure. The initial slope of the stress-strain curve is the flexural modulus of the material, which is a measure of the stiffness of the material and its propensity to withstand bending. The modulus of the composite materials can be calculated through several different models. The simple rule of mixing, shown in Equation 3, provides an upper bound for the possible moduli. The inverse rule of mixing, shown in Equation 4, provides a lower bound for the possible moduli. If the moduli lay between these two models, the composite is acting as would be expected.

$$\sigma_f = \frac{FL}{\pi R^3}$$

Equation 1: Flexural stress as a function of force, length, and radius

σ_f=breaking stress (MPa); F=load (N); L=length (mm); R=radius (mm)

$$\epsilon_f = \frac{12Rd}{L^2}$$

Equation 2: Flexural strain as a function of radius, displacement, and length

ε_f=breaking stress; R=radius; d=displacement (mm); L=length (mm)

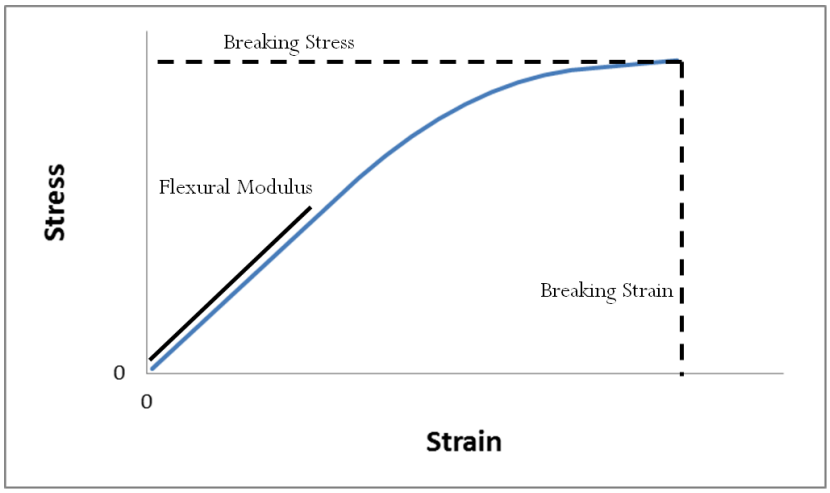

Figure 3: Example of a Stress-Strain Curve

$$E_c = \omega_1 E_1 + \omega_2 E_2$$

Equation 3: Simple Rule of Mixing

E_c=modulus of composite; ω_1=weight fraction of component 1; E_1=modulus of component 1; ω_2=weight fraction of component 1; E_2=modulus of component 1

$$E_c = \frac{1}{\frac{\omega_1}{E_1} + \frac{\omega_2}{E_2}}$$

Equation 4: Inverse Rule of Mixing

E_c=modulus of composite; ω_1=weight fraction of component 1; E_1=modulus of component 1; ω_2=weight fraction of component 1; E_2=modulus of component 1

Three point flexural testing was performed in a Tinius-Olsen Universal Testing Machine, shown in Figure 4, with a three point flexural test attachment. The samples were deflected at a speed of 0.5 in/min and a testing length of 2 inches was used. The testing was performed on the larger 10 mm diameter samples as described previously.

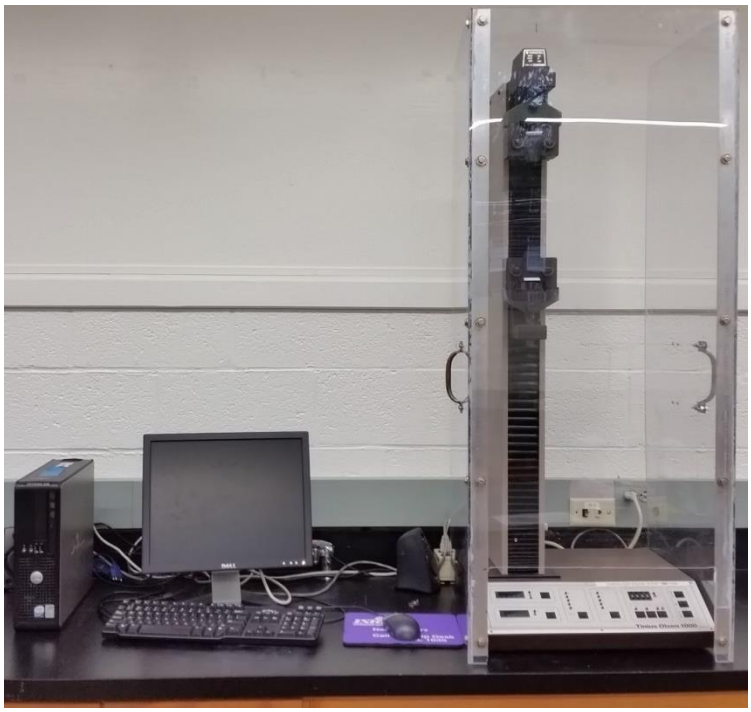

Figure 4: Tinius Olsen Universal Testing Machine

2.2.3. DYNAMIC MECHANICAL ANALYSIS

Dynamic mechanical analysis is a powerful technique used to characterize the mechanical response of materials over a temperature range. Samples are

placed on a base, similar to that used in three point flexural bending, and a comparable testing head is placed atop the sample. In this method, a sinusoidal strain is applied to the sample at a given rate, and the stress in the material is measured. The storage modulus and loss modulus, two material properties are measured and recorded. The storage modulus measures the elastic properties of the material and is similar to the material's flexural modulus. The loss modulus provides a measure of the mechanical properties of the viscous component of the polymer. This provides an additional measure of the materials resistance to deformation. By measuring these properties over a range of temperatures, the ability of the material to withstand temperature changes can be approximated.

Additionally, the storage and loss moduli can be used to calculate the phase angle of the material. The phase angle, δ, and more importantly its tangent, tan(δ), allow the glass transition temperature, or T_g, of the material to be found; the T_g is located at the peak value of tanδ. The glass transition temperature denotes the thermal boundary of an amorphous solid polymer, beyond which the material properties change as it becomes increasingly viscous or rubbery. T_g also provides an identifier of the polymer being tested, as identical polymers will always have the same glass transition temperature. The storage modulus beyond the glass transition temperature provides a measure of the number average molecular weight of the network chains between crosslinks, or $\bar{M}_c$, and is calculated using Equation 5. This value measures the molecular weight of

crosslinked chains in the polymer and provides and estimate of the degree of crosslinking in the polymer. Higher degrees of crosslinking suggest that the polymer is more interconnected and can produce improved properties. An example of the information produced by this test can be found in Figure 5.

$$\bar{M}_c = \frac{3\rho RT}{E}$$

Equation 5: $\bar{M}_c$ as a function of storage modulus, density, and temperature

$\bar{M}_c$=molecular weight between chains (g/mol); ρ=density (g/ml); R=ideal gas constant (8.314 MPa*mL/K*mol); T=temperature (K); E=modulus (MPa)

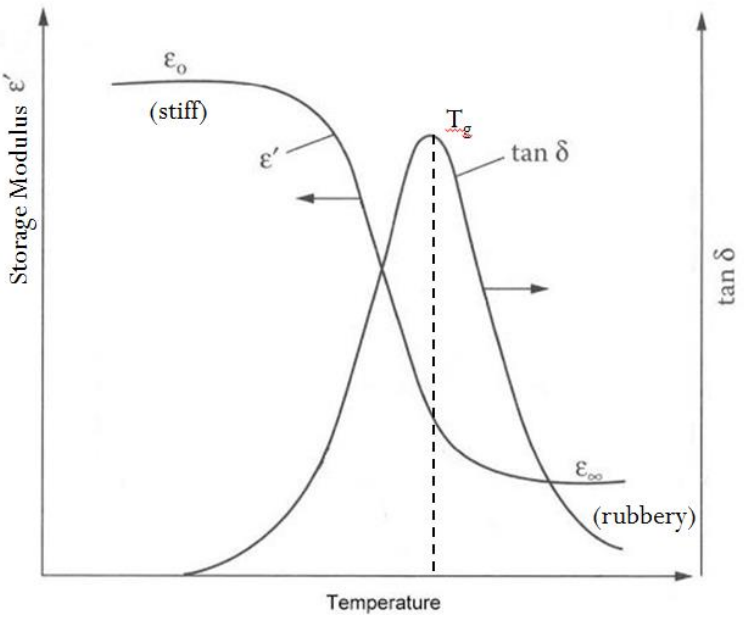

Figure 5: Example of an Output of a Dynamic Mechanical Analysis

To determine these properties of the copolymers and composites, dynamic mechanical analysis was performed using a RSA3 Rheometrics System Analyzer, shown in Figure 6. The smaller 8 mm diameter samples were loaded into the machine. The program for the testing assumes rectangular samples as the standard rather than cylindrical, so the programmed measurements for the samples were altered slightly to account for the difference in formulae used to calculate the stress.

Figure 6: RSA3 Rheometrics System Analyzer

The testing procedure was selected to be the dynamic temperature ramp test, performed at a ramp rate of 1 °C/min with a frequency of 1 Hz. As the

physical properties in question were not all observable at the same temperature ranges, two different temperature ranges were used for each sample; the majority of samples used a range of 30 to 100 °C, while the pure AESO samples used a range of -10 to 50 °C. The testing used a strain of 0.01 with a constant static force applied as a compression.

2.2.4. IMPACT TESTING

Impact testing is a method of determining the energy necessary to break a material, also known as the breaking energy. A sample of the material is notched, whereby a small, consistent indentation is placed in the sample. The sample is then placed in a holder, after which a weighted pendulum is released to contact the material, breaking it. The energy that the pendulum loses due to breaking the material is the breaking energy of the material. The breaking energy is often reported as energy per width; however, for this experimentation, all samples were constructed identically and the length was not factored in. The breaking energy of the sample provides a measure of the brittleness of the material. The less total energy that a material can withstand before failure, the more brittle the material is determined to be.

To determine the breaking energy of the copolymers and composites, impact testing was performed using a Tinius-Olsen Model 92T Impact Tester, shown in Figure 7. The samples were notched using a Dynisco Automatic Sample

Notcher to produce consistent notches in the samples. The larger 10 mm diameter samples were used for this process and were broken at the notch consistently.

Figure 7: Tinius Olsen Model 92T Impact Tester

2.2.5. DUROMETER MEASURMENTS

Durometer measurement, also known as Shore durometer, is a method of determining the hardness of a material. Hardness, unlike other material properties, does not have a commonly defined unit of measurement; instead, several different measures exist by which to provide hardness of materials. Durometer measurements use a material's resistance to penetration under a fixed load as one

measurement of hardness. This method is frequently applied to polymers, as other methods cannot easily incorporate the properties of polymers. Several different durometer scales exists, with A and D being the most often used for soft and hard polymers, respectively. Each scale is standardized between values of one and one hundred, with higher values denoting a harder material.

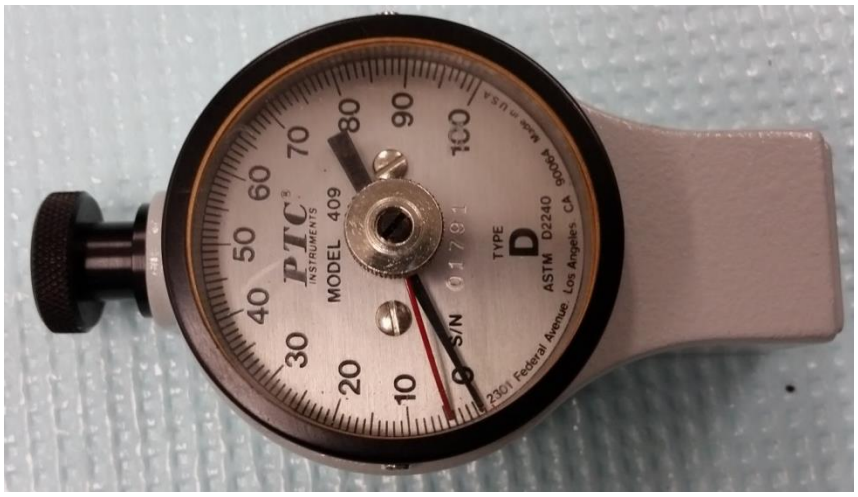

Figure 8: PTC Model 409 Type D Durometer

To determine the hardness of the copolymers and composites, durometer measurements were performed using a PTC Model 409 Type D Durometer, shown in Figure 8. The samples were created by cutting off a small piece of material and imbedding it in a fast curing acrylic base. The acrylic base was created by combining SamplKwick liquid 20-3568 and SamplKwick powder 20-3566. The resulting sample was polished to produce a smooth surface on which to

develop accurate hardness measurements. The durometer was then placed swiftly atop the sample, indenting it slightly and producing a measurement along the scale. Several samples produced values higher than the intended scale would allow; for these, metered estimates above the 100 mark were made.

3. ACRYLATED EPOXIDIZED SOYBEAN OIL COPOLYMERS

3.1. SCANNING ELECTRON MICROSCOPY

Scanning electron microscopy was used to develop images of the fracture surface of several blends of AESO and styrene in copolymers. Selected images are shown in Figures 9 through 11. A full collection of SEM images take of these blends is available in Figures 70-74 in Appendix E.

As seen in Figure 9, the fracture surface of a styrene polymer is relatively smooth. Small cracks occur at the beginning of the fracture site, but do not extend very far into the sample. Additionally, the notching site is also relatively smooth, indicating that the cracks can propagate easily through the polymer. In Figure 10, the fracture surface of the AESO polymer contains more topographical elements. Small striations can be seen at the beginning of the fracture site, but again, do not extend far into the sample. The notching site displays an altogether different appearance. Many striations permeate throughout the site, displaying no smooth plane whatsoever. This corroborates the expected increase in crosslinking, as the crack path is impeded by the more interwoven polymer. In Figure 11, the fracture surface of the heteropolymer is incredibly different. The entire surface is covered with topographical features, with striations and wave-like patterns permeating the entire surface. The surface contains no smooth surfaces and does not seem to have broken along any particular plane. The topographical dissonance is likely caused

by the two comonomers forming separate regions within the polymer, leading to the crack permeation leaping and changing directions.

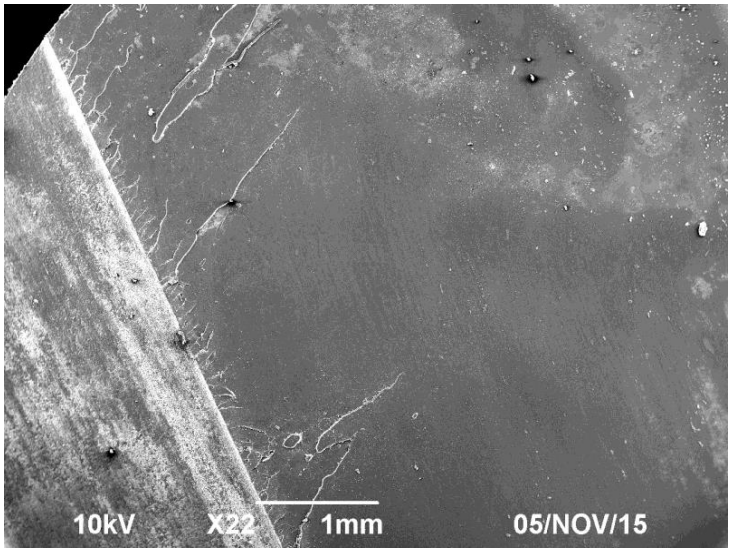

Figure 9: SEM Image of Styrene Polymer Fracture Site

Figure 10: SEM Image of AESO Polymer Fracture Site

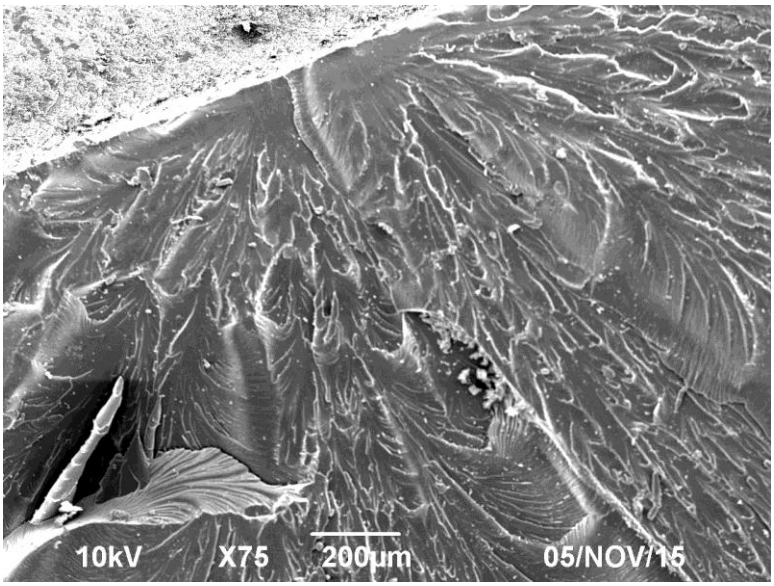

Figure 11: SEM Image of 50:50 AESO/Styrene Copolymer

3.2. THREE POINT FLEXURAL TESTING

The breaking stress, breaking strain, and flexural modulus were measured for samples of various combinations of acrylated epoxidized soybean oil and styrene using three point flexural testing. Five samples were created for each blend ratio. The samples of the same composition were averaged, and plotted as functions of AESO content in Figures 12 through 14. The standard deviation of the measurements was also calculated and is included as of error bars. A full listing of averaged physical properties obtained through three point flexural testing is available in Table 2 in Appendix A.

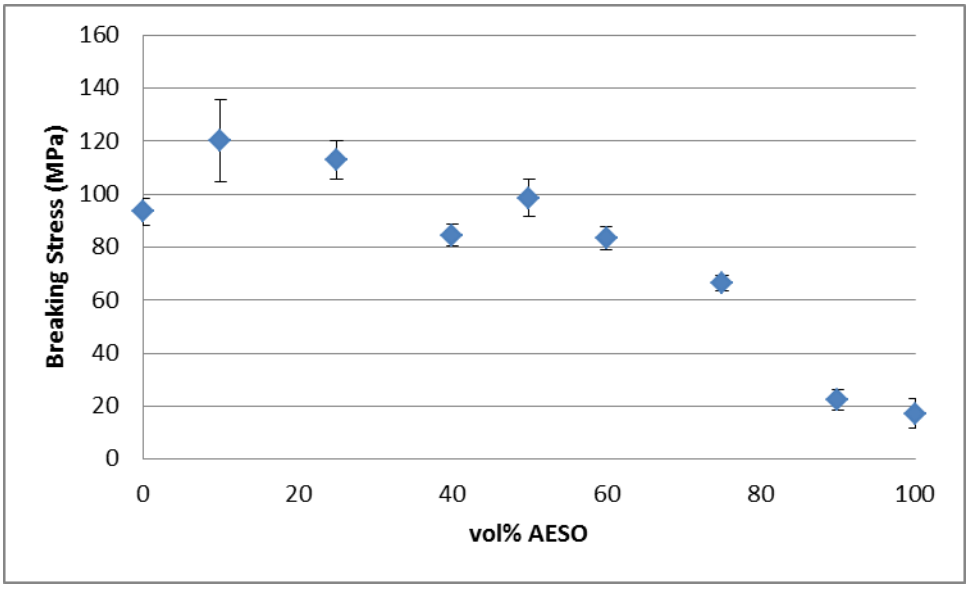

Figure 12: Average Flexural Stress of AESO/Styrene Copolymers

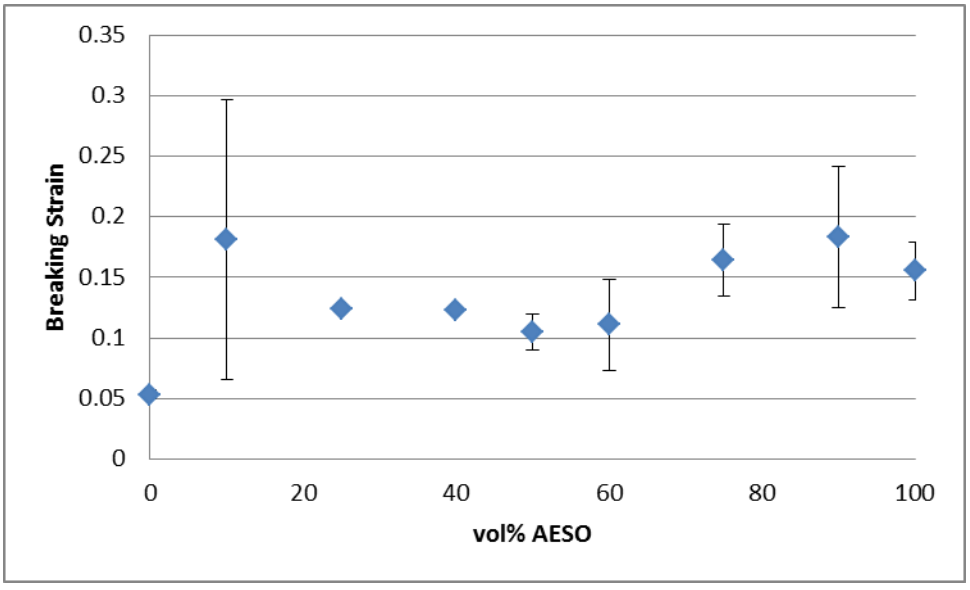

Figure 13: Average Flexural Strain of AESO/Styrene Copolymers

As shown below in Figure 13, the breaking strain of pure polystyrene is lower than all of the copolymers tested, with a peak initially, followed by a decrease after approximately 10 vol% AESO, increasing again after approximately 50 vol% AESO. In general, higher amounts of AESO result in a more flexible copolymer and increase the breaking strain. This trend is slightly less pronounced than the trends in the breaking stress shown previously. The final peak is likely due to AESO being more ductile than the pure styrene. The initial peak, however, could be caused by the aforementioned increasing of crosslinking that was theorized to cause the increase in breaking stress.

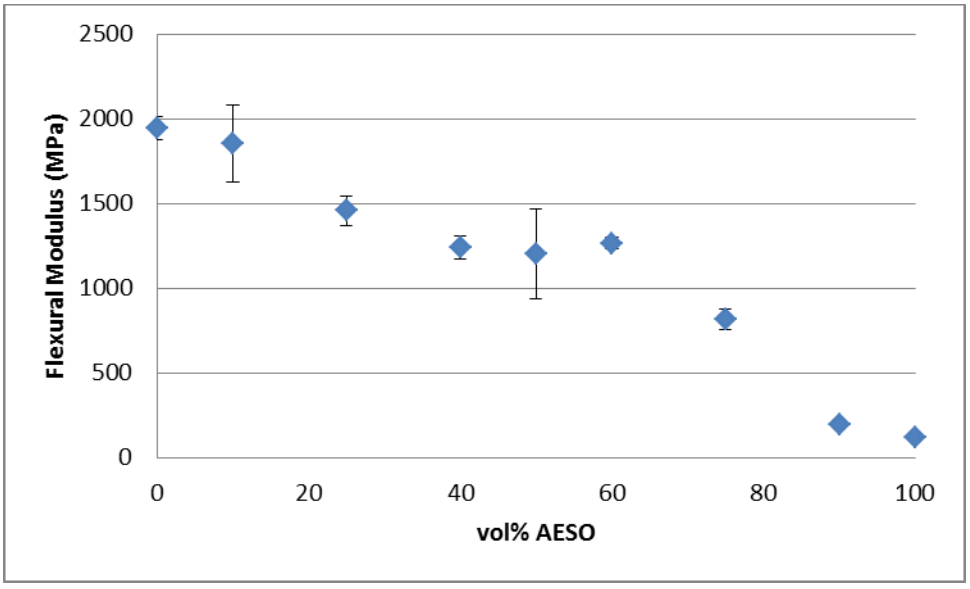

Figure 14: Average Flexural Modulus of AESO/Styrene Copolymers

As shown in Figure 14, the flexural modulus decreases fairly steadily as volume percentage of AESO increases. Unlike the previous properties, the flexural modulus does not seem to be greatly affected by the theorized initial increase in crosslinking. Between roughly 40 and 60 vol%, the flexural modulus appears to level off slightly. Higher amounts of styrene result in a stiffer polymer, while AESO makes the copolymer significantly less stiff. The decrease in modulus in such a linear fashion was not seen in previous studies investigating AESO/styrene blends, with no trend occurring as AESO content changed. [50]

3.3. DYNAMIC MECHANICAL ANALYSIS

Using dynamic mechanical analysis, the room temperature storage modulus, storage modulus as a function temperature, glass transition temperature, and number average molecular weight of network chains were determined. The room temperature storage modulus was plotted against the AESO weight percentage in each sample and graphed in Figure 15. The storage modulus of different blend compositions was plotted against temperature and graphed in Figure 16. In addition, the expected glass transition temperatures for each non-pure blend was calculated using the Fox equation, listed in Equation 6, and graphed in comparison to each measured glass transition temperature in Figure 17. The equation uses weight fractions of each component of the copolymer, is assumed to be the same as in the blend of monomers. The number average

molecular weight of the network chains of each composition blend at 100 ^{o}C was calculated and graphed in Figure 18. A full listing of data used is available in Tables 14 through 17 in Appendix D.

$$\frac{1}{T_g} = \frac{w_1}{T_{g,1}} + \frac{w_2}{T_{g,2}}$$

Equation 6: Fox Equation for Predicting T_g of Copolymer blends. T_g=glass transition temperature of copolymer (K); ω_1=weight fraction of polymer 1; $T_{g,1}$=glass transition temperature of polymer 1; ω_2=weight fraction of polymer 2; $T_{g,2}$=glass transition temperature of polymer 2

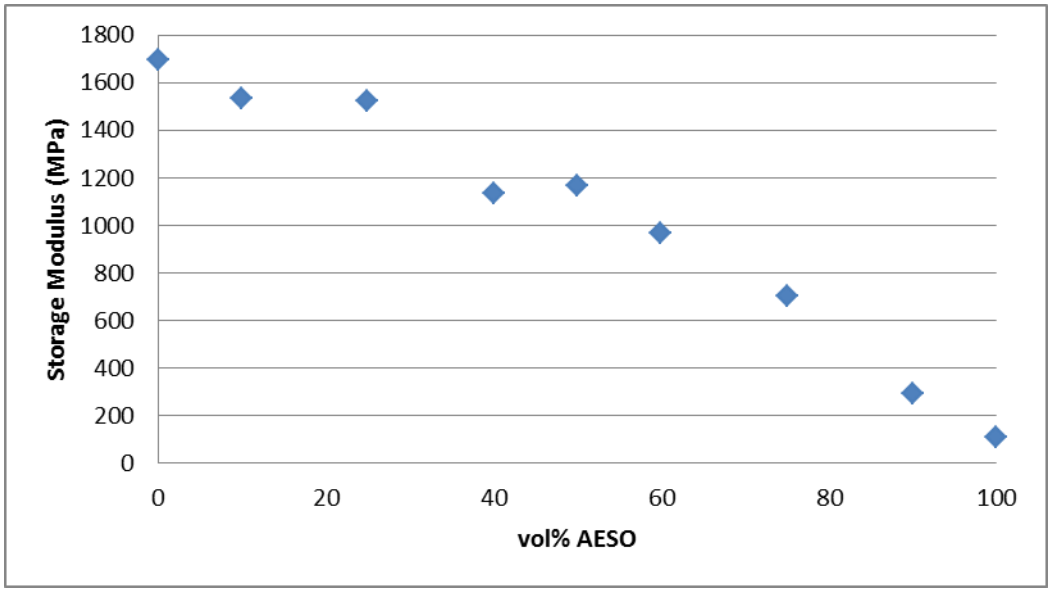

Figure 15: 30 °C Storage Modulus of AESO/Styrene Copolymers

As shown in Figure 15, the storage modulus decreases almost linearly as the weight percentage of AESO increase in the copolymer blends. This result is as expected, as the modulus of a copolymer normally exists as a weighted average of the modulus of the two pure polymers. The room temperature storage moduli under cyclic loading conditions are a measure of stiffness and are expected to be similar in trend and value of moduli from flexural testing. As seen in Figure 9, the trends and values are quite similar, corroborating the experimental results.

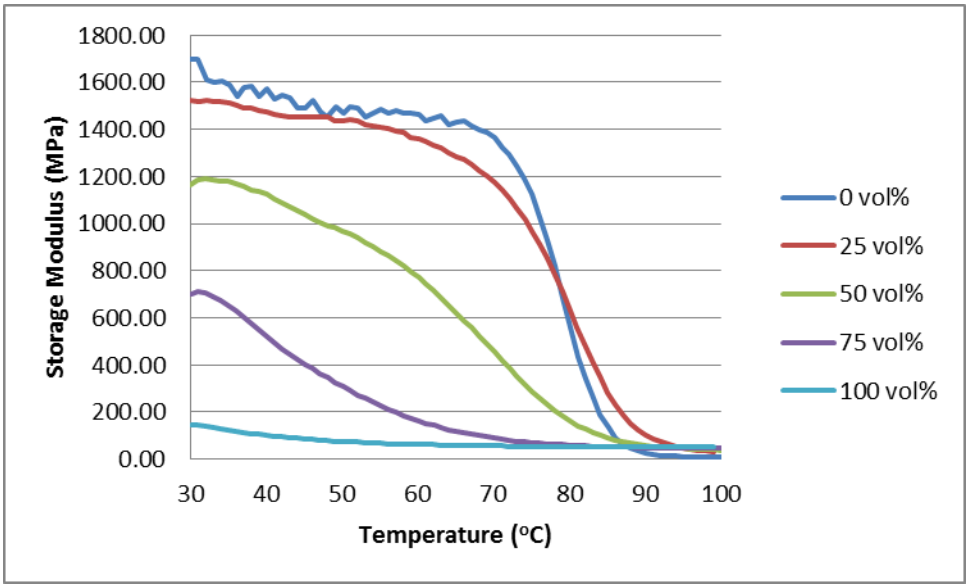

Figure 16: 30-100 °C Storage Modulus of AESO/Styrene Copolymers

As seen in Figure 16, increasing amounts of AESO also decreases the thermal stability of the copolymers. At 0 vol% AESO, the storage modulus

remains fairly constant, before experiencing a sharp decline beginning around 75 ^{o}C. As the amount of AESO increases, this decrease comes earlier and less sharply. This rapid decline is associated with the glass transition temperature. Below the T_g, the copolymer is fairly rigid and glassy; above the T_g, low stiffness of the material is caused by the rubbery or viscous nature of the copolymer. This signifies that small changes in temperature could result in severely differing material properties.

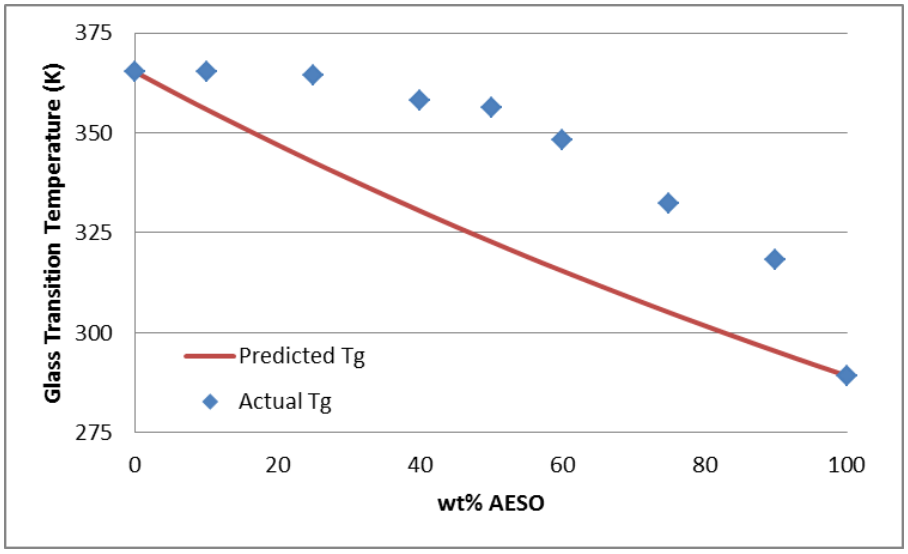

Figure 17: Measured and Predicted Tg of AESO/Styrene Copolymers

As shown in Figure 17, the glass transition temperatures of the blends found by the tanδ were found to decrease as weight percentage of AESO was increased; the change was fairly gradual at first and then increased more rapidly at

higher AESO contents. The glass transition temperatures between those of the homopolymers were observed to be slightly higher than those predicted by the Fox equation; the glass transition temperatures remained fairly high up to 40 wt% AESO, which may be related to the crosslinking and some of the unusual trends in the strength and stiffness previously observed.

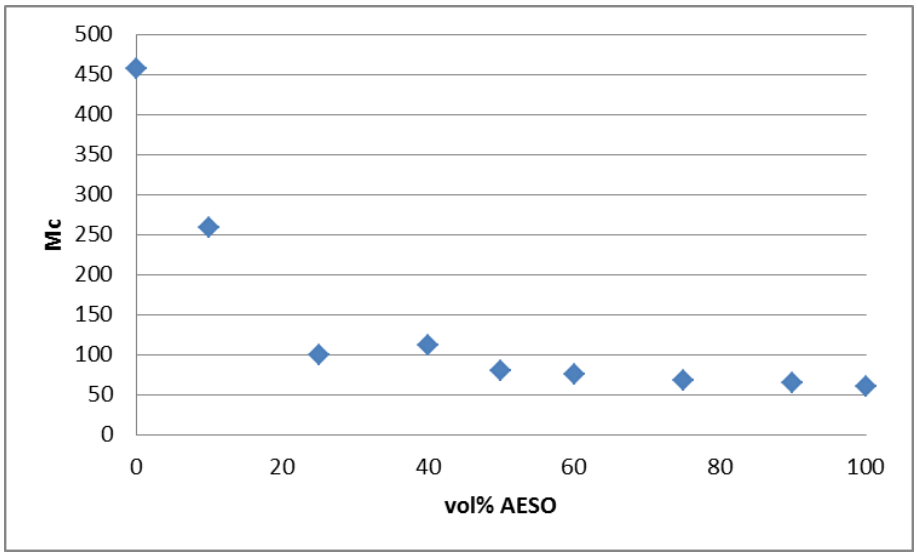

Figure 18: $\bar{M}_c$ of AESO/Styrene Copolymers

The number average molecular weight of the network chains is as shown in Figure 18, the number average molecular weight of the network chains initially decreases sharply as AESO content increases. After approximately 50 vol%, however, the $\bar{M}_c$ remains remarkably constant, with each measurement falling between 50 and 100. This confirms the theory that a significant increase in cross

linking occurs with a small amount of AESO content. It also shows that higher AESO contents do not greatly increase the crosslinking beyond the initial escalation. The $\bar{M}_c$ was calculated at 100 °C for all of the copolymer belnds, as all of the blends had a T_g below this value. A slight decrease in the T_g of the copolymer blends was also seen in previous studies, but at lower overall temperatures. Glass transiiton temperature was seen to decrease from 317 K at 30 vol% AESO to 310 K at 80 vol% AESO [48]

3.4. IMPACT TESTING

Using impact testing, the breaking energy of various compositions of AESO and styrene were measured. The samples of the same composition were then averaged, and plotted as functions of AESO content in Figure 19. In addition, the standard deviation of the measurements was calculated and plotted in the aforementioned graphs in the form of error bars. A full listing of the measurements obtained through impact testing is available in Table 6 in the Appendix B.

As shown below in Figure 19, the breaking energy increases initially as AESO content increases, before leveling off after 50 vol%. Between 50 and 100 vol% AESO, the breaking energies are nearly indistinguishable, with the breaking energy of 100 vol% AESO measuring slightly lower. The pure styrene polymer was by far the most brittle, with the brittleness of copolymers with high volume

fractions of AESO remaining fairly constant. Similar to the strain, the addition of the weaker, more flexible AESO component leads to a modest decrease in brittleness. The increase in breaking energy was not seen in previous studies investigating AESO/styrene blends. A general trend in breaking energy as AESO content changed could not be ascertained, with slight increases and decreases occurring as the AESO content varied. [50]

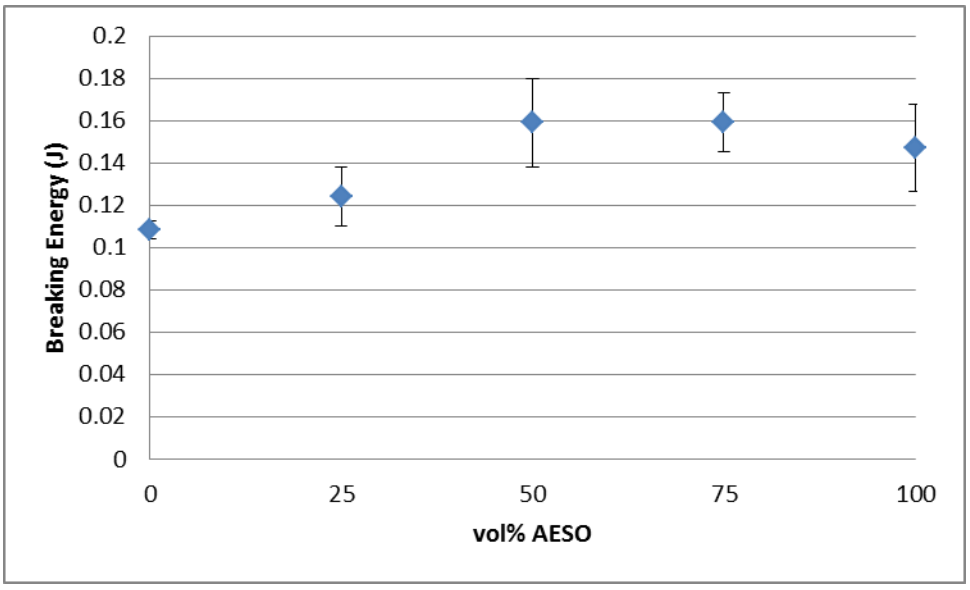

Figure 19: Average Breaking Energy of AESO/Styrene Copolymers

3.5. DUROMETER MEASURMENTS

Using durometer measurements, the hardness of various compositions of AESO and styrene were measured. The samples of the same composition were

then averaged, and plotted as functions of AESO content in Figure 20. In addition, the standard deviation of the measurements was calculated and plotted in the aforementioned graphs in the form of error bars. A full listing of measurements obtained through durometer measurements is available in Table 10 in Appendix C.

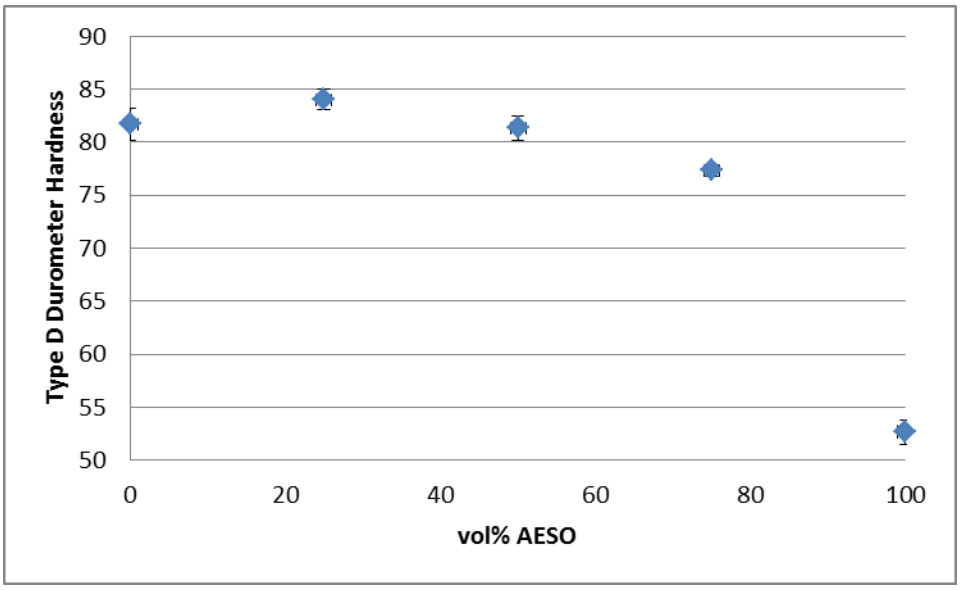

Figure 20: Average Durometer Hardness of AESO/Styrene Copolymers

As seen in Figure 20, as AESO content increases initially, the durometer hardness stays relatively constant, with perhaps a slight increase at approximately 25 vol% AESO. After 50 vol% AESO, however, the hardness drops off significantly, before reaching its lowest value for 100 vol% AESO. The lack of decrease in hardness initially is promising, as it allows for up to 50 vol% AESO to

be incorporated without experiencing a significant compromise in hardness. The decrease in hardness in any noticeable trend was not seen in previous studies investigating AESO/styrene blends. The hardness did not vary linearly with a change in AESO content, showing no general trend. [50]

4. SUMMARY OF FILLED COMPOSITES

The following section will serve to summarize the findings of the investigation into filler type in composites with AESO/Styrene copolymer as a filler. An overview and comparison of the properties of all three filled composite types is presented below. Additional detail and discussion for pecan nut shell flour, egg shell calcium, and organically modified clay filled composites can be found in section 5.2, 5.3, and 6.2, respectively.

As one of the primary goals of the project was overall reduction of nonrenewable components of the material, higher filler loadings are beneficial. Of the three filler types, egg shell calcium was able to achieve the highest filler loading at 36 vol%. Pecan nut shell flour was able to achieve the next highest loading at 23 vol%, while organically modified clay was able to be added at a mere 4 vol%. The high loading of ESC, and to lesser degree of PNSF, indicates that they are superior filler candidates.

The addition of all filler types was found to decrease the strength and the flexibility of the composite. The highest loadings of the PNSF, ESC, and OMC achieved a breaking stress of 54, 83, and 74 MPa and a breaking strain, of 0.04, 0.02, and 0.06, respectively. The reduction in breaking stress and strain is thought to be a result of poor adhesion between the filler and matrix, causing the composite to break prematurely. All of the samples produced a material of a lower strength than polystyrene (σ=93 MPa); however, the ESC filled sample was only

moderately weaker. The OMC filled samples were able to produce a material marginally more flexible than polystyrene (ε=0.05), although polystyrene is already such a brittle material that the slight differences between the neat polymer and the composites is essentially irrelevant. The breaking stress and strain of the composites in comparison to polystyrene is summarized in Figures 21 and 22.

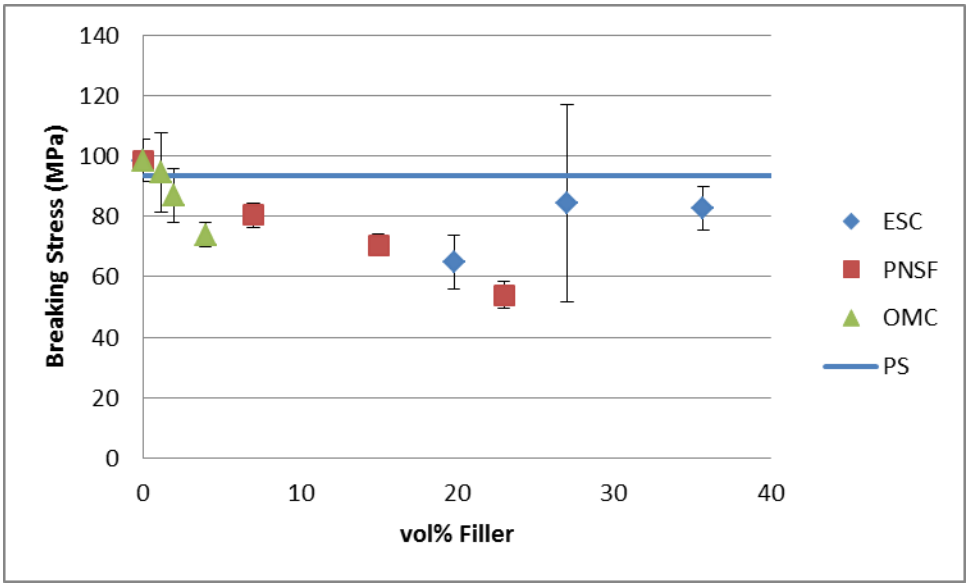

Figure 22: Breaking Stress of Filled Composites and Polystyrene

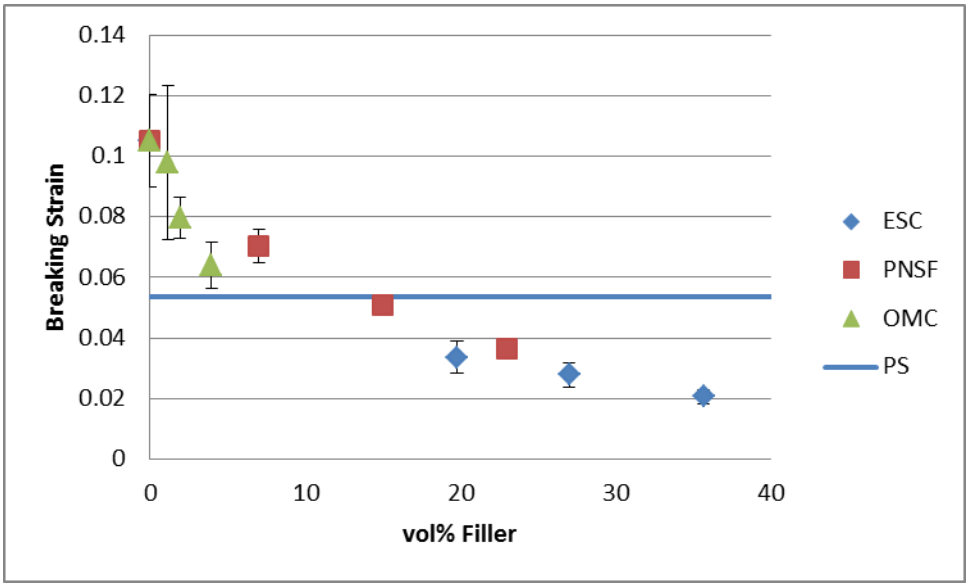

Figure 22: Breaking Strain of Filled Composites and Polystyrene

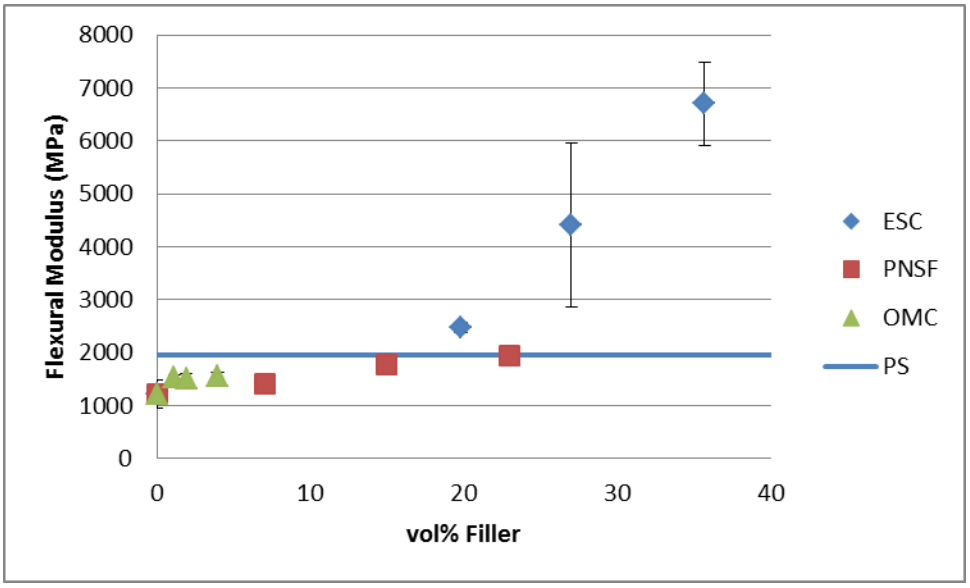

Figure 23: Flexural Modulus of Filled Composites and Polystyrene

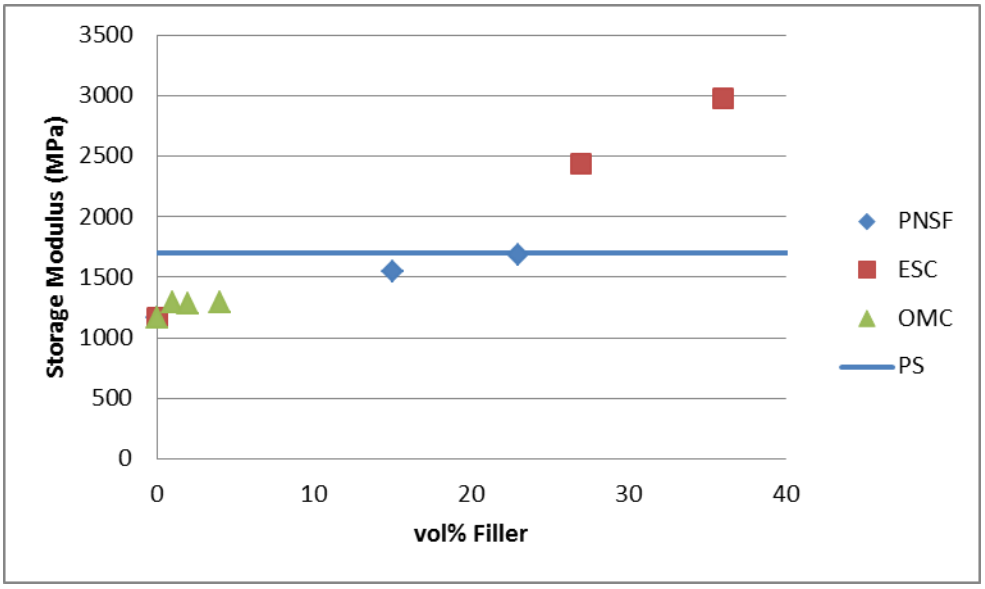

Figure 24: Storage Modulus of Filled Composites and Polystyrene

The filled composites had nearly identical glass transition temperatures to that of the 50:50 AESO/Styrene copolymer matrix at 356 K. The lack of deviation indicates that the polymer was not altered by polymerizing around the fillers, causing neither positive nor negative contributions. These are lower than the glass transition temperature of pure polystyrene (T_g=365 K), but are not meaningfully different. All of the composites had nearly identical breaking energies, ranging between 0.08 and 0.10 J. These are slightly lower than polystyrene at 0.11 J, although not enough to be detrimental. The decrease in breaking energy is likely caused by incomplete cohesion between the matrix and the filler, causing premature fracturing within the composite. The glass transition temperatures and

breaking energies of the composites in comparison to polystyrene is summarized in Figures 25 and 26.

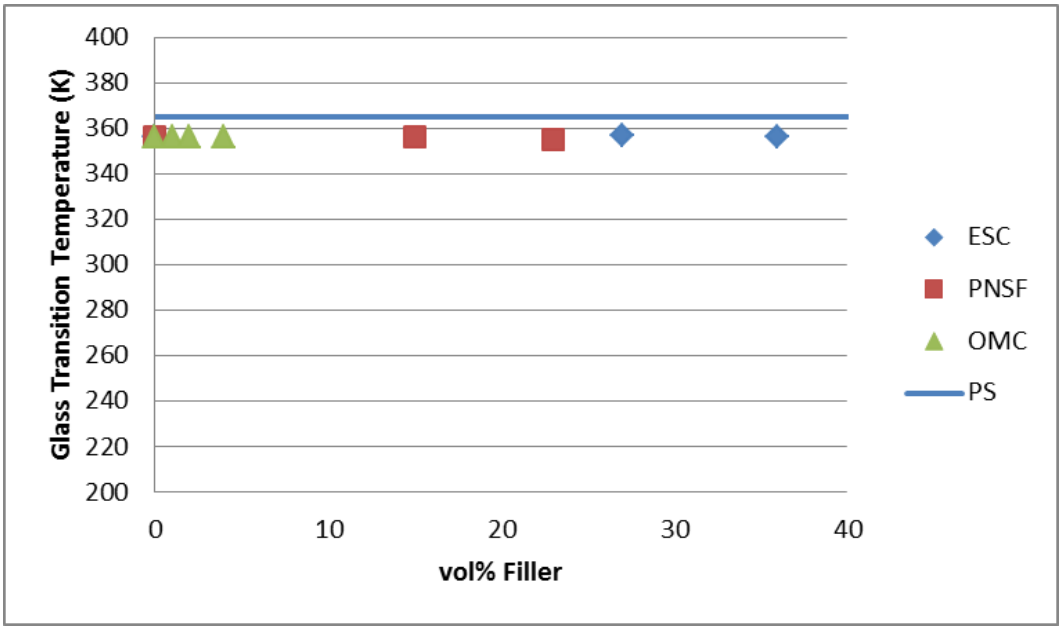

Figure 25: T_g of Filled Composites and Polystyrene

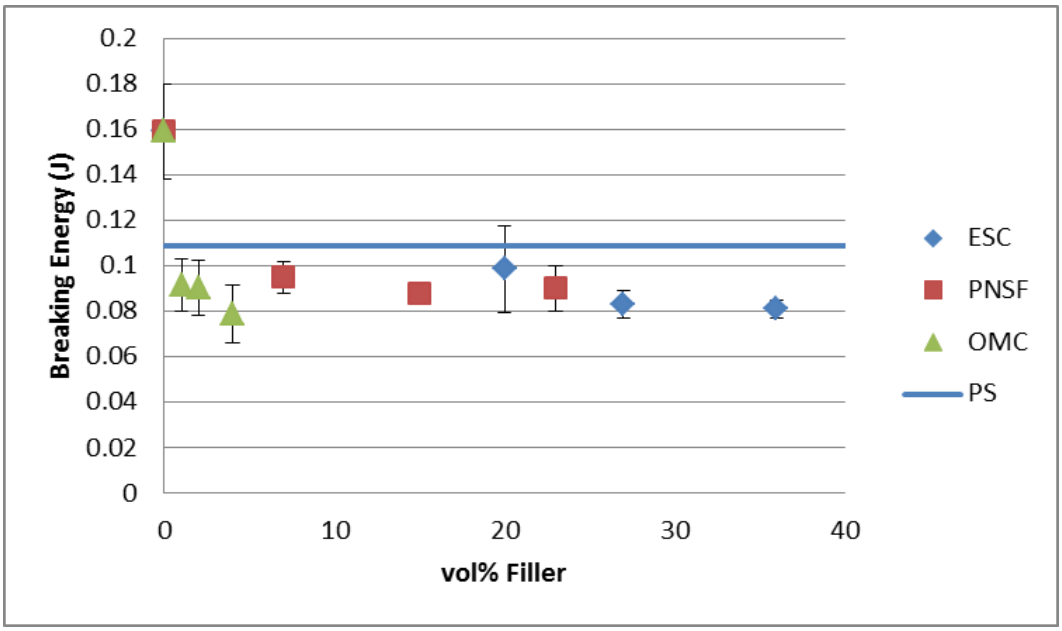

Figure 26: Breaking Energy of Filled Composites and Polystyrene

The hardness of the composites was all significantly improved by the addition of polystyrene. The PNSF, ESC, and OMC filled samples achieved hardnesses of 97, 143, and 88, respectively. These were all higher than the hardness of pure polystyrene at 82. While ESC improved the hardness by the most at nearly double the measured value, all of the fillers were successful at improving the hardness of the material. The improvement to the hardness is likely caused by the filler being substantially harder than the starting copolymer. The hardness of the composites in comparison to polystyrene is summarized in Figures 27.

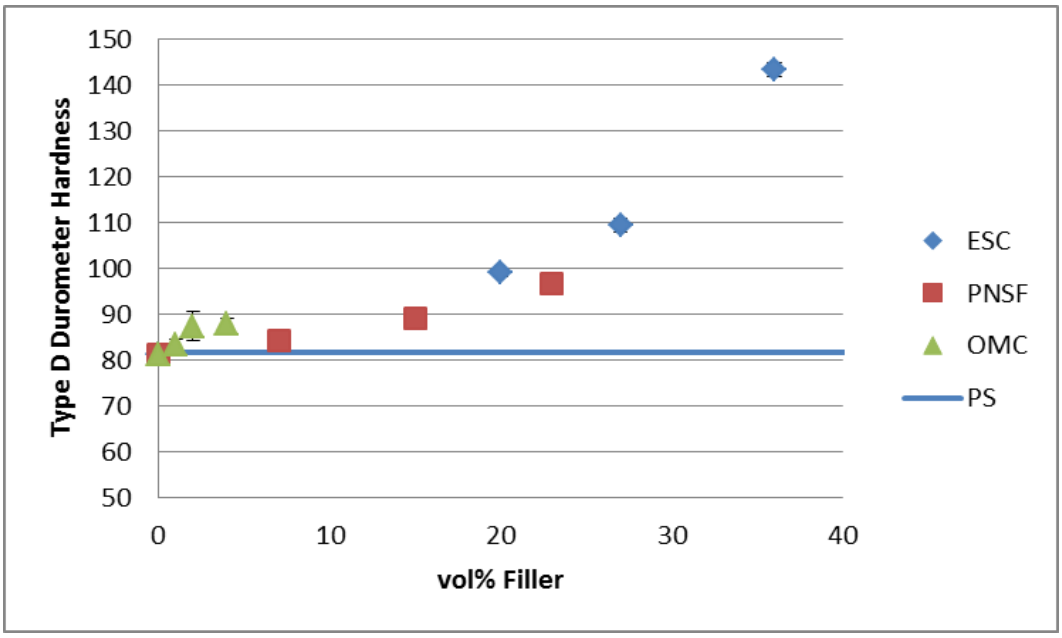

Figure 27: Hardness of Filled Composites and Polystyrene

5. COMPOSITES WITH BULK FILLERS

5.1. BENEFITS OF BULK FILLERS

Bulk fillers offer many potential benefits when used in polymeric composites. Bulk fillers are composed of large, macro sized particles, visible under standard light microscopy. The materials chosen are typically stiffer and stronger than the polymer matrix, so that the incorporation might increase the stiffness, strength, and hardness. They are normally made of pulverized materials, which mean they can be created easily from renewable resources. Additionally, large amounts of the filler can be added to the copolymer and still produce a material able to undergo polymerization. While fillers are generally added in small amounts to improve the properties of the material, high filler contents can also make the product more biorenewable if the fillers are themselves biorenewable. Unfortunately, these fillers also tend to chemically different from the polymeric material; meaning the material as a whole may lack cohesion between the filler and the polymer, which could in fact compromise properties.

5.2. PECAN NUT SHELL FLOUR FILLER

5.2.1. SCANNING ELECTRON MICROSCOPY

Scanning electron microscopy was used to achieve images of the surface of pecan nut shell flour filled composites. Selected low magnification images, shown below in Figures 28-30, demonstrate the dispersion of PNSF in the

composite. Selected high magnification images, seen in Figures 31-33, depict the particle size of the filler in the material. A full listing of SEM images take of these blends is available in Figures 75-92 in Appendix E.

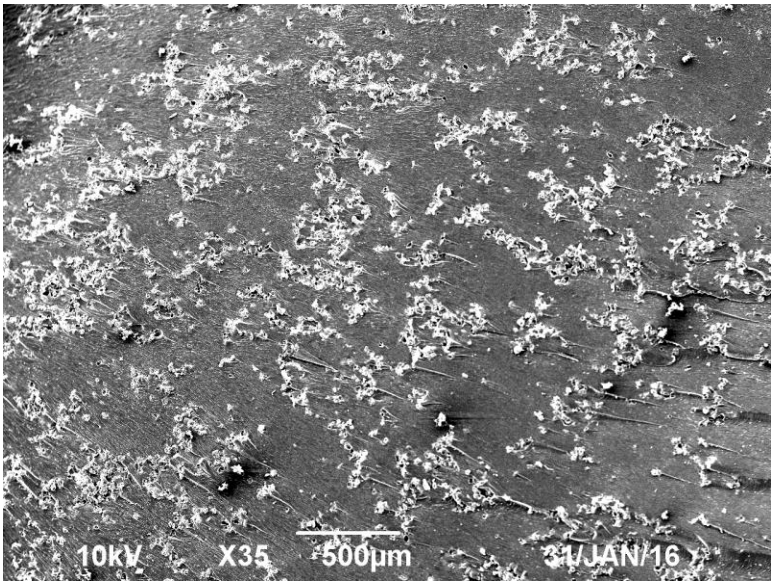

Figure 28: Low Mag SEM Image of 7 vol% PNSF Filled Composite

As shown in Figure 28, the dispersion of 7 vol% PNSF in the composite is only moderately uniform. The filler is not spread uniformly throughout the sample, with regions of high filler density and regions with essentially no filler. The regions tend to be quite small, with the largest measuring no more than 500 µm wide. This creates reasonable dispersion throughout the sample, but poor dispersion in specific areas.

At higher rates of filler, the dispersion of 15 vol% PNSF in the material is significantly improved, as seen in Figure 29. The PNSF is spread very uniformly throughout the composite, with every section looking visually similar to nearly any other. Small regions of low PNSF density do exist, but measure less than 100 μm across. In Figure 30, the dispersion of 23 vol% PNSF in the composite is maximized, with high visual density throughout. No regions of low PNSF density exist, with every area achieving an appreciable concentration of the filler. Small agglomerates, approximately 25-50 μm in diameter, have begun appearing on the surface of the sample. These are likely insignificant, as there are relatively few of them and they are fairly scattered in the sample.

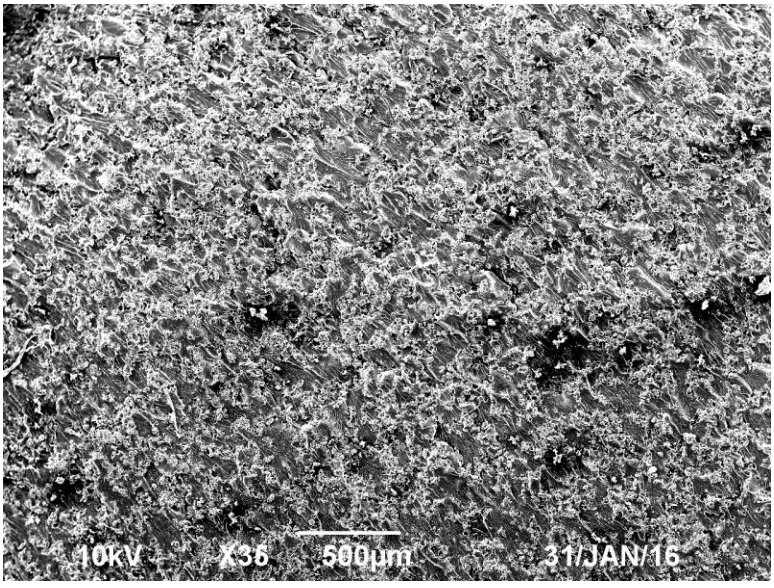

Figure 29: Low Mag SEM Image of 15 vol% PNSF Filled Composite

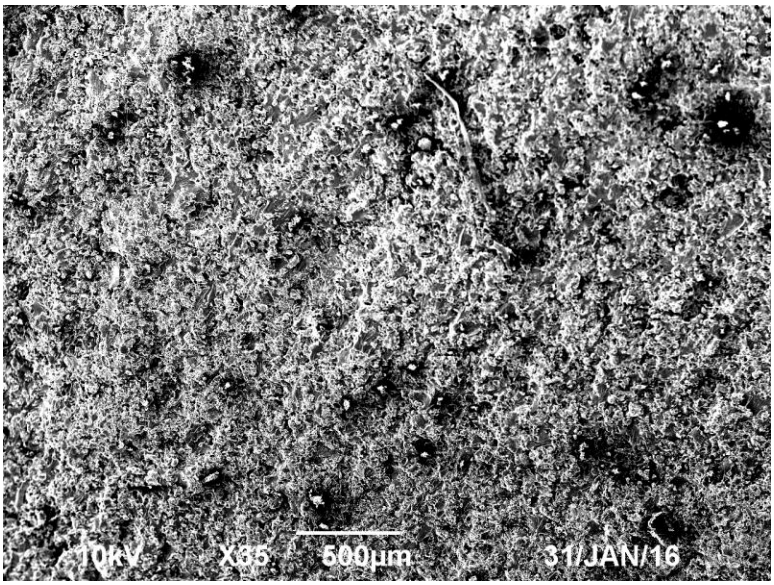

Figure 30: Low Mag SEM Image of 23 vol% PNSF Filled Composite

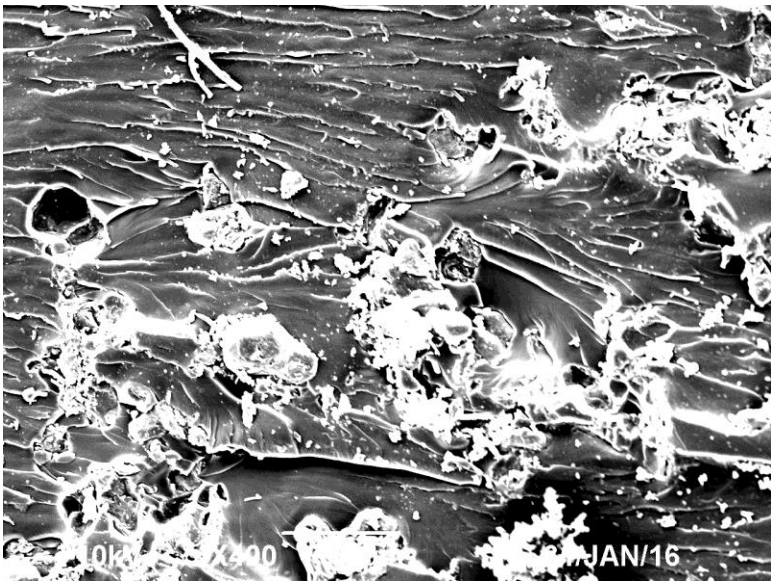

Figure 31: High Mag SEM Image of 7 vol% PNSF Filled Composite

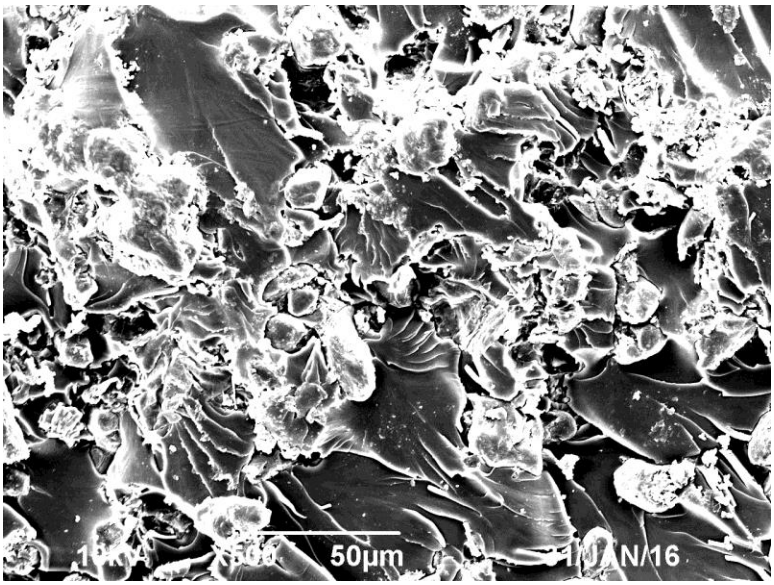

Figure 32: High Mag SEM Image of 15 vol% PNSF Filled Composite

As seen in the high magnification image of 7 vol% in Figure 31, the particle size is reasonably small. The particles appear to be under 50 μm in size, with no noticeable agglomerations of the filler forming. In Figure 32, the particle size remains relatively constant in the 15 vol% PNSF filled material. Individual particles are again measured at 50 μm or less in diameter, with most appearing at under 25 μm. Agglomerations of particles have begun to form, with some reaching almost 100 μm across, but these are still reasonable small and are not widespread. In Figure 33, the particle size of the filler in the 23 vol% PNSF filled composites has decreased. The largest particles seem to be no greater than 10 μm in diameter, with the majority measuring much less than that. The increased PNSF

loading has allowed for the PNSF to bond more freely with the copolymer, reducing the self-bonding that caused the larger particles to form.

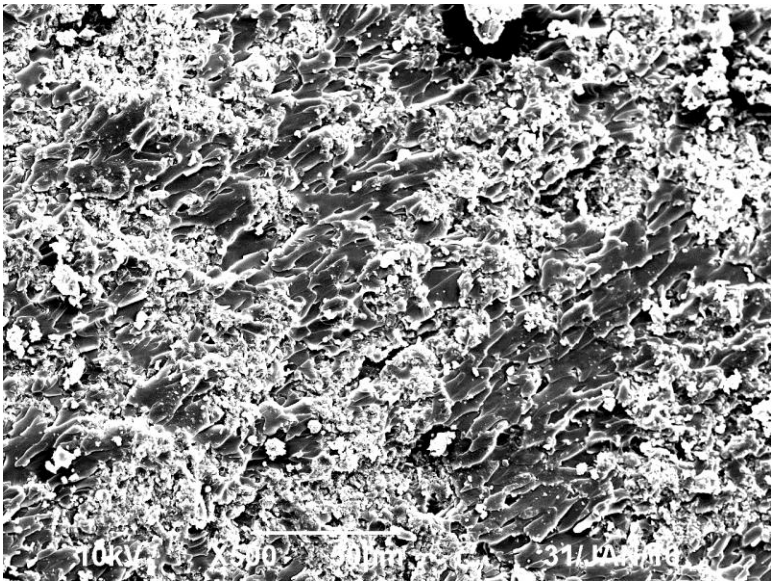

Figure 33: High Mag SEM Image of 23 vol% PNSF Filled Composite

5.2.2. THREE POINT FLEXURAL TESTING

Using three point flexural testing, the breaking stress, breaking strain, and flexural modulus were measured for pecan nut shell flour filled composites. The samples of the same composition were then averaged, and plotted as functions of PNSF content in Figures 34 through 36. In addition, the standard deviation of the measurements was calculated and plotted in the aforementioned graphs in the form of error bars. A full listing of averaged physical properties obtained through three point flexural testing is available in Table 3 in Appendix A.

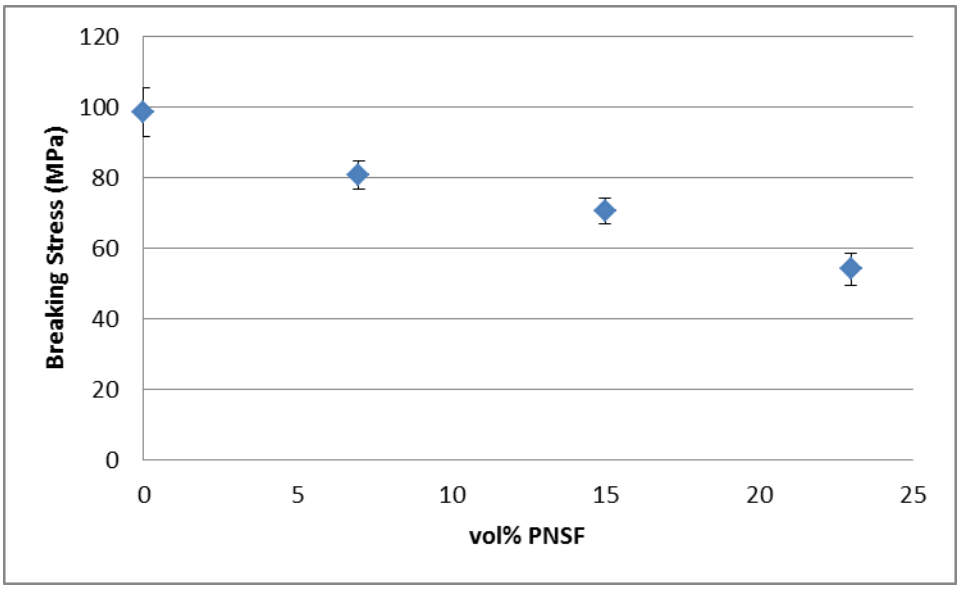

Figure 34: Average Flexural Breaking Stress of PNSF Filled Composites

As shown in Figure 34, the average flexural breaking stress decreases steadily as the PNSF content increases. The drop is fairly linear between the bounds, with the breaking stress hitting a maximum at 0 vol% PNSF and reaching a minimum at 23 vol% PNSF. This trend is likely caused by a lack of complete bonding between the filler and the copolymer. As the amount of filler increases, material becomes increasingly less cohesive, allowing fractures to move easily throughout the interior of the samples. The added interface from larger PNSF contents likely act as preexisting flaws, which ease the propagation of cracks in the material. A similar decrease in strength due to added cellulosic filler has been

seen in other studies; however, the previous studies saw an over 80% decrease due to filler content, down to 8.1 MPa at 40 wt% filler in poly(lactic acid) (PLA). [54] Alternatively, other studies saw an increase in the flexural strength at higher loadings, ranging from moderate 10 MPa increases at 30 wt% in recycled high density polyethylene (rHDPE) [55] to nearly 3 fold increase at 25 vol% in linseed oil resin (LOR) [51].

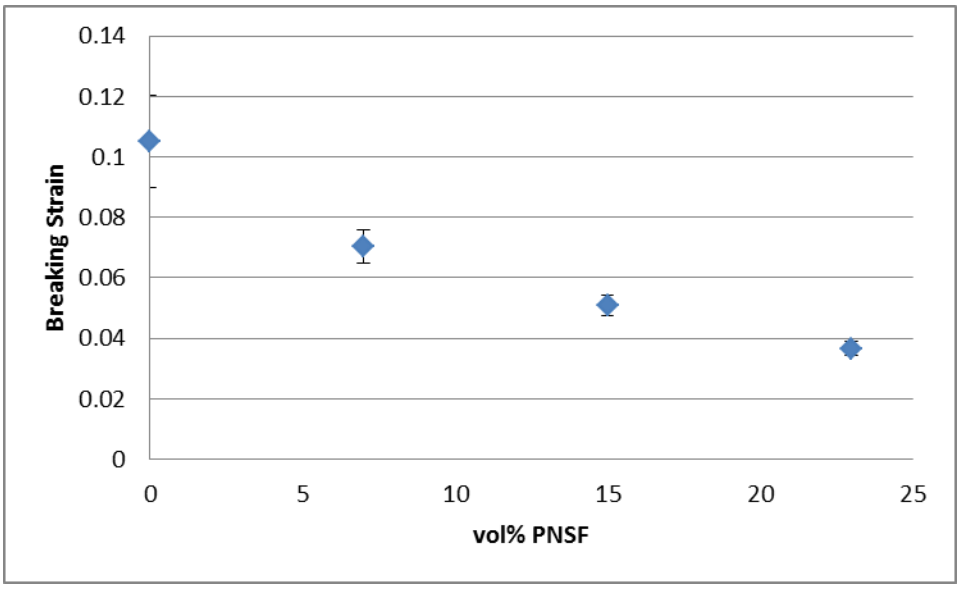

Figure 35: Average Flexural Breaking Strain of PNSF Filled Composites

As shown in Figure 35, the average flexural breaking strain also decreases as the amount of PNSF in the composites increases. The decrease begins rapidly, before beginning to level out after approximately 15 vol% PNSF. This trend can again be explained by a lack of cohesion between the filler and the copolymer.

With the PNSF supporting little to none of the induced strain, the remaining copolymer must support the vast majority of it. As the amount of copolymer in the more PNSF filled composites is lower, the strain decreases. The flexural strain has previously been identified to decrease slightly due to increased loading of cellulosic filler in the composite, dropping from strains of 0.159 to 0.056 at 40 wt% filler in PLA. [54]

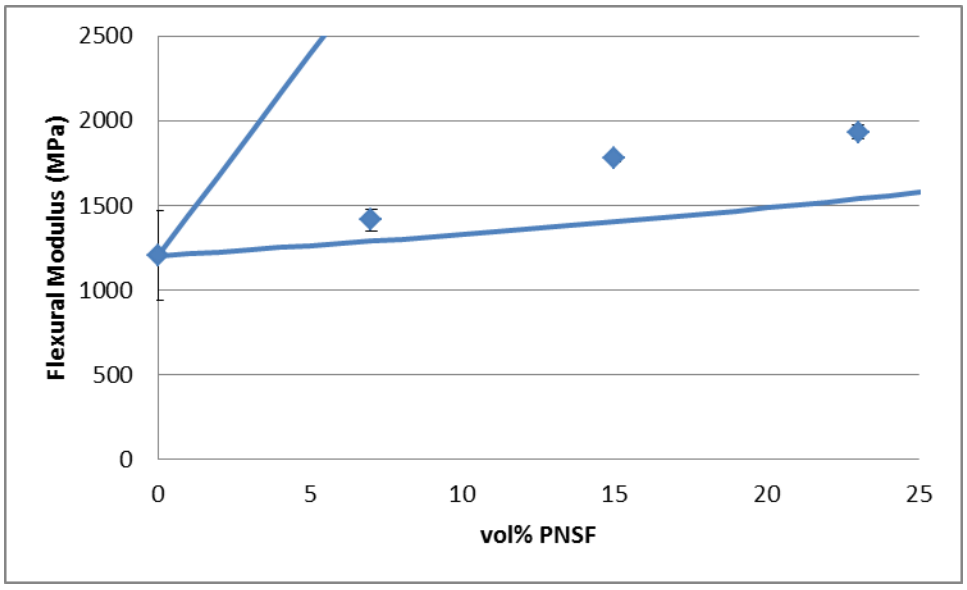

Figure 36: Average Flexural Modulus of PNSF Filled Composites

In contrast, as shown in Figure 36, the addition of PNSF substantially increases the stiffness of the neat copolymer. The increase is relatively linear, rising steadily from 0 vol% PNSF to a maximum at approximately 23 vol% PNSF. The 23 vol% PNSF, the highest level tested, increased the modulus of the

composite by a factor of 1.8 over the pure copolymer. This is likely caused by the modulus of the pure PNSF being much greater than that of the pure copolymer. While the lack of complete bonding decreased the other material properties, the nature of the flexural modulus likely avoided this problem. Flexural modulus is related to the initial change in the stress and strain, before critical cracks and a fracture in the material develops. The measured moduli all lie between the two bounds provided by the simple and inverse rules of mixing, indicating the composite is behaving as expected. An increase in the modulus of the composite due to the increased cellulosic filler content has been seen in previous research, up to 1500 MPa at 25 vol% in LOR [51] or 1700 MPa at 40 wt% in rHDPE [55]. Alternatively, an increase in filler content has been seen to cause a slight decrease in modulus, causing a 50% decrease in stiffness at 40 wt% filler in PLA. [54]

5.2.3. DYNAMIC MECHANICAL ANALYSIS

Using dynamic mechanical analysis, the room temperature storage modulus, storage modulus as temperature varies, glass transition temperature of pecan nut shell flour filled composites were measured. Values at 7 vol% PNSF were unable to be attained, as the filler did not stay sufficiently suspended in copolymer during polymerization in the smaller 8 mm tubes. The room temperature storage modulus and the glass transition temperatures were plotted against the PNSF content in each sample and graphed below in Figures 37 and 39,

respectively. The storage modulus of different blend compositions were plotted against temperature and graphed below in Figure 38. A full listing of data used is available in Tables 18 through 20 in Appendix D.

As seen in Figure 37, the room temperature storage modulus increases steadily as the amount of PNSF in the material increases. The increase in modulus is likely caused by the higher stiffness of PNSF than the neat copolymer. The moduli measured by this method are similar to those measured in the three point flexural testing, corroborating the results of each technique. These experiments confirm the conclusion that the addition of PNSF as a filler leads to an increase in the stiffness of the composite.

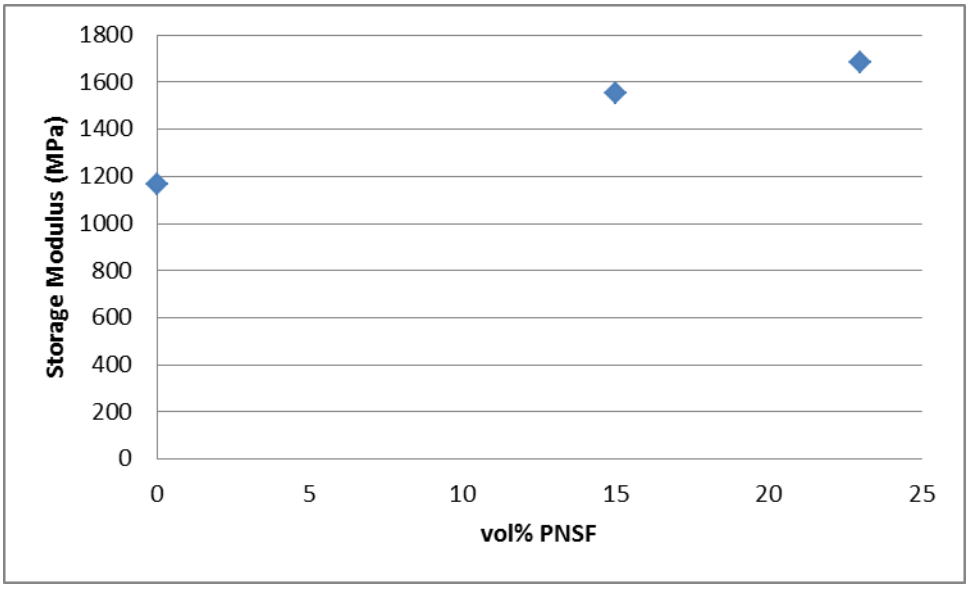

Figure 37: 30 °C Storage Modulus of PNSF Filled Composites

As shown in Figure 38, the addition of PNSF leads to higher storage moduli at all temperatures. This result was expected, as the glass transition temperature of cellulose, the main component of PNSF is much higher than that of the neat copolymer. The PNSF does not seem to increase the thermal stability of the composite greatly. The rapid decrease in the storage modulus still occurs at roughly the same temperature, and the slope of the decline does not vary significantly with changes in PNSF content. While the material properties are improved with higher PNSF contents, they are no less prone to loss due to temperature shifts.

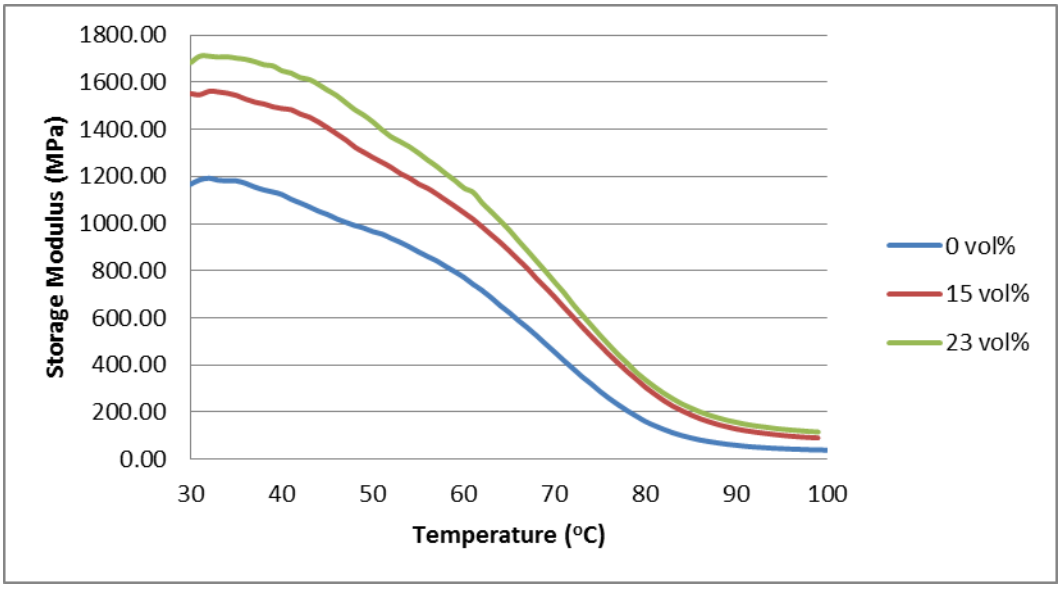

Figure 38: 30 -100 °C Storage Modulus of PNSF Filled Composites

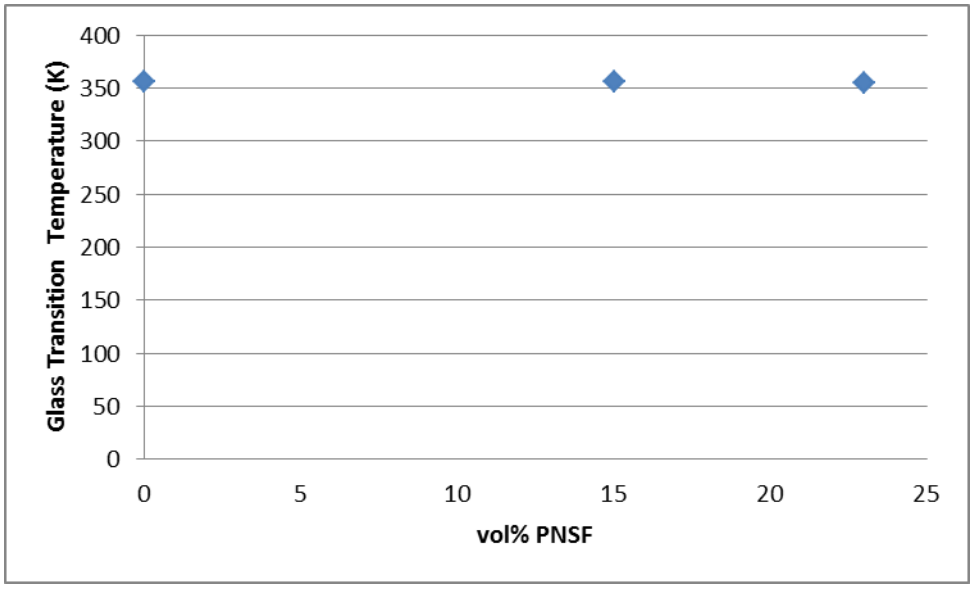

Figure 39: Glass Transition Temperature of PNSF Filled Composites

The similarity of this temperature response is further illustrated in Figure 39. The glass transition temperature, as measured by the tanδ peak, does not change with the addition of PNSF. The identical glass transition temperatures indicate that the response of chains in the copolymer matrix within the composites has not changed with the addition of PNSF as a filler. The decreases in the modulus with temperature changes are in all cases due to the softening of the matrix polymer. Conversely, the addition of PNSF does nothing to increase the glass transition temperature. A higher T_g would produce greater thermal stability and improve the performance of the material. Any effect of filler particles on behavior of individual chains in the matrix is limited to the matrix-filler

interfaces, which make up a small fraction of the volume of the matrix polymer. The lack of change in glass transition temperature has been seen in previous studies, with a slight decrease in T_g from 330 K to 325K at 40 wt% cellulosic filler in PLA. [54] Alternatively, increases in T_g have been seen to increase as filler content from 350 K to 400 K at 30 wt% filler in LOR.[51]

5.2.4. IMPACT TESTING

Using impact testing, the breaking energy of pecan nut shell flour filled composites was measured. The samples of the same composition were then averaged, and plotted as functions of PNSF content in Figure 40. In addition, the standard deviation of the measurements was calculated and plotted in the aforementioned graphs in the form of error bars. A full listing of the measurements obtained through impact testing is available in Table 7 in the Appendix B.

As seen in Figure 40, the PNSF filled samples were much more brittle than that of the neat copolymer. The breaking energy experiences an immediate drop as the PNSF content initially increases. After roughly 7 vol% PNSF, however, the breaking energy levels off and remain fairly constant between 0.08 and 0.1 J. The drop is likely caused by the lack of cohesion between the filler and the copolymer in the composite and is caused by a similar mechanism that resulted in decreased breaking strain. Once PNSF is added, the fracture in the

material has less polymer to fracture through, decreasing the energy needed to propagate through. Unlike the breaking strain, additional PNSF beyond 7 vol% did not further compromise the composite's breaking energy. This could indicate that the brittleness of the material is not affected by the total addition of filler, merely by the fact that filler had been added. Previous studies had identified similar drop in breaking energy as cellulosic filler content increase, showing a 50% decrease as filler content increased to 40 wt% in rHDPE. [55]

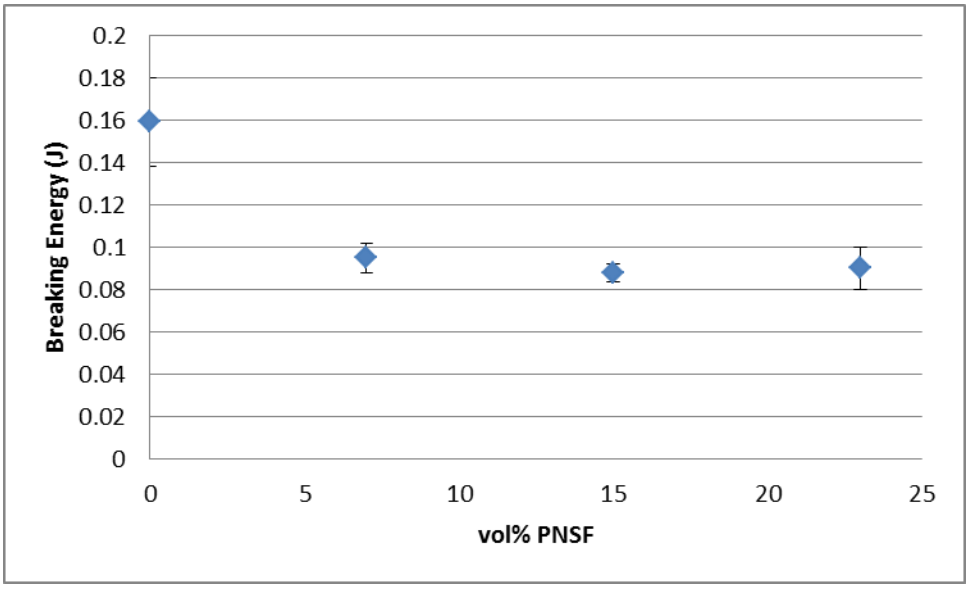

Figure 40: Average Breaking Energy of PNSF Filled Composites

5.2.5. DUROMETER MEASUREMENTS

Using durometer measurements, the hardness of pecan nut shell flour filled composites was measured. The samples of the same composition were then averaged, and plotted as functions of AESO content in Figure 41. In addition, the standard deviation of the measurements was calculated and plotted in the aforementioned graphs in the form of error bars. A full listing of measurements obtained through durometer measurements is available in Table 11 in Appendix C.

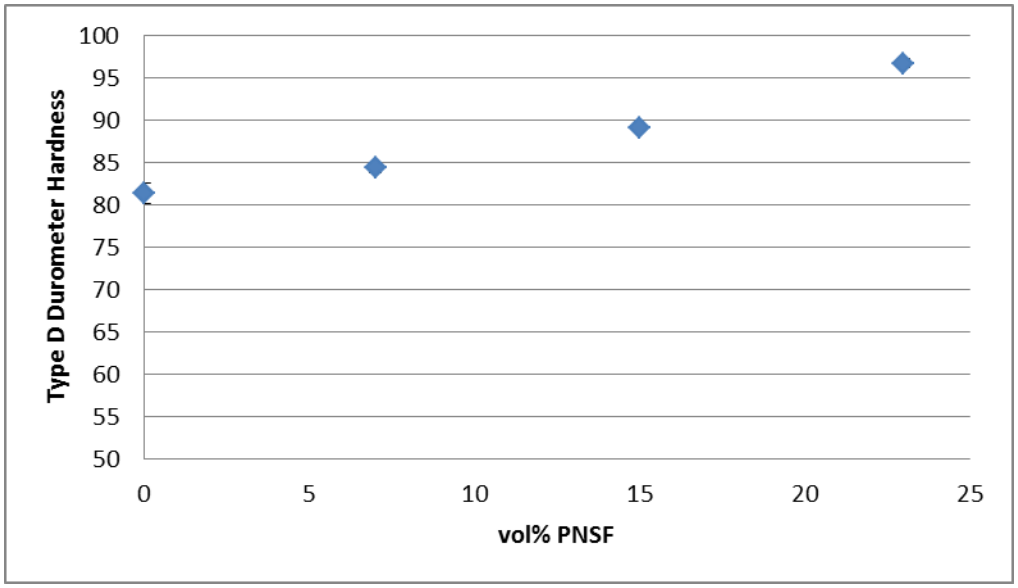

Figure 41: Average Durometer Hardness of PNSF Filled Composites

As seen in Figure 41, the hardness of the composite increase as the PNSF content increases. The rise begins gradually, with a greater rate of increase at higher loadings of PNSF. The 23 vol% PNSF, the highest loading tested, showed an increase in hardness of nearly 20%. The increase in the measured hardness was expected; the filler used in the composite was harder on its own than the pure copolymer. The greater hardness could be promising, as it indicates that this material property could be easily controlled and improved through the addition of this filler.

5.3. EGG SHELL CALCIUM FILLER

5.3.1. SCANNING ELECTRON MICROSCOPY

Scanning electron microscopy was used to achieve images of the surface of egg shell calcium filled composites. Selected low magnification images, shown in Figures 42-44, demonstrate the dispersion of ESC in the composite. Selected high magnification images, seen below in Figures 45-47, depict the particle size of the filler in the material. A full listing if SEM images take of these blends is available in Figures 93-110 in Appendix E.

As shown in Figure 42, the dispersion of 20 vol% ESC in the composite is fairly high. The filler is spread uniformly throughout the sample, with few regions of high filler density and few regions with essentially no filler. The filler does not seem to be very clustered, with the ESC mixed evenly throughout. The regions of

low ESC density tend to be quite small, with the largest measuring no more than 200 μm wide. This creates reasonable dispersion throughout the sample. In Figure 43, the dispersion of 27 vol% ESC in the material is improved. The ESC is spread very uniformly throughout the composite, with every section looking visually similar to nearly any other. Small regions of low ESC density do exist, but measure less than 50 μm across. In Figure 44, the dispersion of 36 vol% ESC in the composite is very high. Low ESC density regions exist, but the surface is packed with filler. Agglomerates, approximately 200 μm in diameter, have begun appearing on the surface of the sample. These are significant, as pockmarks have been left where the masses have been broken off.

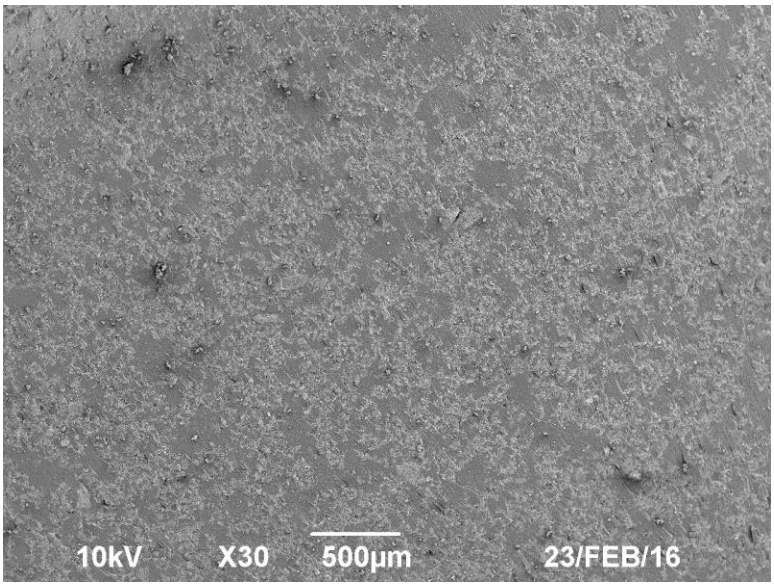

Figure 42: Low Mag SEM Image of 20 vol% ESC Filled Composite

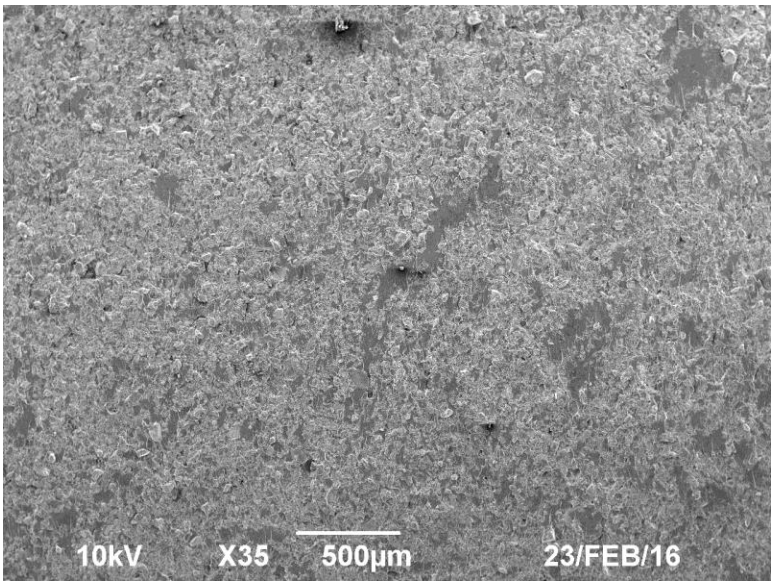

Figure 43: Low Mag SEM Image of 27 vol% ESC Filled Composite

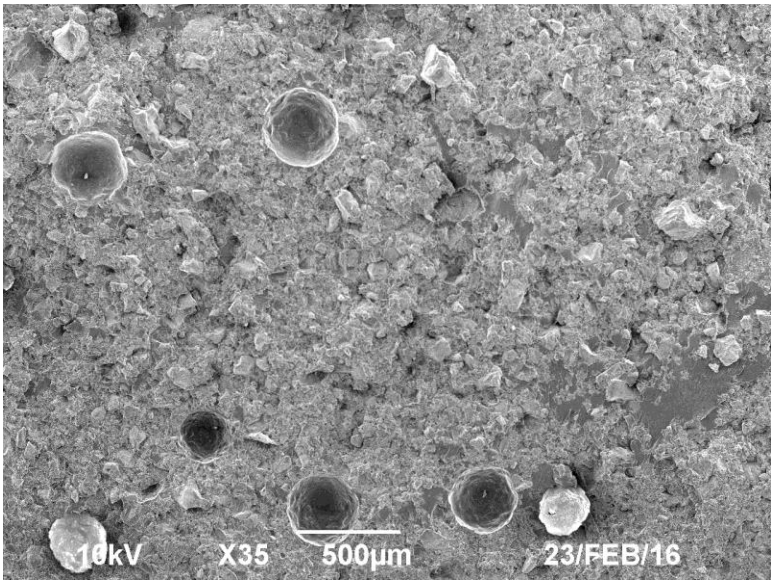

Figure 44: Low Mag SEM Image of 36 vol% ESC Filled Composite

As seen in Figure 45, the particle size of the ESC in the 20 vol% ESC filled composite is reasonably small. The particles appear to be under 20 μm in size, with no noticeable agglomerations of the filler forming. In Figure 46, the particle size remains relatively constant in the 27 vol% ESC filled material. Individual particles are again measured at 20 μm or less in diameter, with most appearing at under 10 μm. Agglomerations of particles have begun to form, with some reaching almost 50 μm across, but these are still reasonable small and are not widespread. In Figure 47, the particle size of the filler in the 36 vol% ESC filled composites has increased. The largest particles are measured at upwards of 100 μm in diameter, with agglomerations forming even larger species. This reinforces the results seen at the low magnification of this composition, and suggests that this loading may be too high for efficient material usage.

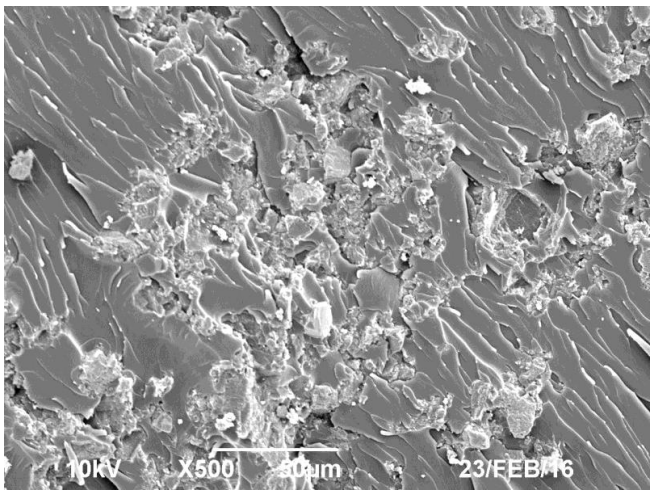

Figure 45: High Mag SEM Image of 20 vol% ESC Filled Composite

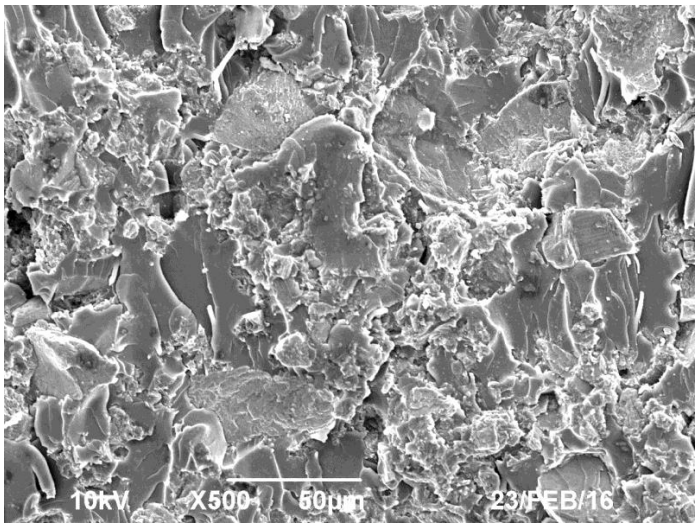

Figure 46: High Mag SEM Image of 27 vol% ESC Filled Composite

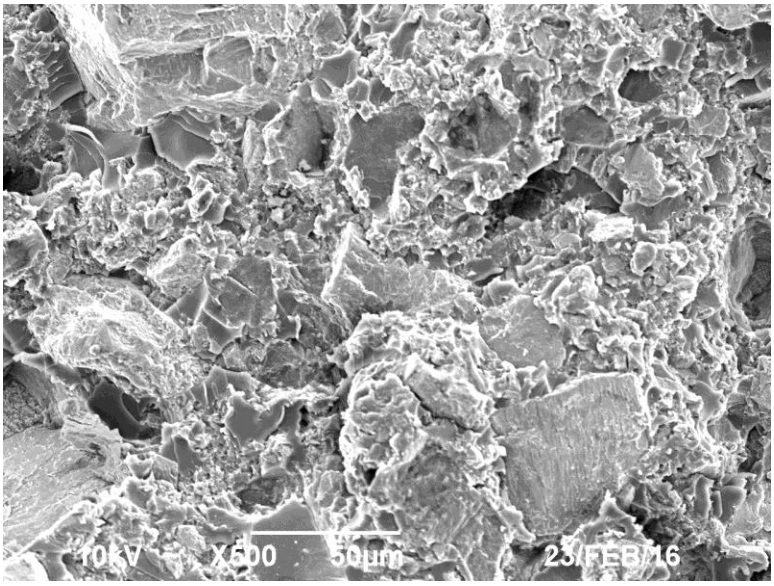

Figure 47: High Mag SEM Image of 36 vol% ESC Filled Composite

5.3.2. THREE POINT FLEXURAL TESTING

Using three point flexural testing, the breaking stress, breaking strain, and flexural modulus were measured for egg shell calcium filled composites. The samples of the same composition were then averaged, and plotted as functions of ESC content in Figures 48 through 50. In addition, the standard deviation of the measurements was calculated and plotted in the aforementioned graphs in the form of error bars. A full listing of averaged physical properties obtained through three point flexural testing is available in Table 4 in Appendix A.

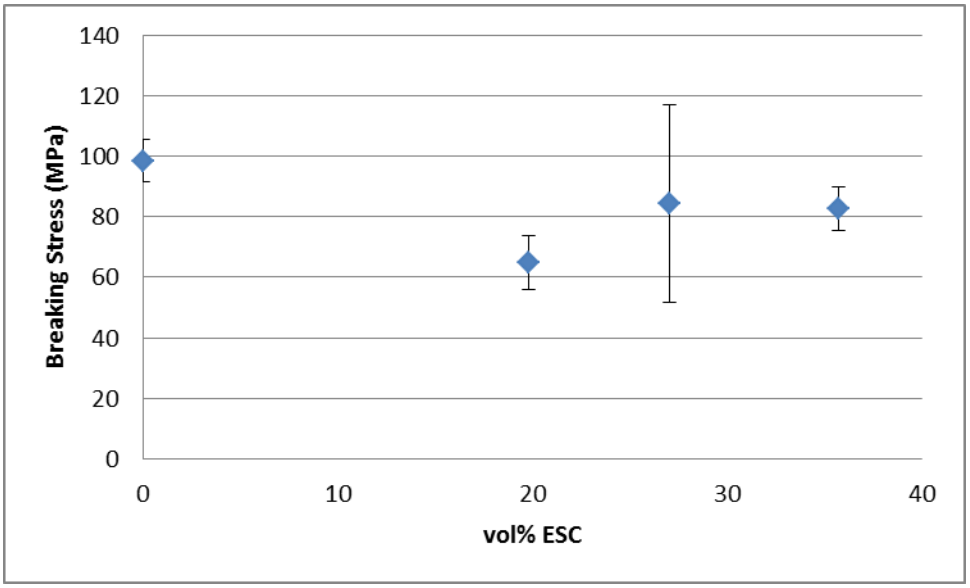

Figure 48: Average Flexural Breaking Stress of ESC Filled Composites

As shown in Figure 48, the flexural breaking strain decreases initially as the ESC content increases. After 20 vol% ESC, the breaking stress increases slightly, but does not hold to any overall trend. The chaotic nature of this result could be due to the connection between the filler and the copolymer. At lower ESC loadings, the lack of cohesion within the material could lead to the copolymer taking the majority of the stress. At higher loadings, the ESC could begin to bear more of the force, resulting in an increase in overall stress.

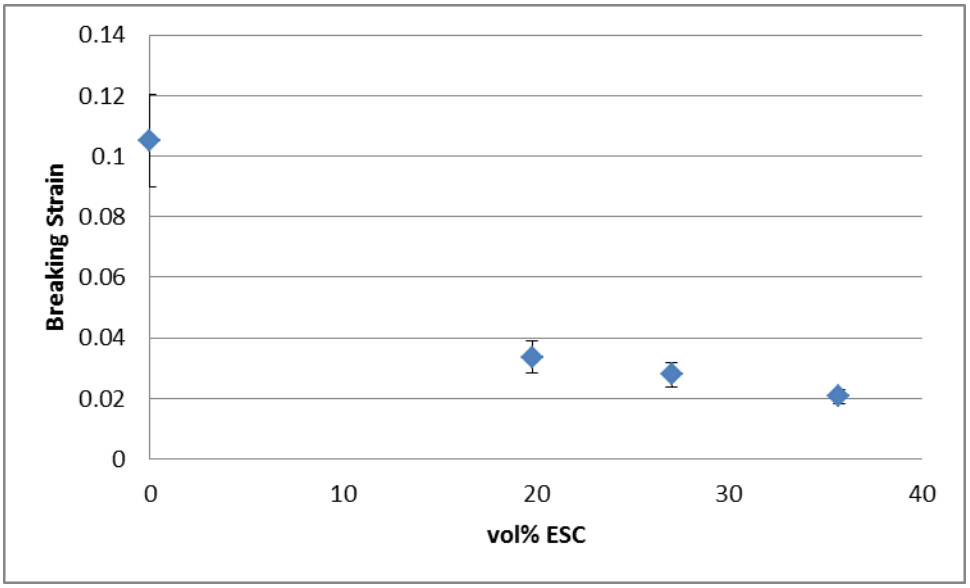

Figure 49: Average Flexural Breaking Strain of ESC Filled Composites

As seen in Figure 49, the flexural breaking strain decreases as the amount of ESC in the material increases. The pure copolymer can withstand the most

strain, while the addition of any filler immediately causes a decrease. This trend is likely caused by the inflexible nature of the pure filler; ESC is primarily calcium carbonate, which cannot withstand significant strain. The decrease could also be the result of a lack of bonding between the filler and the copolymer. Without bonding occurring, the ESC could be taking no strain at all, with only the reduced copolymer amount bearing the force.

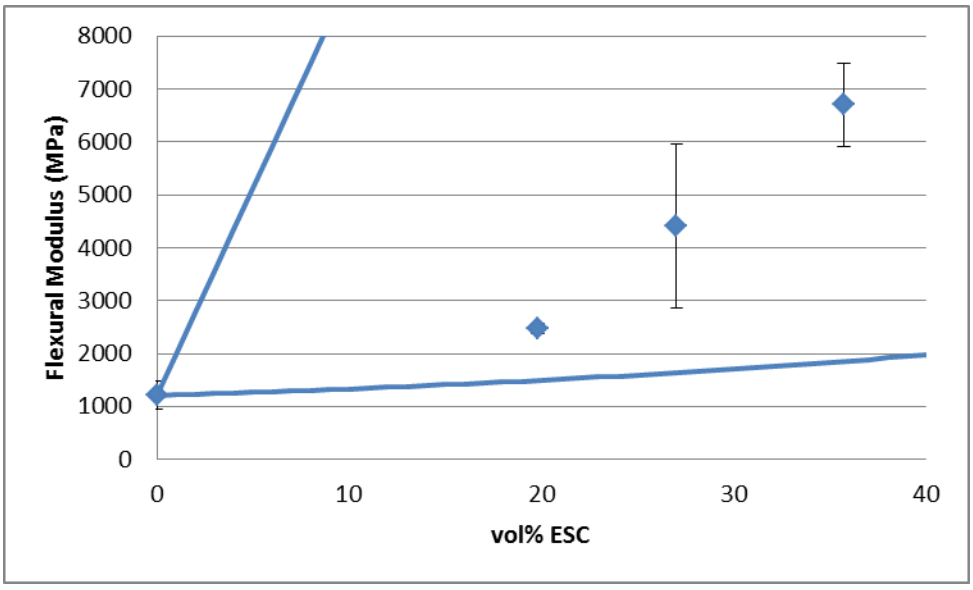

Figure 50: Average Flexural Modulus of ESC Filled Composites

As shown in Figure 50, the flexural modulus significantly increases with an increase in ESC content. The pure copolymer has the lowest measured modulus, with every ESC filled composite experiencing a more than doubled

modulus. This trend is likely caused by the ESC being much stiffer than the copolymer. The large increase, however, is unusual and will need to be substantiated by similar increases in other material properties. The measured moduli all lie between the two bounds provided by the simple and inverse rules of mixing, indicating the composite is behaving as expected. Previous studies involving calcium carbonate based fillers saw no significant trend in modulus as filler content increased in polypropylene. [52]

5.3.3. DYNAMIC MECHANICAL ANALYSIS

Using dynamic mechanical analysis, the room temperature storage modulus, storage modulus as temperature varies, glass transition temperature of egg shell calcium filled composites were measured. Values at 20 vol% ESC were unable to be attained, as the filler did not stay suspended in copolymer during polymerization in the smaller 8 mm tubes. The room temperature storage modulus and the glass transition temperatures were plotted against the ESC content in each sample and graphed in Figures 51 and 53, respectively. The storage modulus of different blend compositions were plotted against temperature and graphed in Figure 52. A full listing of data used is available in Tables 21 through 23 in Appendix D.

As seen in Figure 51, the room temperature storage modulus increases as the amount of ESC in the material increases. The increase in modulus is likely

caused by the ability of the ESC to withstand more force with less strain than the copolymer. The moduli measured by this method are significantly lower than those measured by the three point flexural testing. This could be the cause for some trepidation at the utilization of the previously reported data. The moduli are still significantly higher than that of the copolymer, but the exact values are not as comparable.

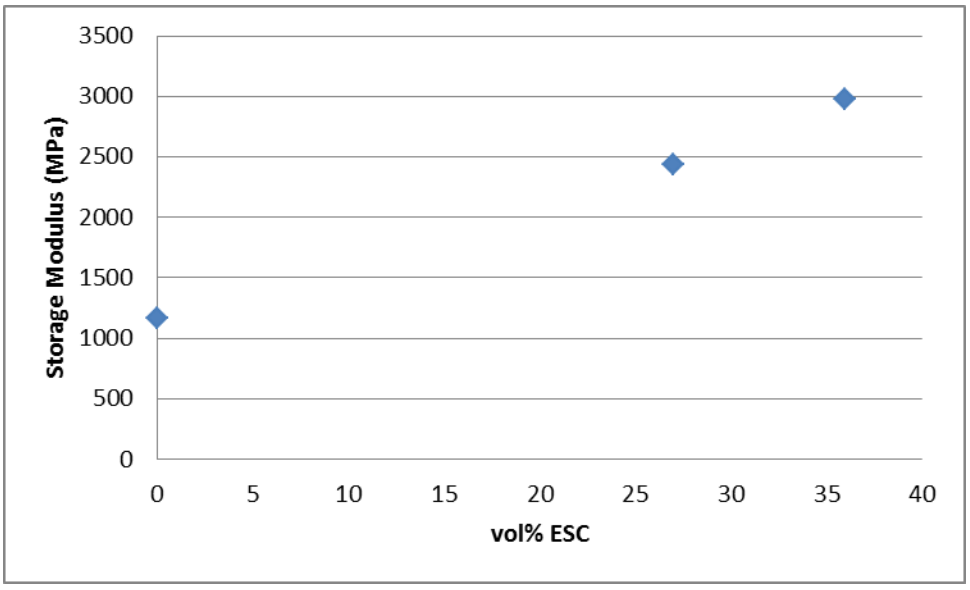

Figure 51: 30 °C Storage Modulus of ESC Filled Composites

As shown in Figure 52, storage modulus increases as ESC content increases at all temperatures. This result was expected, as the ESC was not a polymer and was therefore less susceptible to changes in material properties as

temperature changes. The ESC does not seem to increase the thermal stability of the composite greatly. The decrease is the storage modulus still occurs at roughly the same temperature, and the slope of the decline does not vary significantly with changes in ESC content. While the material properties are improved with higher ESC contents, they are no less prone to loss due to temperature shifts.

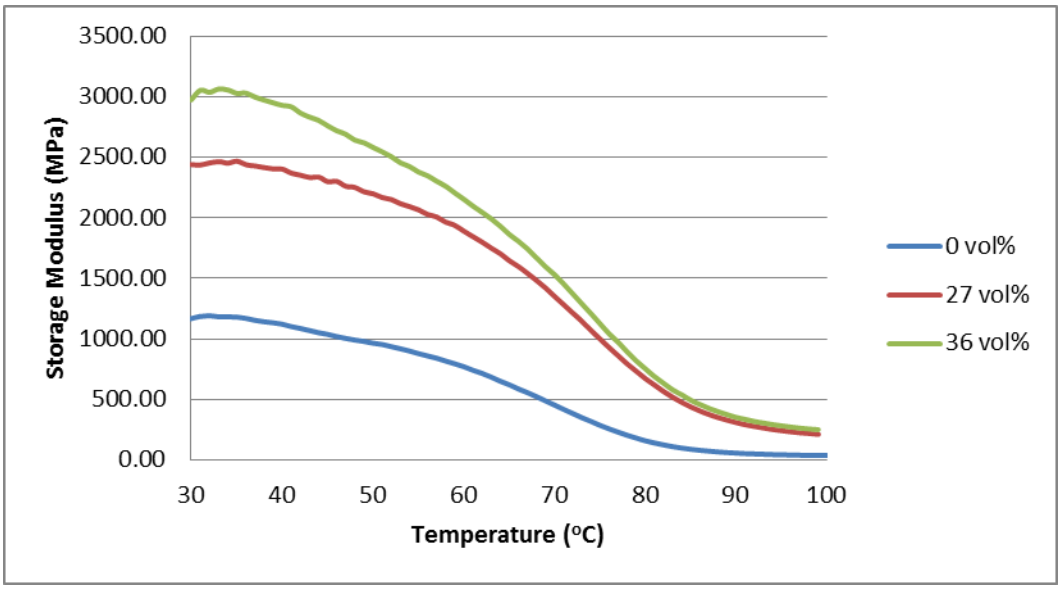

Figure 52: 30-100 °C Storage Modulus of ESC Filled Composites

As seen in Figure 53, the glass transition temperature does not change with the addition of ESC. This result is beneficial, as identical glass transition temperatures indicate that the copolymer in the composites has not changed with the addition of ESC as a filler. The material properties expected of the copolymer

should still be expected, as the chemical structure has likely remained the same. Conversely, the addition of ESC does nothing to increase the glass transition temperature. A higher Tg would produce greater thermal stability and improve the performance of the material.

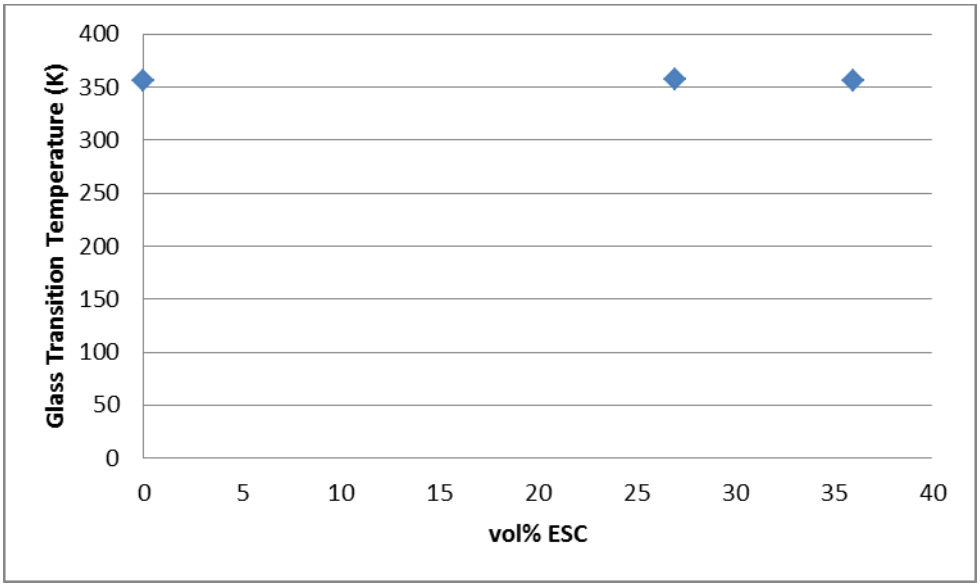

Figure 53: Glass Transition Temperature of ESC Filled Composites

5.3.4. IMPACT TESTING

Using impact testing, the breaking energy of egg shell calcium filled composites was measured. The samples of the same composition were then averaged, and plotted as functions of PNSF content in Figure 54. In addition, the standard deviation of the measurements was calculated and plotted in the aforementioned graphs in the form of error bars. A full listing of the

measurements obtained through impact testing is available in Table 8 in the Appendix B.

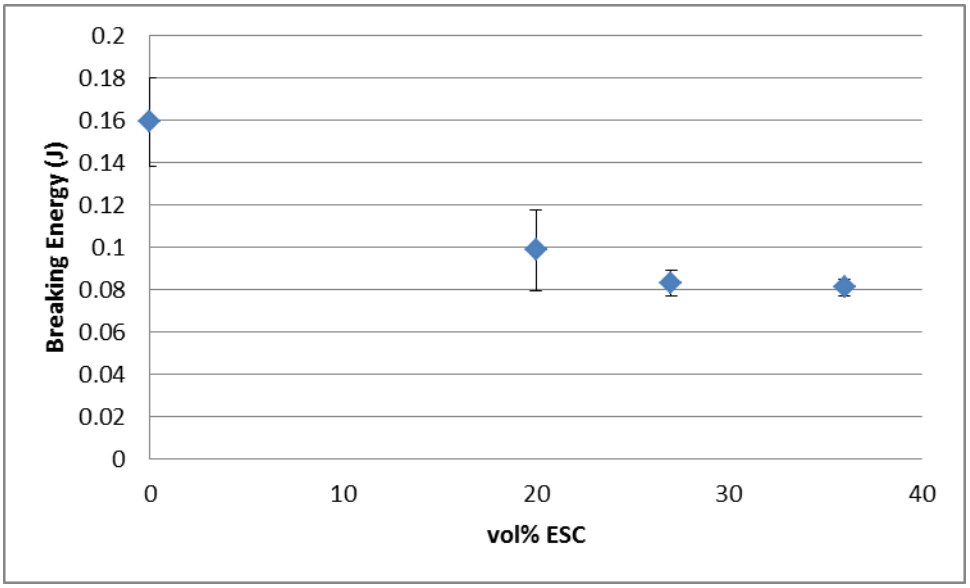

Figure 54: Average Breaking Energy of ESC Filled Composites

As seen in Figure 54, the breaking energy experiences an immediate drop as the ESC content initially increases. After roughly 20 vol% ESC, the breaking energy decreases more slowly before leveling off after 27 vol% ESC. The initial drop is likely caused by the lack of cohesion between the filler and the copolymer in the composite. Once ESC is added, the fracture in the material has less AESO to jump between, decreasing the energy needed to propagate through. The consistency once ESC is added could indicate that the energy needed to separate

the ESC from the copolymer remains fairly constant as ESC content increases. The breaking strain could be more directly related to the energy of separation and less caused by the energy to fracture copolymer in the composite.

5.3.5. DUROMETER MEASURMENTS

Using durometer measurements, the hardness of egg shell calcium filled composites were measured. The samples of the same composition were then averaged, and plotted as functions of AESO content in Figure 55. In addition, the standard deviation of the measurements was calculated and plotted in the aforementioned graphs in the form of error bars. A full listing of measurements obtained through durometer measurements is available in Table 12 in Appendix C.

As seen in Figure 55, the hardness of the composite increase as the ESC content increases. The rise begins gradually, with the greatest rate of increase between 27 and 36 vol% PNSF. The values above 100 are not precise measurements; the hardness scale used only makes measurements up to 100, so higher values were visually estimated. The increase in the measured hardness was expected; the filler used in the composite was harder on its own than the pure copolymer. The greater hardness could be promising, as it indicates that this material property could be easily controlled through the addition of this filler. Conversely, the values of this hardness are all higher than that of the pure styrene

polymer, indicating that a change in this material property will need to be accounted for if using these blends.

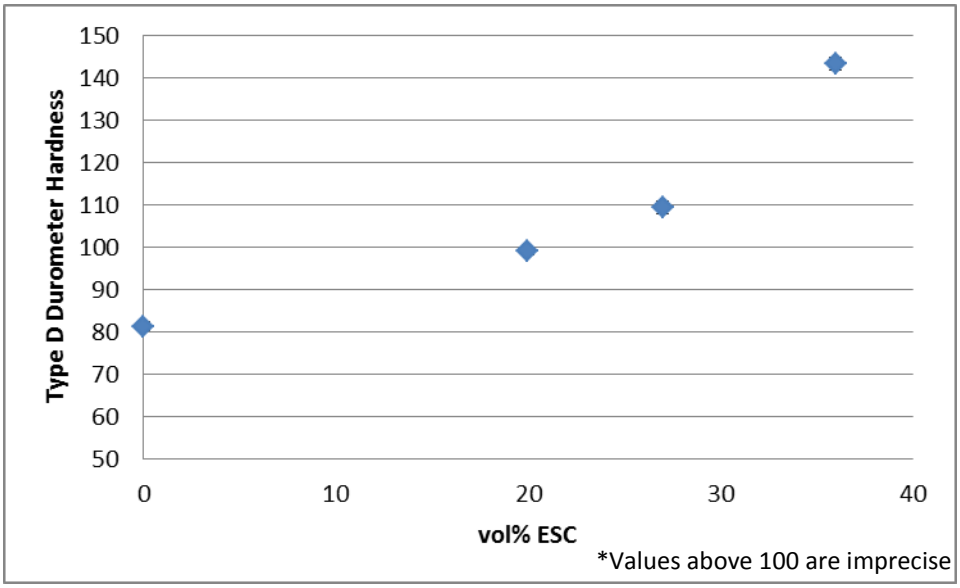

Figure 55: Average Durometer Hardness of ESC Filled Composites

6. COMPOSITES WITH NANOFILLER

6.1 BENEFITS OF NANOFILLERS

Nanofillers offer many potential benefits when used in polymeric composites. Nanofillers consist of incredibly small particles, only visible to microscopy on the nanoscale. They are normally made of specially engineered material, which adds a level of complexity to their production. Additionally, only small amounts of material can be added to a monomer mixture and still produce a material able to undergo polymerization. While fillers are generally added in small amounts to improve the properties of the material, it would be ideal if larger amounts could be added, so long as the filler is itself biorenewable. The small size also allows for modification of the filler to be easily performed, allowing for increase cohesion between the filler and the polymer matrix.

6.2 ORGANICALLY MODIFIED CLAY FILLER

6.2.1. SCANNING ELECTRON MICROSCOPY

Scanning electron microscopy was used to achieve images of the surface organically modified clay filled composites. Selected low magnification images, shown in Figures 56-58, demonstrate the dispersion of OMC in the composite. Selected high magnification images, seen below in Figures 59-61, depict the particle size of the filler in the material. A full listing if SEM images take of these blends is available in to Figures 111-129 in Appendix E.

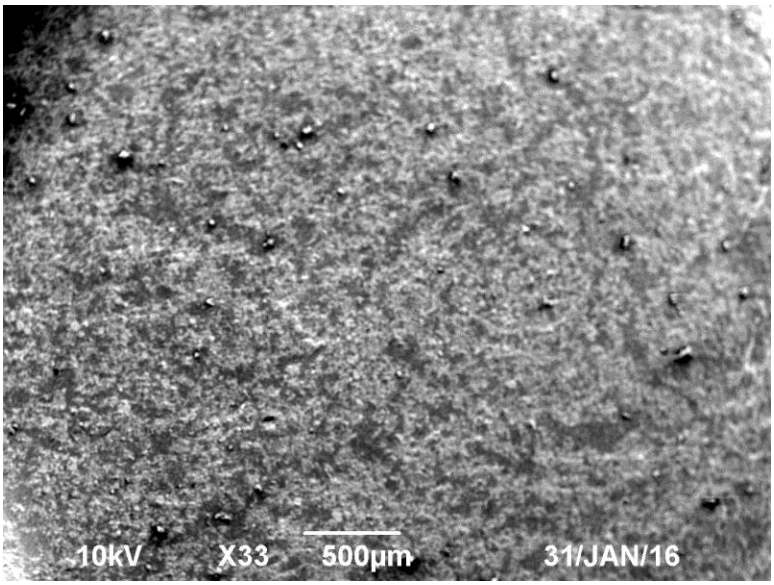

Figure 56: Low Mag SEM Image of 1 vol% OMC Filled Composite

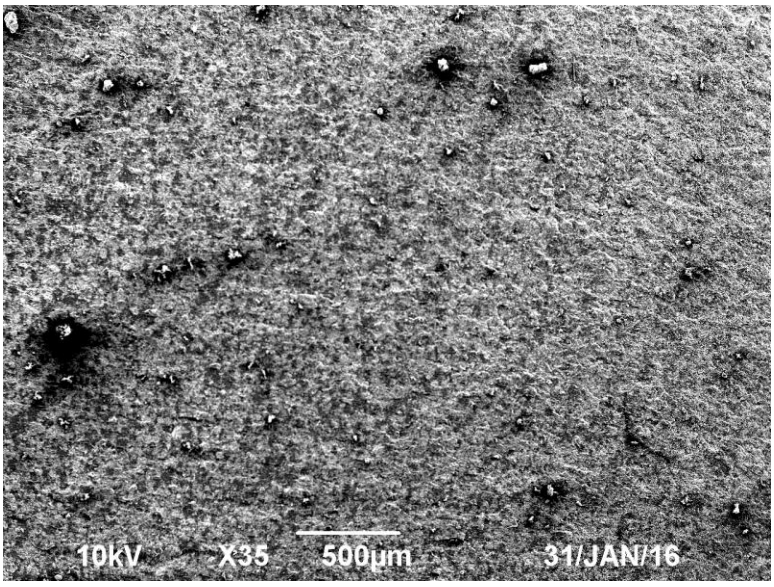

Figure 57: Low Mag SEM Image of 2 vol% OMC Filled Composite

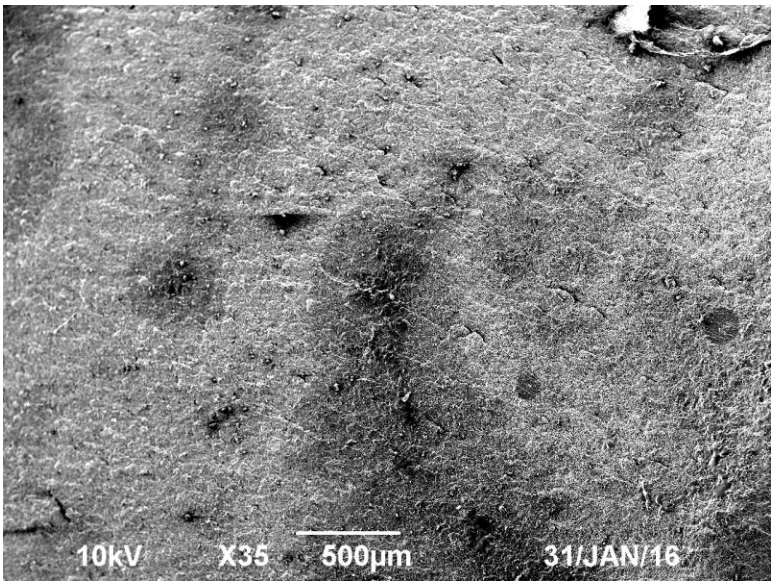

Figure 58: Low Mag SEM Image of 4 vol% OMC Filled Composite

As shown in Figure 56, the dispersion of 1 vol% OMC in the composite is very high. The filler is spread uniformly throughout the sample, with high filler density throughout the composite. The filler does not seem to be very clustered, with the OMC mixed evenly throughout. The regions of low OMC density tend to be quite small, with the largest measuring no more than 100 µm wide. This creates high dispersion throughout the sample. In Figure 57, the dispersion of 2 vol% OMC in the material is nearly maximized. The OMC is spread very uniformly throughout the composite, with every section looking visually similar to nearly any other. No regions of noticeably low PNSF density can be seen, indicating that the filler is dispersed throughout. In Figure 58, the dispersion of 4

vol% OMC in the composite is as high as is possible. The surface is almost entirely uniform, with a few areas containing only a small decrease in OMC density. No noticeable agglomerations have formed, indicating that all of the OMC is till contained within the composite. This indicates a high efficiency of material usage, but also indicates that the maximum amount of OMC added is severely limited.

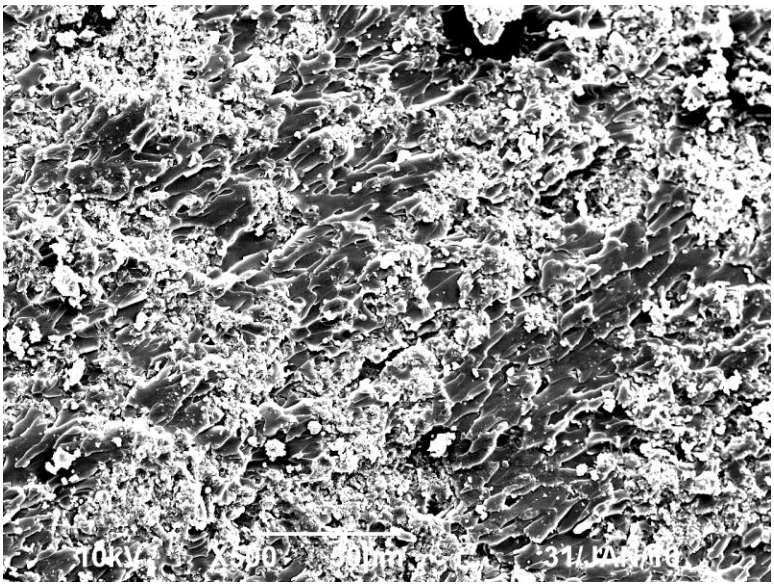

Figure 59: High Mag SEM Image of 1 vol% OMC Filled Composite

As seen in Figure 59, the particle size of the OMC in the 1 vol% OMC filled composite is incredibly small. What particles are visible are very minute and infrequent, measuring at less than 10 μm across. The majority of the filler is smaller than can be measured, which is expected from the use of a nanofiller. In

Figure 60, the visible particle size remains relatively constant in the 2 vol% OMC filled material. Individual particles are again measured at 10 μm or less in diameter, with the majority of the particles remaining smaller than measurable. No agglomerations of particles have formed, with the majority of the filler still in particulate form. In Figure 61, the particle size of the filler in the 4 vol% OMC filled composites is unmeasurable. The entire surface is uniform, appearing as an unvarying mixture of OMC and copolymer. The surface is completely packed with OMC, indicating that no higher amounts of OMC could be added to this copolymer effectively.

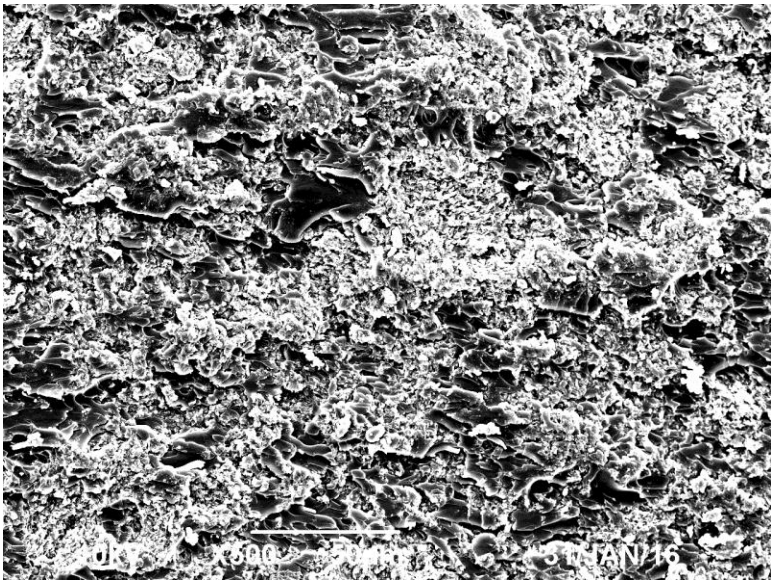

Figure 60: High Mag SEM Image of 2 vol% OMC Filled Composite

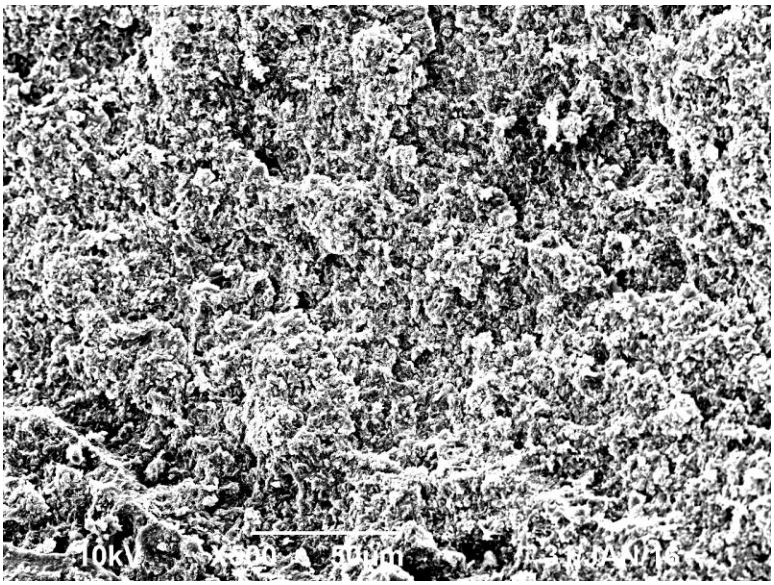

Figure 61: High Mag SEM Image of 4 vol% OMC Filled Composite

6.2.2. THREE POINT FLEXURAL TESTING

Using three point flexural testing, the breaking stress, breaking strain, and flexural modulus were measured for organically modified clay filled composites. The samples of the same composition were then averaged, and plotted as functions of OMC content in Figures 62 through 64. In addition, the standard deviation of the measurements was calculated and plotted in the aforementioned graphs in the form of error bars. A full listing of averaged physical properties obtained through three point flexural testing is available in Table 5 in Appendix A.

As shown above in Figure 62, the average flexural breaking stress decreases steadily as the OMC content increases. The drop is fairly linear, with

the breaking stress peaking at 0 vol% OMC and reaching the nadir at 4 vol% OMC. This trend is likely caused by the breaking strain of pure OMC being substantially lower than that of the pure copolymer. As more OMC is added to the composite, the material can withstand less force and fractures. Magnitude of the decrease in the breaking stress is somewhat unexpected, as a drop in breaking stress of over 20% is experienced with only 4 vol% OMC. Previous studies had indicated a moderate increase as nanoclay filler content increased, raising 10 MPa as the filler content increased to 5 wt% in a conjugated soybean oil/styrene copolymer. [58]

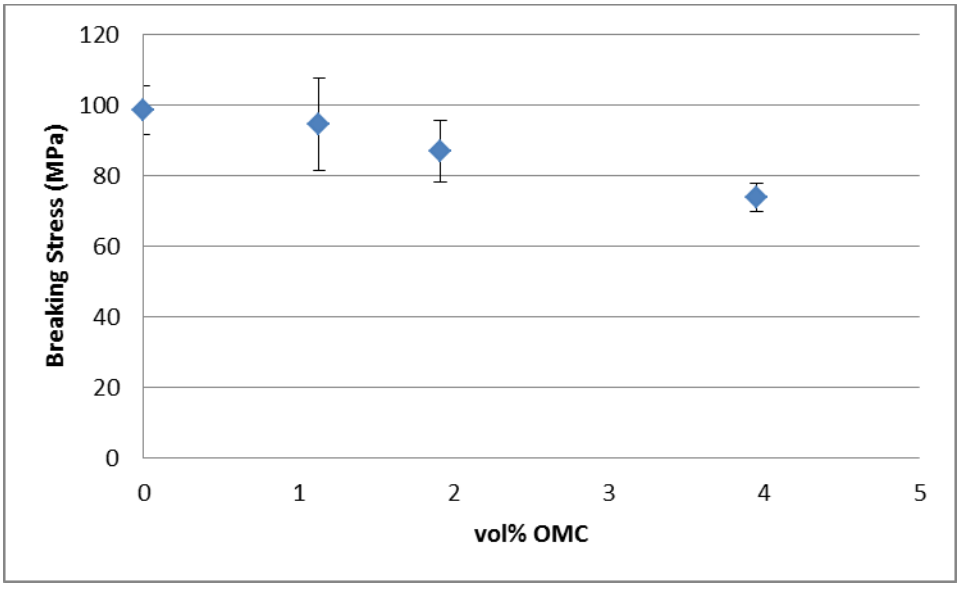

Figure 62: Average Flexural Breaking Stress of OMC Filled Composites

As seen above in Figure 63, the average flexural breaking strain decreases as the amount of OMC in the composites increases. The decrease is fairly linear, with consistent decreases as high OMC contents are used. This trend can again be explained by the breaking strain of pure OMC being significantly lower than that of the copolymer. The significant decrease, seen in the breaking stress, is also seen in the breaking strain, with a drop of almost 40% occurring with only 4 vol% OMC. The flexural strain has previously been identified to increase due to increased loading of nanoclay filler in the composite. A loading of 5 wt% filler was found to increase the flexural strain from by 0.10 in a conjugated soybean oil/styrene copolymer. [58]

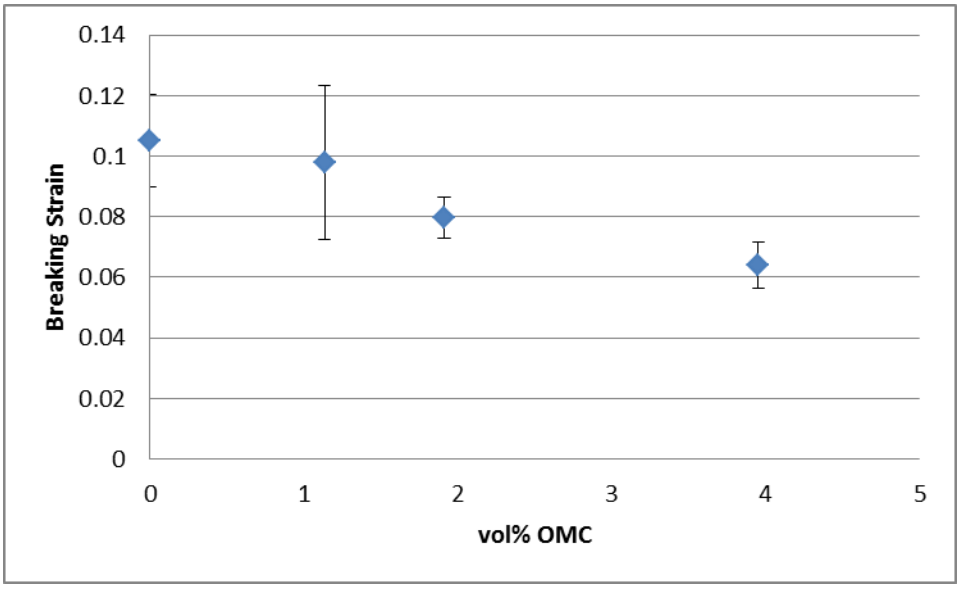

Figure 63: Average Flexural Breaking Strain of OMC Filled Composites

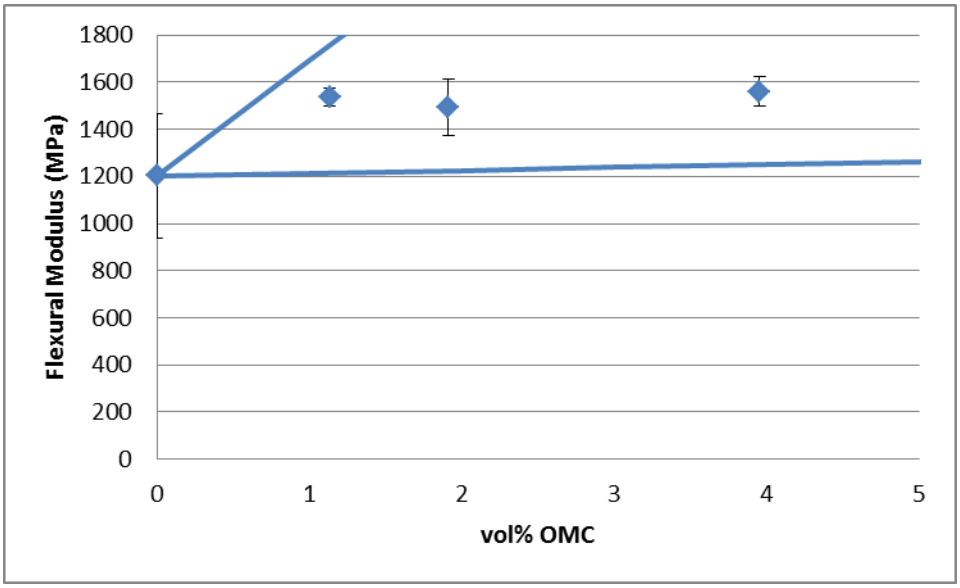

Figure 64: Average Flexural Modulus of OMC Filled Composites

As shown in Figure 64, the flexural modulus initially increases as the OMC content increases. The modulus then levels out above 1 vol% OMC, with no significant change at any higher loadings. Regardless of the amount of OMC added to the copolymer, the modulus does not seem to increase above 1600 MPa. This result is not particularly useful, as it signifies that using less copolymer does not produce significantly improved properties. On the other hand, only a small amount of filler is needed to produce any change in the modulus, which could be useful as a small additive. The measured moduli all lie between the two bounds provided by the simple and inverse rules of mixing, indicating the composite is behaving as expected. An increase in the modulus of the composite due to the

increased nanofiller content has been seen in previous research. The exact magnitude of the increase has varied, with some studies showing only a slight increase of 40% MPa at 5 wt% filler in conjugate soybean oil/styrene copolymers [58] and others showing a significant 300% increase at 3 wt% filler in AESO/styrene copolymers [59].

6.2.3. DYNAMIC MECHANICAL ANALYSIS

Using dynamic mechanical analysis, the room temperature storage modulus, storage modulus as temperature varies, glass transition temperature of organically modified clay filled composites were measured. The room temperature storage modulus and the glass transition temperatures were plotted against the OMC content in each sample and graphed in Figures 65 and 67, respectively. The storage modulus of different blend compositions were plotted against temperature and graphed in Figure 66. A full listing of data used is available in Tables 24 through 26 in Appendix D.

As seen in Figure 65, the room temperature storage modulus increases initially as the amount of OMC in the material increases. After the initial increase, the modulus remains fairly constant, with no change as the amount of OMC in the filler increases. This corresponds with the result from the three point flexural testing, where a similar trend was seen in Figure 64. The increase in the modulus

is not as severe as that seen in the previous testing, but the overall pattern continues.

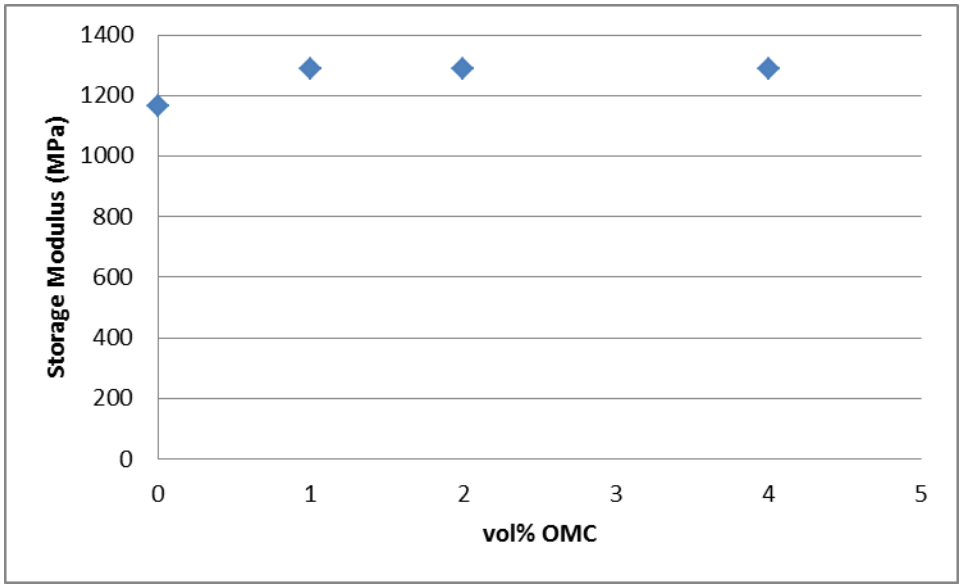

Figure 65: 30 °C Storage Modulus of OMC Filled Composites

As shown in Figure 66, storage modulus increases as OMC content is added at all temperatures. This result was expected, as the OMC was not a polymer and was therefore less susceptible to changes in material properties as temperature changes. Increased amounts of OMC, however, do not seem to increase the modulus at any given temperature. This was somewhat expected, as the modulus remained the same at room temperature. The OMC does not seem to increase the thermal stability of the composite greatly. The decrease is the storage

modulus still occurs at roughly the same temperature, and the slope of the decline does not vary significantly with changes in OMC content. While the material properties are improved with added OMC, they are no less prone to loss due to temperature shifts.

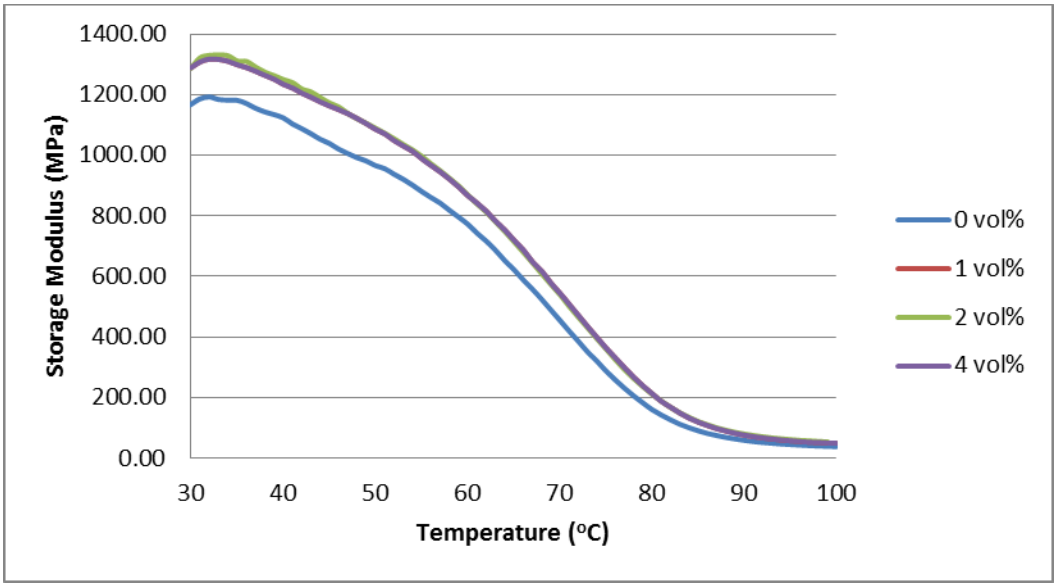

Figure 66: 30-100 °C Storage Modulus of OMC Filled Composites

As seen in Figure 67, the glass transition temperature does not change with the addition of OMC. This result is beneficial, as identical glass transition temperatures indicate that the copolymer in the composites has not changed with the addition of OMC as a filler. The material properties expected of the copolymer should still be expected, as the chemical structure has likely remained

the same. Conversely, the addition of OMC does nothing to increase the glass transition temperature. A higher T_g would produce greater thermal stability and improve the performance of the material. Previous studies have shown a slight variation in glass transition temperature with the addition of nanofillers, either trending upward with a 20 K increase at 3 wt% filler in an ESO/styrene copolymer [59] or slightly downward with a 5 K decrease at 5 wt% filler in a conjugated soybean oil/styrene copolymer [58].

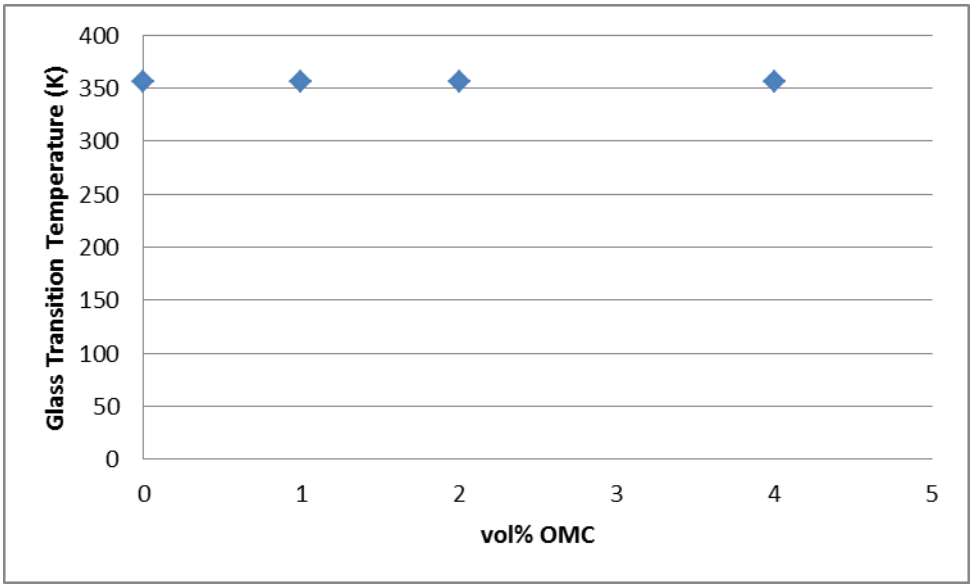

Figure 67: Glass Transition Temperature of OMC Filled Composites

6.2.4. IMPACT TESTING

Using impact testing, the breaking energy of organically modified clay filled composites was measured. The samples of the same composition were then averaged, and plotted as functions of OMC content in Figure 68. In addition, the standard deviation of the measurements was calculated and plotted in the aforementioned graphs in the form of error bars. A full listing of the measurements obtained through impact testing is available in Table 9 in the Appendix B.

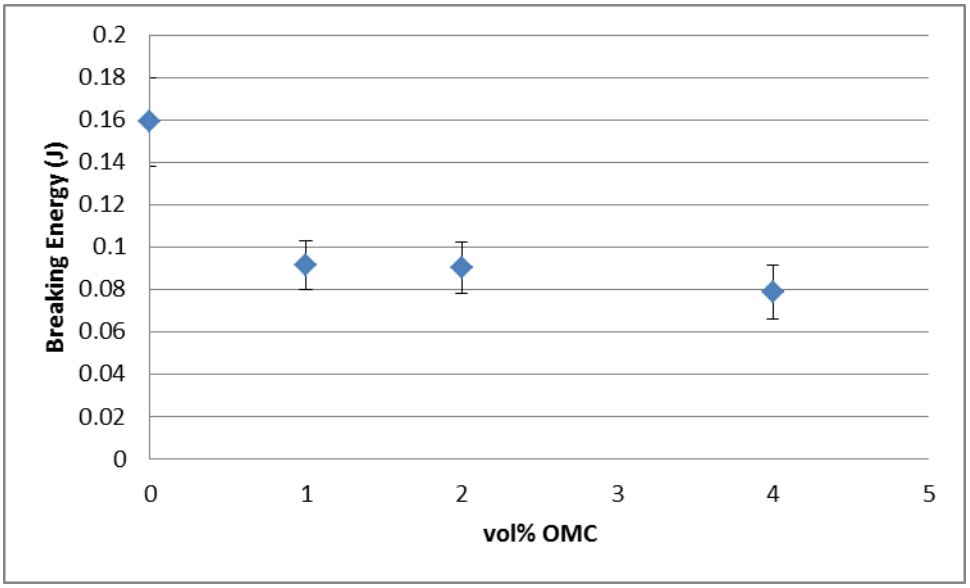

Figure 68: Average Breaking Energy of OMC Filled Composites

As seen in Figure 68, the breaking energy experiences an immediate drop as the OMC content initially increases. After roughly 1 vol% OMC, however, the breaking energy levels off and remain fairly constant. This result is surprising, as a significant drop off occurs with very little filler added. The decrease does not seem to be related to the amount of OMC added, as the same breaking energy is needed regardless of how much OMC is contained within the composite, so long as it contains some. This result is useful, as it shows that higher loadings of OMC do not produce any further decrease in breaking energy.

6.2.5. DUROMETER MEASURMENTS

Using durometer measurements, the hardness of organically modified clay filled composites were measured. The samples of the same composition were then averaged, and plotted as functions of ESC content in Figure 69. In addition, the standard deviation of the measurements was calculated and plotted in the aforementioned graphs in the form of error bars. A full listing of measurements obtained through durometer measurements is available in Table 13 in Appendix C.

As seen in Figure 69, the hardness of the composite increases as the OMC content increases. The rise is fairly linear between 0 and 2 vol% OMC, but remains fairly constant from 2 vol% OMC to 4 vol% OMC. Unlike previous fillers examined in this study, the added OMC does not take the hardness of the

material significantly past that of the pure styrene polymer. This is potentially beneficial, as it indicates that OMC can be added as a filler without exceeding the hardness expected of polystyrene. It also indicates that OMC cannot be used to increase the hardness of the polymer beyond what was already expected.

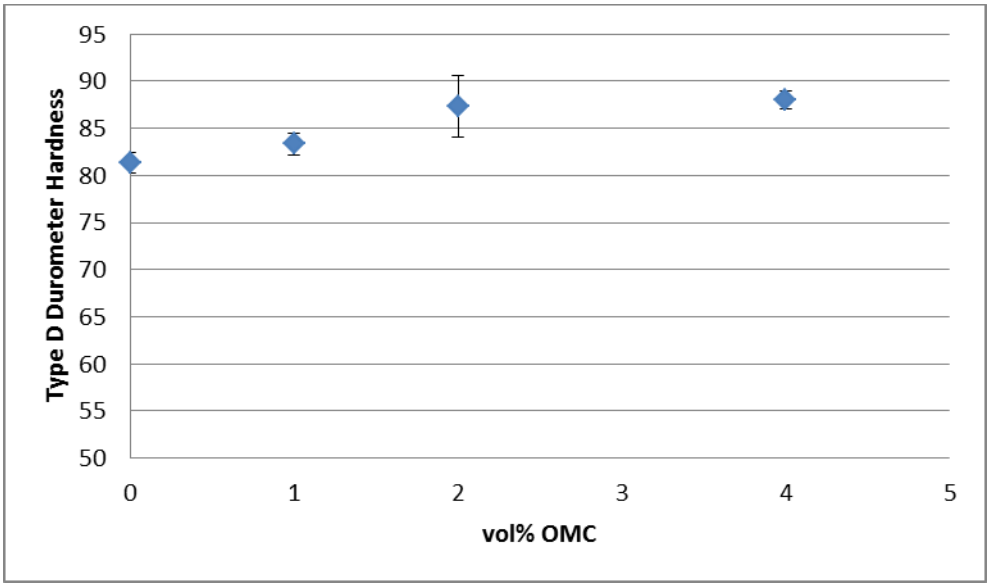

Figure 69: Average Durometer Hardness of OMC Filled Composites

7. CONCLUSIONS

AESO and styrene were successfully polymerized throughout the entire composition range, with the samples ranging from hard and rigid with more styrene to soft and rubbery with more AESO. As the amount of acrylated epoxidized soybean oil in the copolymer increased, the mechanical and physical properties of the material changed. The strength and stiffness both decreased, while the flexibility increased. The brittleness decreased initially, before becoming relatively constant. The hardness decreased, but more slowly than was expected. The thermal stability of the material decreased significantly. The glass transition temperature decreased, but not as severely as was predicted. The crosslinking within the copolymer increased significantly, but only initially.

These properties show that the additional of AESO, in general creates an inferior copolymer to polystyrene. While some of the properties did not diminish as badly as was expected, there was still a decrease in properties that would need to be addressed before use of this polymer. The increased breaking energy and the decreased $\bar{M}_C$ do point toward a slight improvement; they do not make up for the overall worsening of the polymer. The composition of the copolymer can be used to tune these properties toward a specific application, depending on the exact material properties needed. The copolymers provide a suitable starting material for the production of filled plastics.

In general, the addition of any filler in the copolymer had a similar effect to the flexural properties. All fillers caused a decrease in the flexural breaking stress and strain of the composite. They did all, however, manage to increase the flexural modulus to levels at or above polystyrene. The bulk fillers, pecan nut shell flour and egg shell calcium, both increased the flexural modulus above that of polystyrene, with higher loadings of ESC greatly exceeding those of the polymer. The nanofiller, organically modified clay, did increase the modulus to that of polystyrene, but the addition of more filler did not improve the modulus further. The bulk fillers were better at creating composites that improved upon polystyrene, while the nanofiller could create a composite that acted similarly to polystyrene.

The addition of fillers to the composite decreased the breaking energy of the material for every filler tested. Each filler caused a nearly identical pattern, with a sudden jump occurring when the filler was first added, but with little to no change when high amounts of filler were used. All of the fillers, however, did not lower the breaking energy significantly below that of polystyrene. In general, these fillers can be added without producing breaking energies worse than that of polystyrene.

As more filler was added to the composite, the hardness of the material increased. The addition of OMC improved the hardness to that of polystyrene, while the addition of PNSF increased the hardness to levels above that of

polystyrene. The ESC produced the hardest composites, with the hardness measurements technically exceeding the hardness scale used. All of these fillers can be added to improve the hardness of the copolymer to match that of polystyrene. The bulk fillers can be used to produce harder materials, but higher loadings of these will also produce materials that may be harder than is needed for a particular usage.

The room temperature storage moduli of these composites roughly confirmed the three point flexural testing, with the flexural moduli of the ESC filled composites slightly exceeding them. The addition of the fillers did nothing to improve the thermal stability of the composites, leaving them all still susceptible to temperature changes. The glass transition temperatures of the composites remained the same, indicating that the polymer was neither changed by the filler nor improved by it.

All three of the fillers achieve good dispersion and small particle size in their composites. The PNSF filled composites had better dispersion as the filler content increased, which also improved the particle size of the material. The ESC filled composites initially had better dispersion and smaller particle size as the filler content increased, but the high filler content led to agglomeration into large masses, indicating a poor use of materials. The OMC filled composites had the greatest dispersion and smallest particle size, which was expected due to the nature of nanofillers; the highest loading of OMC tested produce a perfectly

uniform sample, with particle sized blurring into one composite. The dispersion of the bulk fillers could be improved, but does not seem to be severely hindering.

Out of all of the composites tested, 36 vol% ESC compared the most favorably to polystyrene, summarized below in Table 1. The breaking stress and strain decreased slightly, but not greatly. The composite was also slightly more brittle than polystyrene. However, as many of these properties are already low for polystyrene compared to other polymers, the decrease is not appreciable important. The stiffness of the material greatly exceeded that of the polymer, by a factor of two to three depending on the precise measurement. The hardness was also greatly increase, achieving almost double that of polystyrene. Overall the composite was able to achieve potentially practical set of properties and could be implemented as a commercially viable material.

Property	Material		Advantage
	Polystyrene	ESC Filled Composite	
Flexural Modulus	1900 MPa	6700 MPa	ESC Filled Composite
Breaking Stress	93 MPa	83 Mpa	Polystyrene
Breaking Strain	0.05	0.02	Polystyrene
30° Storage Modulus	1700 MPa	3000 MPa	ESC Filled Composite
Breaking Energy	0.11 J	0.08 J	Polystyrene
Hardness	82	143	ESC Filled Composite

Table 1: Comparison of Polystyrene and 36 vol% ESC Filled Composite

8. RECOMMENDATIONS

Based on these findings, bulk fillers appear to be better suited for use in biorenewable composites. Initially, more filler can be used, which correlates to less styrene usage and less usage of nonrenewable resources. Several material properties, such as modulus and hardness, can be improved to make the composite perform better than polystyrene. While the thermal properties and breaking energy cannot be improved, they are also made no worse by the addition of the bulk fillers. The nanofiller did have better dispersion and smaller particle sizes, but not significantly enough to warrant its usage. Specifically, egg shell calcium is recommended to be used as a filler, as higher loadings of it can be added and it improves the properties more than any other filler tested.

Much further research can be performed based on this study. The exact benefit of the other components to the copolymer besides the comonomers should be determined. Exactly how much the divinylbenzene actually improves the crosslinking and how much is required to be used should be investigated. Alternative polymerization methods, such as UV polymerization, should be investigated to determine if the results are similar. In terms of composites, alternative blends of AESO in the copolymer, such as 75 or 90 vol%, should be researched. This will demonstrate how effective these fillers are at improving the properties of the composites and how little nonrenewable resources can be used to make them. The use of bonding agents in the composites could greatly improve

the properties of the materials. One of the largest problems with the fillers is their lack of cohesion with the polymer, which diminishes their physical properties. The addition of bonding agents could further improve the properties and help make even better biorenewable materials.

9. BIBLIOGRAPHY

1. Lligadas I Puig, G. “Biobased Thermosets from Vegetable Oils: Synthesis, Characterization, and Properties” *Universitas Rovira I Virgili* (2006)
2. Greene, D.; Hopson, J.; Li, J. “Running Out of and Into Oil: Analyzing Global Oil Depletion and Transition Through 2050” *Journal of the Transportation Research Board* (2003)
3. Khot, S. N.; Lascara, J.J.; Can, E.; Moyre, S.S.; Williams, G.I.; Palmese, G.R. Kusefoglu, S.H.; Wool, R.P. “Development and application of triglyceride-based polymers and composites” *Journal of Applied Polymer Science* (2001)
4. Eissen, M.; Metzger, J.O.; Schmidt, E.; Schneidewind, U. “10 Years After Rio – Concepts on the Contribution of Chemistry to a Sustainable Development” *Angewandte Chemie-International Edition* (2010)
5. Meier, M.A.R.; Metzger, J.O.; Schubert, U.S. “Plant Oil Renewable Resources as Green Alternatives in Polymer Science” *Chemical Society Reviews* (2007)
6. Gandini , A. “ Polymers from Renewable Resources: A Challenge for the Future of Macromolecular Materials” *Macromolecules* (2008)
7. Lu, Y.; Larock, R.C “Novel Polymeric Materials from Vegetable Oils and Vinyl Monomers: Preparation, Properties, and Applications” *ChemSusChem* (2009)

8. Raquez J.M.; Deleglise, M.; Lacrampe, M.F.; Krawczak, K. "Thermosetting (Bio)Materials Derived from Renewable Resources: A Critical Review" *Progress in Polymer Science* (2010)
9. Vieira, M.G.A.; da Silva, M.A.; dos Snatos, L.O.; Beppu, M.M. "Natural-Based Plasticizers and Biopolymer Films: A Review" *European Polymer Journal* (2011)
10. Shogren, R.L.; Petrovic, Z; Liu, Z.; Erhan, S.Z "Biodegradation Behaviour of Some Vegetable Oil-Based Polymers" *Journal of Polymers and the Environmental Impact* (2004)
11. Petrovic, Z.S. "Polyurethanes from Vegetable Oils" *Polymer Reviews* (2008)
12. Nayak, P.L. "Natural Oil-Based Polymers: Opportunities and Challenges" *Journal of Macromolecular Science Polymer Reviews* (2000)
13. Güner, F.S.; Yagci, Y.; Erciyes, A.T. "Polymers from Triglyceride Oils" *Progress in Polymer Science* (2006)
14. Lligadas, G.; Ronda, J.C.; Galia, M.; Cadiz, V. "Plant Oils as Platform Chemicals for Polyurethane Synthesis: Current State-of-the-Art" *Biomacromolecules* (2011)
15. Wool R.P, Sun, X.S. "Bio-Based Polymers and Composites" *Elsevier Academic Press: San Diego, California/London, UK* (2005)

16. Pelletier, H.; Gandini, A. “Preparation of Acrylated and Urethanted Triglycerols” *European Journal of Lipid Science and Technology* (2006)
17. Sharma, V.; Kundu, R.P. “Condensation Polymers from Natural Oils” *Progress in Polymer Science* (2008)
18. Sacristán, M.; Ronda, J.C.; Galia, M.; Cadiz, V. “Silicon-Containing Soybean-Oil-Based Copolymers: Synthesis and Properties” *Biomacromolecules* (2009)
19. Sacristán, M.; Ronda, J.C.; Galia, M.; Cadiz, V. “Sytheis and Properties of Boron-Containing Soybean Oil Based Thermosetting Copolymers” *Biomacromolecules* (2010)
20. De Espinosa, l.M.; Meier, M.A.R.; “Plant Oils: The Perfect Renewable Resource for Polymer Science?!” *European Polymer Journal* (2011)
21. Campanella, A.; Bonnaillie, L.M.; Wool, R.P. “Polyurethane Forams from Soyoil-Based Polyols” *Journal of Applied Polymer Science* (2009)
22. Bonnaillie, L.M.; Wool, R.P. “Thermosetting Foam with a High Bio-Based Content from Acrylated Epoxidized Soybean Oil and Carbon Dioxide” *Journal of Applied Polymer Science* (2007)
23. Can, E.; Wool, R.P.; Kusefoglu, S. “Soybean and Castor Oil Based Monomers: Synthesis and Copolymerization with Styrene” *Journal of Applied Polymer Science* (2006)

24. Li, F.; Hasjim, J.; Larock, R.C. “Synthesis, Structure, and Thermophysical and Mechanical Properties of New Polymers Prepared by the Cation Copolymerization of Corn Oil, Styrene, and Divinylbenzene” *Journal of Applied Polymer Science* (2003)
25. Boyd S. E.; La Scala J. J.; Palmese G. R. “Molecular Relaxation Behavior of Fatty Acid-Based Vinyl Ester Resin” *Journal of Applied Polymer Science* (2008)
26. Raghavachar R.; Letasi R. J.; Kola P. V.; Chen Z.; Massingill J. L.; “Rubber-Toughening Epoxy Thermosets With Epoxidized Crambe Oil” *Journal of the American Oil Chemists’ Society* (1999)
27. Lu, J.; Wool, R.P. “Additive Toughening Effects on New Bio-Based Thermosetting Resins from Plant Oils” *Composites Science and Technology* (2008)
28. Grishchuk, S.; Karger-Kocsis, J. “Hybrid Thermosets from Vinyl Ester Resin and Acrylated Epoxidized Soybean Oil (AESO)” *eXPRESS Polymer Letters* (2011)
29. Eren, T.; Kusefoglu, S.H. “Synthesis and Polymerization of the Bromoacrylated Plant Oil Triglycerides to Rigid, Flame-Retardant Polymers” *Journal of Applied Polymer Science* (2003)

30. Hong, C.K; Wool, R.P. “Development of a Bio-Based Composite Material from Soybean Oil and Keratin Fibers” *Journal of Applied Polymer Science* (2005)
31. Khot, S. N.; Lascara, J.J.; Can, E.; Moyre, S.S.; Williams, G.I.; Palmese, G.R. Kusefoglu, S.H.; Wool, R.P. “Development and application of triglyceride-based polymers and composites” *Journal of Applied Polymer Science* (2001)
32. Yang, L.; Dai, H.; Yi, A.; Lin, B.; Li, G. “Structure and Properties of Partially Epoxidized Soybean Oil” *Journal of Thermal Analysis and Calculations* (2008)
33. Cai, C.; Dai, H.; Chen, R.; Su, C. “Studies on the Kinets of In Situ Epoxidation of Vegetable Oils” *European Journal of Lipid Science and Technology* (2008)
34. La Scall, J.J, Wool, R.P. “The Effect of Fatty Acid Composition on the Acrylation Kinetics of Epoxidized Triacylglycerol” *Journal of American Oil Chemistry* (2008)
35. Thames, S.F.; Smith, O.W.; Evans, J.M.; Dutta, S.; Chen, L. “Functionalized Vegetable Oil Derivatives, Latex Compositions and Coatings” *US Patent 7361710* (2008)

36. Behera, D.; Banthai, A.K. “Synthesis, Characterization, and Kinetics Study of Thermal Decomposition of Epoxidized Soybean Oil Acrylate” *Journal of Applied Polymer Science*
37. Mika, A.M.; Childs, R.F.; Dickson, J.M. “Chemical Valves Based on Poly(4-Vinylpyridine)-Filled Microporous Membranes” *Journal of Membrane Science* (1999)
38. Mosiewicki, M.; Aranguren, M.I.; Borrajo, J. “Mechanical Properties of Linseed Oil Monoglyceride Maleate/Styrene Copolymers” *Journal of Applied Polymer Science* (2005)
39. Mosiewicki, M.; Rojas, O.; Sibaja, M.R.; Borrajo, J.; Aranguren, M.I. “Aging Study of Linseed Oil Resin/Styrene Thermosets and their composites with Wood Flour” *Polymer International* (2007)
40. La Scala, J.; Wool, R.P. “Property Analysis of Triglyceride-Based Thermosets” *Polymer* (2005)
41. Jang, N.R.; Kim, H.; Hou, C.T; Kim, B.S. “Novel Biobased Photo-Crosslinked Polymer Networks Prepared from Vegetable Oil and 2,4-Furan Diacrylate” *Polymer Advanced Technologies* (2013)
42. Cristea, M.; Ionita, D.; Doroftei, F.; Simionecu, B.C. “Effect of Long-Term and Short-Term Dynamic Mechanical Evaluation of Network Based on Urethane and Soybean Oil” *Journal of the Mechanical Behavior of Biomedical Materials* (2013)

43. Li, Y.; Fu, L.; Lai, S.; Cai, X.; Yang, L. “Synthesis and Characterization of Cast Resin Based on Different Saturation Epoxidized Soybean Oil” *European Journal of Lipid Science and Technology* (2010)
44. Oprea, S.; Potolinca, V.O. “The Synthesis and Properties of Binary Acrylate Oligomer Mixtures and Their Blends with Different Soybean Oil Contents” *High Performance Polymers* (2013)
45. Palacios-Jaimes, M.; Cortes-Guzman, F.; Gonzales-Martinez, D.A; Gomez-Espinosa, R.M. “Surface Modification of Polypropylene Membrane by Acrylate Epoxidized Soybean Oil to be Used in Water Treatment” *Journal of Applied Polymer Science* (2011)
46. Saithai, P.; Lecomte, J.; Dubreucq, E.; Tanrattanakul, V. “Effects of Different Epoxidation Methods of Soybean Oil on the Characteristics of Acrylated Epoxidized Soybean Oil-Co-Poly(Methyl Methacrylate) Copolymer” *eXPRESS Polymer Letters* (2013)
47. Senoz, E.; Stanzione, J.F.; Reno, K.H.; Wool, R.P.; Miller, M.E.N. “Pyrolyzed Chicken Feather Fibers for Biobased Composite Reinforcement” *Journal of Applied Polymer Science* (2013)
48. Fu, L.; Yang, L.; Dai, C.; Zhao, C.; Ma, L. “Thermal and Mechanical Properties of Acrylated Epoxidized-Soybean Oil-Based Thermosets” *Journal of Applied Polymer Science* (2010)

49. Sharma, V.; Kundu, R.P. “Additional Polymers from Natural Oils: A Review” *Progress in Polymer Science* (2006)
50. Boronat, T.; J.M. Espana; I. Rico; O. Fenollar; R. Balart. "Processing and Characterization of New Organic Matrix for Composite Materials Based on Acrylated Epoxidized Vegetable Oils." *Advances in Materials Processing Technologies* (2012)
51. Mosiewicki, M.; Borrajo, J.; Aranguren, M. I. “Mechanical Properties of Woodflour/Linseed Oil Resin Composites” *Polymer International* (2005)
52. Sivarao; Vijayaram, T. R. “Determination of Tensile, Flexural Properties and Microstructural Characterization of Calcium Carbonate Filler Reinforced Polypropylene Matrix Composites” *Transactions of the Indian Institute of Metals* (2009)
53. Obrzud, R.; Truty, A.; “The Hardening Soil Model – A Practical Guidebook” *Z Soil* (2012)
54. Sutivisedsak, Nongnuch; Cheng, Huai N. “Use of Nutshells as Fillers in Polymer Composites” *Journal of Polymers and the Environment* (2012)
55. Tong, Jia Ying; Royan, Nishata Royan Rajendran; Ng, Yong Chuen; Ab Ghani, Mohd Hafizuddin; Ahmad, Shahrim “Study of the Mechanical and Morphology Properties of Recycled HDPE Composite Using Rice Husk Filler*” Advances in Materials Science and Engineering* (2014)

56. Haecker, C. J.; Garboczi, E. J.; Bullard, J. W.; Bohn, R. B.; Sun, Z.; Shah, S. P.; Voigt, T. “Modeling the Linear Elastic Properties of Portland Cement Paste” *Cement and Concrete Research* (2005)
57. Eichhorn, S. J.; Yound, R. J. “The Young’s Modulus of a Microcrystalline Cellulose” *Cellulose* (2001)
58. Lu, Y.; Larock, R. C. “Novel Biobased Nanocomposites from Soybean Oil and Functionalized Organoclay” *Biomacromolecules* (2006)
59. Albayrak, O.; Sen, S.; Cayli, G.; Ortac, B. “Bio-Based Polymer Nanocomposites Based on Layered Silicates Having a Reactive and Renewable Intercalant” *Journal of Applied Polymer Science* (2013)

APPENDIX A: Three Point Flexural Testing Data

vol% AESO	Stress (MPa)	St. Dev.	Strain	St. Dev.	Modulus (MPa)	St. Dev.
0	93.28	5.16	0.0536	0.0034	1946.23	67.14
10	120.07	15.56	0.1812	0.1159	1853.80	228.14
25	112.77	7.35	0.1237	0.0029	1457.35	85.84
40	84.37	4.15	0.1232	0.0026	1239.75	68.96
50	98.54	6.91	0.1050	0.0152	1201.70	266.36
60	83.32	4.29	0.1110	0.0374	1266.74	35.85
75	66.34	2.77	0.1648	0.0297	816.88	59.35
90	22.37	3.74	0.1831	0.0581	197.13	8.38
100	17.03	5.56	0.1553	0.0240	120.02	12.84

Table 2: Three Point Flexural Data of AESO/Styrene Copolymers

vol% PNSF	Stress (MPa)	St. Dev.	Strain	St. Dev.	Modulus (MPa)	St. Dev.
0	98.54	6.91	0.1050	0.0152	1201.70	266.36
7	80.49	4.01	0.0703	0.0054	1413.24	63.88
15	70.45	3.58	0.0509	0.0032	1777.00	19.49
23	54.02	4.42	0.0366	0.0022	1931.39	43.05

Table 3: Three Point Flexural Data of PNSF Filled Composites

vol% ESC	Stress (MPa)	St. Dev.	Strain	St. Dev.	Modulus (MPa)	St. Dev.
0	98.54	6.91	0.1050	0.0152	1201.70	266.36
20	64.77	8.85	0.0336	0.0052	2468.44	101.31
27	84.36	32.58	0.0279	0.0040	4416.00	1545.63
36	82.67	7.24	0.0207	0.0023	6696.08	774.73

Table 4: Three Point Flexural Data of ESC Filled Composites

vol% OMC	Stress (MPa)	St. Dev.	Strain	St. Dev.	Modulus (MPa)	St. Dev.
0	98.54	6.91	0.1050	0.0152	1201.70	266.36
1	94.50	13.16	0.0978	0.0254	1536.20	40.08
2	86.89	8.72	0.0796	0.0069	1492.83	119.75
4	73.88	4.00	0.0639	0.0076	1560.97	61.36

Table 5: Three Point Flexural Data of OMC Filled Composites

APPENDIX B: Impact Testing Data

vol% AESO	Trial 1	2	3	4	5	Average	St. Dev
0	0.1121	0.1031	0.1068	0.1121		0.1085	0.0044
25	0.1197	0.1281	0.1076	0.1404		0.1240	0.0138
50	0.1450	0.1738	0.1699	0.1296	0.1777	0.1592	0.0209
75	0.1465	0.1481	0.1707	0.1722		0.1594	0.0140
100	0.1419	0.1243	0.1488	0.1738		0.1472	0.0205

Table 6: Impact Testing Data of AESO/Styrene Copolymers

vol% PNSF	Trial 1	2	3	4	5	Average	St. Dev
0	0.1450	0.1738	0.1699	0.1296	0.1777	0.1592	0.0209
7	0.0978	0.1023	0.0866	0.0926		0.0948	0.0068
15	0.0888	0.0829	0.0926	0.0866		0.0877	0.0041
23	0.0933	0.0978	0.0755	0.0933		0.0900	0.0099

Table 7: Impact Testing Data of PNSF Filled Composites

vol% ESC	Trial 1	2	3	4	5	Average	St. Dev
0	0.1450	0.1738	0.1699	0.1296	0.1777	0.1592	0.0209
20	0.0971	0.1172	0.0972	0.0679	0.1127	0.0984	0.0193
27	0.0770	0.0866	0.0898	0.0790		0.0831	0.0061
36	0.0746	0.0810	0.0814	0.0834	0.0842	0.0809	0.0038

Table 8: Impact Testing Data of ESC Filled Composites

vol% OMC	Trial					Average	St. Dev
	1	2	3	4	5		
0	0.1450	0.1738	0.1699	0.1296	0.1777	0.1592	0.0209
1	0.0934	0.0971	0.0733	0.0895	0.1046	0.0916	0.0116
2	0.0696	0.0941	0.0926	0.1016	0.0941	0.0904	0.0121
4	0.0711	0.0971	0.0740	0.0652	0.0852	0.0785	0.0127

Table 9: Impact Testing Data of OMC Filled Composites

APPENDIX C: Durometer Measurement Data

vol% AESO	Trial			Average	St. Dev
	1	2	3		
0	82	80	83	81.7	1.5
25	85	83	84	84.0	1.0
50	82	82	80	81.3	1.2
75	78	77	77	77.3	0.6
100	52	52	54	52.7	1.2

Table 10: Durometer Measurement Data of AESO/Styrene Copolymers

vol% PNSF	Trial			Average	St. Dev
	1	2	3		
0	82	82	80	81.3	1.2
7	85	84	84	84.3	0.6
15	89	89	89	89.0	0.0
23	97	96	97	96.7	0.6

Table 11: Durometer Measurement Data of PNSF Filled Composites

vol% OMC	Trial			Average	St. Dev
	1	2	3		
0	82	82	80	81.3	1.2
1	84	82	84	83.3	1.2
2	86	85	91	87.3	3.2
4	88	89	87	88.0	1.0

Table 12: Durometer Measurement Data of ESC Filled Composites

vol% ESC	Trial			Average	St. Dev
	1	2	3		
0	82	82	80	81.3	1.2
20	98	100	99	99.0	1.0
27	109	111	108	109.3	1.5
36	142	145	143	143.3	1.5

Table 13: Durometer Measurement Data of OMC Filled Composites

APPENDIX D: Dynamic Mechanical Analysis Data

Temp	vol% AESO																	
	0		10		25		40		50		60		75		90		100	
(°C)	Modulus (MPa)	tanδ	Modulus (MPa)	tanδ	Modulus (MPa)	tanδ	Modulus (MPa)	tanδ	Modulus (MPa)	tanδ	Modulus (MPa)	tanδ	Modulus (MPa)	tanδ	Modulus (MPa)	tanδ	Modulus (MPa)	tanδ
30	1697.26	0.02568	1535.32	0.02294	1521.86	0.03835	1133.81	0.03777	1165.68	0.0411	966.08	0.07771	701.94	0.10989	291.96	0.1947	143.36	0.21071
31	1697.26	0.02745	1522.28	0.02439	1516.62	0.04059	1170.84	0.03633	1185.60	0.03877	990.27	0.07631	711.59	0.11075	312.04	0.18977	145.51	0.20711
32	1607.71	0.03039	1535.50	0.02428	1523.24	0.04196	1169.61	0.03577	1192.81	0.03851	996.07	0.07786	704.76	0.11502	319.94	0.18762	140.72	0.20576
33	1601.30	0.0308	1537.90	0.02714	1518.24	0.04186	1175.84	0.03605	1184.44	0.03891	988.40	0.07883	689.92	0.11793	325.87	0.18581	135.11	0.2046
34	1603.67	0.03142	1525.06	0.02695	1518.04	0.04219	1171.37	0.03641	1182.23	0.04087	976.06	0.08222	671.13	0.12268	307.21	0.19265	129.65	0.20135
35	1590.36	0.02989	1542.75	0.02667	1510.24	0.04192	1181.53	0.03822	1181.69	0.04184	968.12	0.08504	651.25	0.1272	273.38	0.19887	124.07	0.19946
36	1537.66	0.03092	1538.64	0.02746	1499.40	0.04292	1170.99	0.03707	1171.25	0.0442	951.78	0.08793	628.30	0.13359	246.16	0.20136	118.52	0.19867
37	1579.86	0.0298	1522.73	0.0284	1490.47	0.04534	1164.22	0.038	1156.07	0.04554	932.75	0.09219	602.70	0.14216	225.57	0.20616	113.26	0.19366
38	1581.82	0.02784	1522.67	0.02939	1490.54	0.04594	1163.31	0.03991	1143.33	0.04808	917.13	0.09715	576.90	0.15101	208.33	0.2067	109.16	0.19095
39	1537.73	0.03162	1508.34	0.0292	1481.38	0.04498	1154.69	0.03889	1134.55	0.04966	899.75	0.10137	549.77	0.16177	194.42	0.21123	104.96	0.18952
40	1572.10	0.03068	1519.63	0.03065	1474.57	0.04774	1145.45	0.04164	1123.65	0.05346	883.64	0.10675	523.00	0.17045	182.17	0.21463	100.75	0.18462
41	1526.59	0.03142	1513.18	0.03229	1460.36	0.0502	1130.48	0.04304	1103.73	0.05726	865.40	0.11075	495.89	0.18019	171.38	0.21722	97.21	0.18359
42	1547.19	0.02999	1508.05	0.03033	1456.88	0.04685	1127.47	0.04547	1088.41	0.06141	851.02	0.11395	468.80	0.19154	161.46	0.21912	93.89	0.1799
43	1533.85	0.03132	1516.20	0.0305	1454.66	0.04951	1127.35	0.04778	1071.60	0.06515	843.75	0.11672	444.10	0.2027	152.34	0.22117	90.52	0.17343
44	1491.65	0.03456	1497.96	0.03019	1453.32	0.05018	1117.02	0.04982	1052.98	0.06848	816.07	0.12483	423.46	0.21061	144.44	0.22039	87.96	0.16963
45	1492.04	0.03632	1488.00	0.03107	1453.03	0.05089	1105.75	0.05358	1039.21	0.07336	796.80	0.13088	402.60	0.22098	137.12	0.2218	85.27	0.16444
46	1521.56	0.03341	1492.05	0.03317	1450.89	0.05108	1097.58	0.05639	1020.86	0.07845	788.22	0.13336	382.97	0.22884	132.03	0.21834	82.91	0.16373
47	1474.37	0.03759	1495.98	0.03271	1452.43	0.05308	1089.37	0.06246	1005.69	0.08333	767.15	0.14297	363.59	0.23578	124.33	0.2193	80.73	0.15673
48	1453.30	0.03974	1490.43	0.03185	1450.86	0.05446	1075.47	0.0632	991.90	0.08971	737.84	0.14792	343.94	0.24314	118.76	0.2166	78.54	0.15514
49	1498.05	0.03625	1482.04	0.03311	1436.78	0.05593	1074.06	0.06678	981.58	0.0943	714.87	0.15387	325.47	0.25076	114.18	0.2153	76.59	0.14948
50	1470.46	0.03804	1482.06	0.03405	1435.74	0.05691	1063.30	0.06863	965.81	0.09851	692.02	0.15959	307.38	0.25909	109.10	0.21049	74.68	0.14458
51	1496.83	0.03772	1484.58	0.03474	1440.60	0.05714	1055.05	0.07455	955.70	0.10541	669.26	0.16774	290.16	0.26553	104.78	0.20776	73.14	0.13877
52	1488.88	0.04095	1484.11	0.03542	1433.85	0.05976	1043.86	0.07647	938.28	0.11018	645.17	0.17594	272.98	0.2723	100.55	0.20299	71.57	0.13858
53	1450.20	0.04553	1471.72	0.03467	1420.57	0.05978	1033.38	0.08071	920.55	0.11502	622.71	0.18316	256.78	0.27793	96.58	0.19962	70.07	0.13091
54	1470.06	0.04497	1464.00	0.0355	1416.29	0.06036	1019.25	0.08569	901.80	0.1209	596.44	0.19028	240.87	0.28473	93.07	0.19658	68.48	0.1268
55	1486.59	0.04561	1465.46	0.03655	1409.17	0.06212	1007.64	0.09073	880.24	0.12646	571.75	0.19842	225.99	0.28664	90.09	0.19064	67.24	0.11906
56	1468.61	0.04069	1464.11	0.03407	1401.61	0.06458	996.64	0.09302	861.50	0.13388	546.58	0.20646	211.65	0.2916	86.79	0.18349	65.95	0.11611
57	1478.76	0.04573	1455.05	0.03831	1392.54	0.06564	986.53	0.09684	842.25	0.14051	521.28	0.21483	198.00	0.29604	84.01	0.17312	64.93	0.11175
58	1469.88	0.04776	1460.04	0.03787	1384.68	0.06764	974.65	0.10334	817.80	0.14954	496.39	0.22503	185.94	0.29817	81.65	0.1725	64.11	0.10713
59	1466.25	0.0477	1457.71	0.03767	1367.02	0.07227	958.08	0.10916	795.50	0.1592	471.01	0.23368	173.96	0.30063	79.16	0.16639	62.94	0.10243
60	1460.41	0.05086	1443.73	0.0394	1359.95	0.0739	943.16	0.11296	771.77	0.16467	444.85	0.24549	162.94	0.30129	76.66	0.16195	62.11	0.10156
61	1433.24	0.05889	1446.72	0.04209	1346.90	0.07522	922.74	0.12108	742.57	0.1735	418.88	0.25719	152.71	0.3035	74.46	0.1578	61.38	0.09311
62	1445.33	0.05653	1436.74	0.04178	1334.97	0.07896	905.26	0.12759	717.15	0.18263	393.46	0.26576	143.11	0.29864	72.84	0.15347	60.80	0.09103
63	1455.84	0.05951	1428.43	0.04516	1319.66	0.07907	876.56	0.13745	686.52	0.19243	368.63	0.27708	134.35	0.29896	70.81	0.14885	59.91	0.08732
64	1421.38	0.06664	1426.97	0.04547	1301.40	0.08372	857.68	0.14407	652.13	0.20343	343.48	0.28612	125.91	0.2962	69.19	0.14002	59.12	0.0819
65	1430.12	0.06832	1418.30	0.04628	1284.83	0.08764	826.73	0.15513	621.56	0.21681	320.03	0.29648	118.31	0.29576	67.56	0.13603	58.55	0.07854
66	1433.91	0.06943	1404.95	0.04996	1270.63	0.0944	801.10	0.16312	588.31	0.2304	297.58	0.30805	111.37	0.29003	66.05	0.13119	57.93	0.0741
67	1415.38	0.07594	1401.35	0.05147	1249.46	0.09903	765.25	0.17741	557.64	0.24155	275.33	0.32033	105.04	0.28163	64.58	0.12539	57.44	0.07325
68	1397.16	0.08624	1389.48	0.05558	1223.13	0.10474	734.93	0.19448	523.27	0.25883	254.59	0.33122	99.03	0.2771	63.73	0.11952	56.97	0.07018
69	1385.67	0.09278	1381.98	0.0584	1200.24	0.10997	700.50	0.21079	489.74	0.27384	233.63	0.3381	93.54	0.26818	62.18	0.11795	56.32	0.06416
70	1363.40	0.10782	1368.64	0.06395	1173.32	0.11904	662.91	0.22908	454.22	0.29003	214.16	0.34805	88.93	0.26095	61.29	0.10941	55.84	0.06254
71	1323.15	0.12325	1346.19	0.06707	1140.32	0.12876	624.58	0.24917	419.23	0.30654	196.17	0.35556	84.28	0.25314	59.98	0.1015	55.77	0.06409
72	1292.00	0.14227	1328.16	0.07298	1103.12	0.13871	581.64	0.27044	384.82	0.32193	179.06	0.3627	80.54	0.24302	59.27	0.09892	54.96	0.0587
73	1244.18	0.16407	1305.91	0.08073	1063.30	0.15075	534.73	0.29556	351.52	0.34265	163.92	0.36908	76.70	0.23492	58.16	0.09434	54.90	0.0543
74	1191.07	0.1918	1284.30	0.09282	1017.82	0.16666	490.25	0.32343	319.35	0.36149	149.92	0.37093	73.36	0.22556	57.37	0.0891	54.53	0.05835
75	1123.47	0.22691	1242.74	0.10553	968.00	0.18179	441.88	0.35424	288.07	0.38022	136.67	0.37596	70.43	0.21523	56.64	0.08232	54.42	0.04832
76	1029.88	0.27008	1201.39	0.12385	911.76	0.20111	395.14	0.3866	258.38	0.39916	125.05	0.37337	67.56	0.20254	56.03	0.07794	53.94	0.04837
77	929.26	0.32373	1140.06	0.15119	852.35	0.22564	349.53	0.42128	231.14	0.41782	113.62	0.37279	65.35	0.19642	55.13	0.07151	53.58	0.04777
78	821.73	0.38994	1069.87	0.18177	782.66	0.25425	304.84	0.46376	205.31	0.43439	104.44	0.36612	62.90	0.18645	54.90	0.07228	53.49	0.04196
79	681.84	0.48006	982.03	0.22719	711.79	0.29095	262.99	0.50465	181.56	0.45021	96.10	0.36174	60.95	0.17882	54.14	0.06563	53.10	0.04217
80	557.50	0.58441	884.04	0.28423	628.62	0.33663	225.12	0.54137	160.64	0.46158	88.52	0.35236	58.94	0.16177	53.60	0.06668	53.02	0.03745
81	432.99	0.70901	774.13	0.35407	556.98	0.37965	189.19	0.58191	142.14	0.46551	81.75	0.34212	57.32	0.15557	53.08	0.05916	52.62	0.03816
82	341.05	0.83716	685.54	0.44527	476.54	0.4368	159.27	0.62259	126.15	0.47122	75.82	0.32896	56.12	0.1446	52.58	0.06146	52.47	0.03772
83	256.91	0.98898	547.68	0.54319	409.14	0.49216	134.54	0.64328	112.03	0.47146	70.88	0.31691	54.74	0.13696	52.25	0.05212	52.32	0.0329
84	187.30	1.157	436.76	0.66488	340.03	0.55657	113.12	0.66951	100.36	0.46311	66.59	0.29727	53.65	0.1274	51.82	0.05279	52.18	0.03162
85	132.68	1.33572	351.42	0.78192	281.52	0.61982	95.95	0.68416	90.46	0.45099	62.82	0.28239	52.26	0.1135	51.56	0.04651	52.04	0.03027
86	91.58	1.52413	255.75	0.90435	230.40	0.68734	81.92	0.67732	81.70	0.44213	59.57	0.26756	51.87	0.10467	50.97	0.04749	51.82	0.03035
87	63.04	1.68537	186.62	1.04391	187.19	0.74645	71.11	0.67139	75.08	0.41796	56.50	0.25068	50.48	0.10533	50.68	0.04334	51.80	0.02727
88	45.08	1.78897	141.26	1.18143	152.24	0.80156	62.05	0.65322	68.79	0.40119	54.26	0.22793	50.06	0.0904	50.49	0.04073	51.36	0.02615
89	33.62	1.81848	106.20	1.30275	125.15	0.84073	54.76	0.62489	63.58	0.38105	51.71	0.21864	49.49	0.08054	50.14	0.03868	51.56	0.02548
90	25.26	1.80654	78.62	1.43407	102.97	0.87355	49.19	0.59528	59.30	0.36055	50.05	0.19925	48.59	0.07944	49.92	0.03362	51.29	0.02395
91	20.45	1.71118	59.26	1.52573	85.05	0.88221	44.50	0.55371	54.91	0.33465	48.30	0.18654	47.98	0.07431	49.52	0.03002	51.37	0.02391
92	16.68	1.5987	46.14	1.59844	71.77	0.87945	40.75	0.51407	51.32	0.31067	46.91	0.1709	47.62	0.06551	49.21	0.03231	51.09	0.02272
93	14.23	1.44544	36.42	1.56545	61.66	0.85564	37.51	0.47277	49.28	0.28327	45.79	0.1524	47.16	0.06333	49.38	0.02901	51.20	0.02344
94	12.01	1.33545	29.05	1.56243	52.57	0.83869	35.04	0.43599	46.90	0.26157	44.69	0.14104	46.73	0.05473	49.07	0.01903	50.87	0.02068
95	10.71	1.19044	23.71	1.52777	45.95	0.79352	32.83	0.39225	45.07	0.24022	43.68	0.13025	46.44	0.04287	48.82	0.02162	51.05	0.0194
96	9.52	1.06863	19.96	1.46325	40.91	0.75198	31.21	0.35515	43.26	0.21656	42.96	0.11288	46.41	0.04447	48.61	0.02198	50.81	0.02189
97	8.65	0.94311	16.78	1.37615	36.92	0.69172	29.70	0.32592	41.71	0.19689	42.05	0.10456	45.88	0.03445	48.42	0.02055	50.90	0.01669
98	7.89	0.83498	15.48	1.18711	33.87	0.6422	28.54	0.28829	40.42	0.17785	41.69	0.08875	45.61	0.04111	48.67	0.02414	50.86	0.01467
99	7.24	0.76392	13.09	1.15244	31.09	0.57762	27.54	0.26149	39.42	0.15701	41.01	0.08046	45.54	0.02754	48.13	0.01789	50.72	0.01865
100	6.79	0.66652	11.98	1.00551	31.09	0.57762	27.54	0.26149	38.55	0.14378	40.52	0.07121	45.21	0.0331	48.06	0.01719	50.72	0.01865

Table 14: DMA Data of AESO/Styrene Copolymers

vol% AESO	Modulus (MPa)
0	1697.3
10	1535.3
25	1521.9
40	1133.8
50	1165.7
60	966.08
75	701.94
90	291.96
100	107.43

Table 15: 30 °C Storage Modulus Data of AESO/Styrene Copolymers

vol% AESO	Measured Tg	Predicted Tg
0	365.23	365.23
10	365.19	355.87
25	364.25	342.71
40	358.21	330.48
50	356.21	322.80
60	348.22	315.47
75	332.2	305.08
90	318.11	295.35
100	289.2	289.20

Table 16: Measured and Predicted T_g Data of AESO/Styrene Copolymers

vol% AESO	Modulus (MPa)	Mc
0	6.8	457
10	12.0	259
25	31.1	100
40	27.5	113
50	38.5	80
60	40.5	77
75	45.2	69
90	48.1	65
100	50.7	61

Table 17: Storage Modulus and $\bar{M}_c$ Data of AESO/Styrene Copolymers

Temp	vol% PNSF					
	0		15		23	
(°C)	Modulus (MPa)	tanδ	Modulus (MPa)	tanδ	Modulus (MPa)	tanδ
30	1165.68	0.0411	1551.97	0.04415	1683.60	0.04361
31	1185.60	0.03877	1547.32	0.04187	1710.72	0.04243
32	1192.81	0.03851	1561.85	0.04289	1710.56	0.04242
33	1184.44	0.03891	1558.85	0.04381	1706.97	0.04285
34	1182.23	0.04087	1553.77	0.04421	1707.98	0.04422
35	1181.69	0.04184	1544.10	0.04449	1702.20	0.04345
36	1171.25	0.0442	1527.97	0.04562	1697.33	0.04437
37	1156.07	0.04554	1515.49	0.0463	1687.06	0.04537
38	1143.33	0.04808	1507.90	0.04829	1674.27	0.04534
39	1134.55	0.04966	1495.59	0.05005	1669.05	0.04851
40	1123.65	0.05346	1488.23	0.0528	1647.88	0.05024
41	1103.73	0.05726	1483.24	0.05424	1638.74	0.05235
42	1088.41	0.06141	1464.95	0.05604	1619.87	0.05342
43	1071.60	0.06515	1451.30	0.05841	1611.27	0.05679
44	1052.98	0.06848	1430.95	0.06145	1590.24	0.06026
45	1039.21	0.07336	1406.92	0.06646	1566.50	0.06374
46	1020.86	0.07845	1380.64	0.07047	1543.46	0.06908
47	1005.69	0.08333	1353.67	0.07572	1513.55	0.07356
48	991.90	0.08971	1324.10	0.08084	1483.71	0.07894
49	981.58	0.0943	1302.18	0.08714	1459.89	0.08474
50	965.81	0.09851	1280.45	0.09249	1430.06	0.09199
51	955.70	0.10541	1259.83	0.09798	1397.51	0.09632
52	938.28	0.11018	1237.57	0.10256	1369.01	0.10148
53	920.55	0.11502	1212.83	0.10806	1347.65	0.10811
54	901.80	0.1209	1192.78	0.1137	1325.18	0.11189
55	880.24	0.12646	1168.42	0.11806	1298.98	0.11605
56	861.50	0.13388	1149.71	0.12488	1271.01	0.1225
57	842.25	0.14051	1125.49	0.13026	1242.57	0.12897
58	817.80	0.14854	1099.76	0.13416	1212.09	0.13415
59	795.50	0.1582	1075.20	0.14241	1182.43	0.14022
60	771.77	0.16467	1046.83	0.14859	1150.96	0.14727
61	742.57	0.1735	1018.44	0.15639	1132.88	0.1537
62	717.15	0.18263	985.75	0.16182	1087.99	0.16328
63	686.52	0.19243	952.49	0.17289	1049.14	0.17143
64	652.13	0.20343	920.55	0.18059	1012.47	0.17942
65	621.56	0.21681	883.68	0.18803	971.84	0.18714
66	588.31	0.2304	845.62	0.19807	927.10	0.1985
67	557.64	0.24155	809.32	0.20866	883.17	0.20833
68	523.27	0.25883	768.62	0.21952	840.50	0.21948
69	489.74	0.27384	728.06	0.23246	796.66	0.23236
70	454.22	0.29003	687.53	0.24489	750.57	0.24614
71	419.23	0.30654	645.05	0.25949	707.04	0.25621
72	384.82	0.32193	603.55	0.27201	656.80	0.27178
73	351.52	0.34265	562.74	0.28675	612.57	0.28471
74	319.35	0.36149	522.23	0.30069	568.16	0.2983
75	288.07	0.38022	481.60	0.31522	524.52	0.31332
76	258.38	0.39916	444.53	0.33038	481.92	0.32606
77	231.14	0.41782	406.60	0.34549	442.52	0.33622
78	205.31	0.43439	369.80	0.35974	404.78	0.34808
79	181.56	0.45021	337.05	0.37029	368.21	0.35752
80	160.64	0.46158	304.63	0.37998	336.18	0.36471
81	142.14	0.46551	275.87	0.38803	306.12	0.36893
82	126.15	0.47122	248.69	0.39781	280.28	0.37043
83	112.03	0.47146	225.81	0.39685	256.19	0.36895
84	100.36	0.46311	205.44	0.39611	234.88	0.36525
85	90.46	0.45099	187.61	0.39095	216.88	0.35648
86	81.70	0.44213	171.92	0.38348	200.85	0.34492
87	75.08	0.41796	158.95	0.36851	186.65	0.33251
88	68.79	0.40119	146.82	0.35417	175.48	0.31705
89	63.58	0.38105	136.88	0.33799	164.91	0.30334
90	59.30	0.36055	128.57	0.3235	156.46	0.28638
91	54.91	0.33465	121.30	0.30467	148.67	0.26396
92	51.92	0.31087	115.25	0.28675	142.16	0.24878
93	49.28	0.28327	110.11	0.26879	136.89	0.23175
94	46.90	0.26157	105.61	0.24881	131.86	0.21541
95	45.07	0.24022	101.32	0.23069	127.34	0.1995
96	43.26	0.21656	97.97	0.21286	123.94	0.18461
97	41.71	0.19689	94.95	0.19877	120.97	0.1695
98	40.42	0.17785	92.36	0.18082	117.95	0.15923
99	39.42	0.15701	90.58	0.16595	115.66	0.14281
100	38.55	0.14378	90.58	0.16595	115.66	0.14281

Table 18: DMA Data of PNSF Filled Composites

vol% PNSF	Modulus (MPa)
0	1165.68
15	1551.97
23	1683.60

Table 19: 30 °C Storage Modulus Data of PNSF Filled Composites

vol% PNSF	Tg (K)
0	356
15	356
23	355

Table 20: Glass Transition Temperature Data of PNSF Filled Composites

Temp	vol% ESC					
	0		27		36	
(°C)	Modulus (MPa)	tanδ	Modulus (MPa)	tanδ	Modulus (MPa)	tanδ
30	1165.68	0.0411	2440.80	0.04768	2973.04	0.04115
31	1185.60	0.03877	2436.05	0.04216	3053.83	0.04022
32	1192.81	0.03851	2453.20	0.0429	3035.80	0.03915
33	1184.44	0.03891	2463.66	0.04273	3063.67	0.03982
34	1182.23	0.04087	2452.21	0.04366	3054.63	0.04128
35	1181.69	0.04184	2468.01	0.04487	3026.55	0.04326
36	1171.25	0.0442	2438.15	0.04572	3030.49	0.04315
37	1156.07	0.04554	2428.71	0.04789	2996.20	0.04457
38	1143.33	0.04808	2415.26	0.04852	2974.38	0.04402
39	1134.55	0.04966	2404.04	0.04985	2950.47	0.04822
40	1123.65	0.05346	2402.10	0.0521	2928.24	0.04855
41	1103.73	0.05726	2369.15	0.05512	2916.82	0.05159
42	1088.41	0.06141	2352.93	0.057	2864.97	0.05345
43	1071.60	0.06515	2333.94	0.05981	2833.09	0.05483
44	1052.98	0.06848	2335.85	0.06349	2805.26	0.05963
45	1039.21	0.07336	2299.05	0.0671	2757.80	0.06095
46	1020.86	0.07845	2301.90	0.07023	2718.75	0.06586
47	1005.69	0.08333	2261.07	0.07472	2689.67	0.06847
48	991.90	0.08971	2251.37	0.07875	2642.56	0.0725
49	981.58	0.0943	2214.75	0.08089	2618.29	0.0741
50	965.81	0.09851	2199.01	0.08375	2582.20	0.07889
51	955.70	0.10541	2168.75	0.08717	2545.91	0.08132
52	938.28	0.11018	2151.23	0.09118	2505.01	0.0868
53	920.55	0.11502	2118.31	0.09609	2454.09	0.08739
54	901.80	0.1209	2093.33	0.09988	2424.95	0.09205
55	880.24	0.12646	2065.80	0.10394	2379.97	0.09609
56	861.50	0.13388	2029.26	0.10853	2347.25	0.099
57	842.25	0.14051	2007.58	0.11362	2302.37	0.10567
58	817.80	0.14854	1964.49	0.11804	2257.68	0.10833
59	795.50	0.1582	1939.20	0.11792	2204.89	0.11491
60	771.77	0.16467	1889.84	0.12801	2153.73	0.12062
61	742.57	0.1735	1846.56	0.13465	2096.96	0.12744
62	717.15	0.18263	1798.30	0.14072	2043.23	0.13341
63	686.52	0.19243	1749.45	0.14791	1990.65	0.13823
64	652.13	0.20343	1704.16	0.15599	1932.58	0.14598
65	621.56	0.21681	1649.76	0.16225	1865.77	0.15531
66	588.31	0.2304	1597.70	0.17062	1807.68	0.16301
67	557.64	0.24155	1544.25	0.17868	1741.09	0.17091
68	523.27	0.25883	1482.88	0.18752	1668.57	0.18049
69	489.74	0.27384	1420.30	0.19774	1596.29	0.19073
70	454.22	0.29003	1351.93	0.20937	1529.06	0.19985
71	419.23	0.30654	1282.77	0.22024	1453.88	0.21324
72	384.82	0.32193	1214.54	0.23118	1371.18	0.2257
73	351.52	0.34265	1145.79	0.24484	1291.31	0.23799
74	319.35	0.36149	1065.79	0.25771	1205.65	0.25049
75	288.07	0.38022	1003.11	0.26836	1129.03	0.26473
76	258.38	0.39916	928.70	0.28133	1045.52	0.27756
77	231.14	0.41782	863.44	0.29444	966.66	0.29007
78	205.31	0.43439	793.73	0.30756	890.14	0.30239
79	181.56	0.45021	732.35	0.31831	820.08	0.31382
80	160.64	0.46158	674.05	0.33003	752.00	0.32304
81	142.14	0.46551	618.36	0.33913	691.23	0.33423
82	126.15	0.47122	566.99	0.34488	633.41	0.33852
83	112.03	0.47146	519.61	0.34929	581.28	0.34163
84	100.36	0.46311	476.96	0.34975	537.31	0.33878
85	90.46	0.45099	438.84	0.3476	494.69	0.33793
86	81.70	0.44213	406.21	0.34151	458.20	0.32881
87	75.08	0.41796	378.14	0.33399	425.86	0.32174
88	68.79	0.40119	351.95	0.32594	399.12	0.3111
89	63.58	0.38105	330.25	0.31413	374.98	0.29933
90	59.30	0.36055	310.13	0.29889	354.08	0.28636
91	54.91	0.33465	293.37	0.28796	336.58	0.26921
92	51.92	0.31087	278.22	0.27379	319.88	0.25775
93	49.28	0.28327	265.04	0.25946	306.62	0.24407
94	46.90	0.26157	253.55	0.24326	294.13	0.22708
95	45.07	0.24022	244.07	0.2291	283.41	0.21455
96	43.26	0.21656	234.50	0.21503	273.50	0.19952
97	41.71	0.19689	226.54	0.20229	265.37	0.18765
98	40.42	0.17785	220.47	0.18594	258.14	0.17271
99	39.42	0.15701	213.82	0.17484	252.39	0.16159
100	38.55	0.14378	213.82	0.17484	252.39	0.16159

Table 21: DMA Data of ESC Filled Composites

vol% ESC	Modulus (MPa)
0	1165.68
27	2440.80
36	2973.04

Table 22: 30 °C Storage Modulus Data of ESC Filled Composites

vol% ESC	Tg (K)
0	356
27	357
36	356

Table 23: Glass Transition Temperature Data of ESC Filled Composites

Temp	vol% OMC							
	0		1		2		4	
(°C)	Modulus (MPa)	tanδ	Modulus (MPa)	tanδ	Modulus (MPa)	tanδ	Modulus (MPa)	tanδ
30	1165.68	0.0411	1288.38	0.05604	1286.53	0.05427	1288.38	0.05604
31	1185.60	0.03877	1308.59	0.05434	1321.46	0.05283	1308.59	0.05434
32	1192.81	0.03851	1317.90	0.05525	1330.16	0.05499	1317.90	0.05525
33	1184.44	0.03891	1316.43	0.05593	1331.07	0.05528	1316.43	0.05593
34	1182.23	0.04087	1310.24	0.05738	1328.71	0.05721	1310.24	0.05738
35	1181.69	0.04184	1298.69	0.05759	1311.12	0.0577	1298.69	0.05759
36	1171.25	0.0442	1289.11	0.06193	1309.80	0.06062	1289.11	0.06193
37	1156.07	0.04554	1277.62	0.06368	1290.93	0.06256	1277.62	0.06368
38	1143.33	0.04808	1263.46	0.06575	1274.68	0.06403	1263.46	0.06575
39	1134.55	0.04966	1251.00	0.06835	1262.97	0.06651	1251.00	0.06835
40	1123.65	0.05346	1234.43	0.07221	1250.05	0.07044	1234.43	0.07221
41	1103.73	0.05726	1221.83	0.07494	1239.61	0.0742	1221.83	0.07494
42	1088.41	0.06141	1205.07	0.07886	1218.47	0.07712	1205.07	0.07886
43	1071.60	0.06515	1190.90	0.08187	1209.24	0.0809	1190.90	0.08187
44	1052.98	0.06848	1176.21	0.08658	1190.82	0.08454	1176.21	0.08658
45	1039.21	0.07336	1162.61	0.09105	1172.64	0.08916	1162.61	0.09105
46	1020.86	0.07845	1150.60	0.09334	1159.82	0.09154	1150.60	0.09334
47	1005.69	0.08333	1137.22	0.09717	1137.78	0.09581	1137.22	0.09717
48	991.90	0.08971	1121.11	0.10183	1120.67	0.09942	1121.11	0.10183
49	981.58	0.0943	1103.82	0.10408	1105.66	0.104	1103.82	0.10408
50	965.81	0.09851	1085.46	0.10948	1088.76	0.10586	1085.46	0.10948
51	955.70	0.10541	1070.42	0.11323	1072.23	0.11122	1070.42	0.11323
52	938.28	0.11018	1049.18	0.11763	1054.92	0.1156	1049.18	0.11763
53	920.55	0.11502	1030.62	0.12221	1035.70	0.12182	1030.62	0.12221
54	901.80	0.1209	1013.23	0.12714	1018.16	0.12772	1013.23	0.12714
55	880.24	0.12646	988.33	0.13166	996.23	0.13521	988.33	0.13166
56	861.50	0.13388	966.93	0.13817	972.55	0.1401	966.93	0.13817
57	842.25	0.14051	944.52	0.14441	948.89	0.14458	944.52	0.14441
58	817.80	0.14854	921.00	0.15127	924.16	0.14952	921.00	0.15127
59	795.50	0.1582	895.28	0.1575	898.85	0.15897	895.28	0.1575
60	771.77	0.16467	865.94	0.16477	868.99	0.16612	865.94	0.16477
61	742.57	0.1735	842.70	0.17193	839.06	0.17321	842.70	0.17193
62	717.15	0.18263	815.25	0.18054	811.40	0.184	815.25	0.18054
63	686.52	0.19243	782.97	0.18897	781.14	0.19066	782.97	0.18897
64	652.13	0.20343	752.36	0.19916	748.23	0.20199	752.36	0.19916
65	621.56	0.21681	719.74	0.20928	715.11	0.21129	719.74	0.20928
66	588.31	0.2304	687.80	0.21945	680.00	0.22304	687.80	0.21945
67	557.64	0.24155	648.09	0.23161	645.23	0.23525	648.09	0.23161
68	523.27	0.25883	617.00	0.24428	608.95	0.24812	617.00	0.24428
69	489.74	0.27384	578.50	0.25879	573.92	0.2625	578.50	0.25879
70	454.22	0.29003	544.57	0.27188	537.78	0.27654	544.57	0.27188
71	419.23	0.30654	507.52	0.28697	501.37	0.29295	507.52	0.28697
72	384.82	0.32193	471.33	0.30153	465.35	0.30756	471.33	0.30153
73	351.52	0.34265	434.52	0.31811	429.92	0.32218	434.52	0.31811
74	319.35	0.36149	398.58	0.33398	393.01	0.34225	398.58	0.33398
75	288.07	0.38022	363.00	0.35286	358.68	0.35955	363.00	0.35286
76	258.38	0.39916	330.02	0.36999	325.50	0.37512	330.02	0.36999
77	231.14	0.41782	297.86	0.38873	293.33	0.39341	297.86	0.38873
78	205.31	0.43439	267.15	0.40436	263.39	0.40689	267.15	0.40436
79	181.56	0.45021	238.57	0.42233	235.72	0.42581	238.57	0.42233
80	160.64	0.46158	212.68	0.43676	210.12	0.43855	212.68	0.43676
81	142.14	0.46551	187.89	0.44823	187.69	0.44831	187.89	0.44823
82	126.15	0.47122	167.72	0.45814	167.10	0.45515	167.72	0.45814
83	112.03	0.47146	148.82	0.46469	149.45	0.45665	148.82	0.46469
84	100.36	0.46311	132.63	0.46435	134.69	0.45405	132.63	0.46435
85	90.46	0.45099	118.82	0.46044	121.08	0.44717	118.82	0.46044
86	81.70	0.44213	107.52	0.45303	109.91	0.43709	107.52	0.45303
87	75.08	0.41796	97.51	0.44052	100.22	0.42434	97.51	0.44052
88	68.79	0.40119	89.49	0.42484	92.09	0.40615	89.49	0.42484
89	63.58	0.38105	82.20	0.40842	85.47	0.38895	82.20	0.40842
90	59.30	0.36055	76.19	0.38558	79.89	0.36773	76.19	0.38558
91	54.91	0.33465	71.12	0.36499	74.95	0.34755	71.12	0.36499
92	51.92	0.31087	67.01	0.34092	70.89	0.32129	67.01	0.34092
93	49.28	0.28327	63.42	0.31784	67.08	0.3057	63.42	0.31784
94	46.90	0.26157	60.33	0.29587	64.28	0.27491	60.33	0.29587
95	45.07	0.24022	57.71	0.27362	61.67	0.25886	57.71	0.27362
96	43.26	0.21656	55.13	0.25311	59.22	0.24234	55.13	0.25311
97	41.71	0.19689	53.43	0.23218	57.57	0.21743	53.43	0.23218
98	40.42	0.17785	51.97	0.20995	55.75	0.20247	51.97	0.20995
99	39.42	0.15701	50.56	0.1954	54.40	0.18635	50.56	0.1954
100	38.55	0.14378	49.36	0.17567	54.40	0.18635	49.36	0.17567

Table 24: DMA Data of OMC Filled Composites

vol% OMC	Modulus (MPa)
0	1165.68
1	1288.38
2	1286.53
4	1288.38

Table 25: 30 °C Storage Modulus Data of OMC Filled Composites

vol% OMC	Tg (K)
0	356
1	356
2	356
4	356

Table 26: Glass Transition Temperature Data of OMC Filled Composites

APPENDIX E: Scanning Electron Microscopy Images

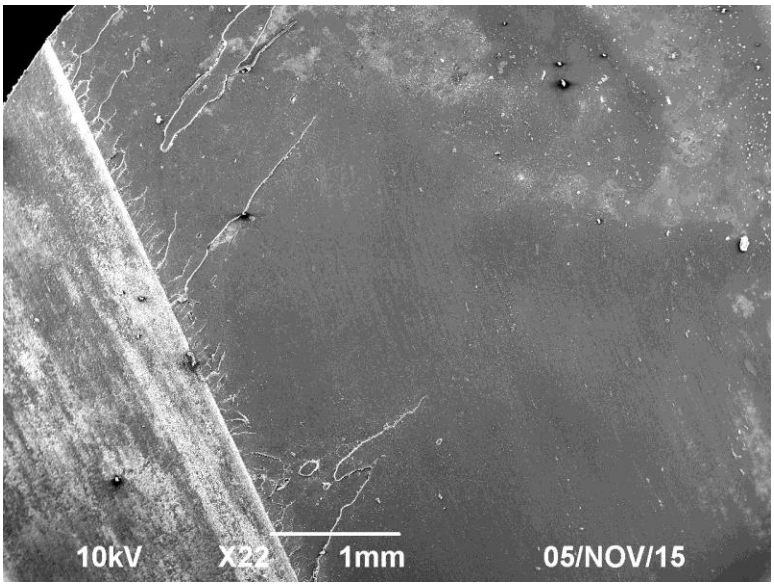

Figure 70: 22x Mag SEM Image of Styrene Polymer Fracture Site

Figure 71: 75x Mag SEM Image of AESO Polymer Fracture Site

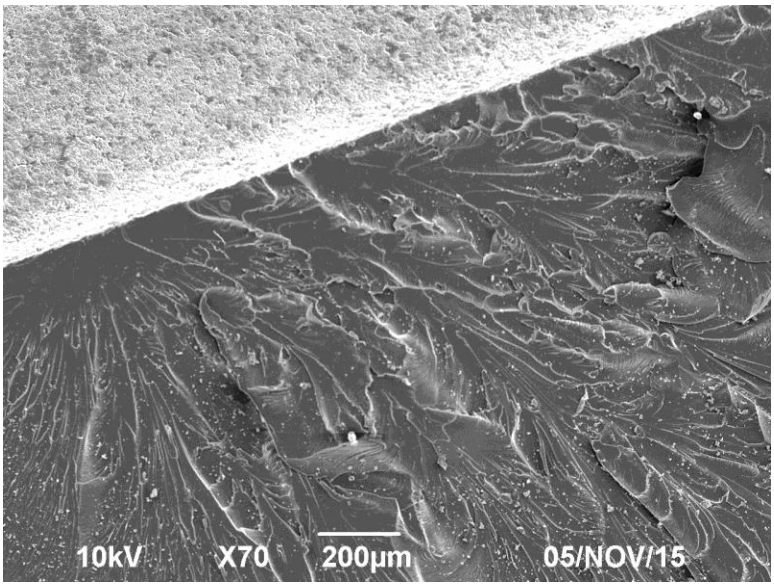

Figure 72: 70x Mag SEM Image of 50:50 AESO/Styrene Copolymer

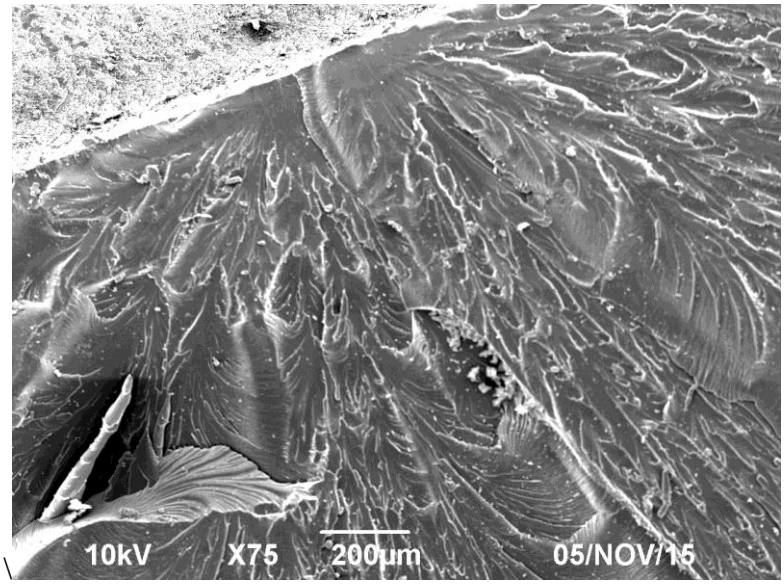

Figure 73: 75x Mag SEM Image of 50:50 AESO/Styrene Copolymer

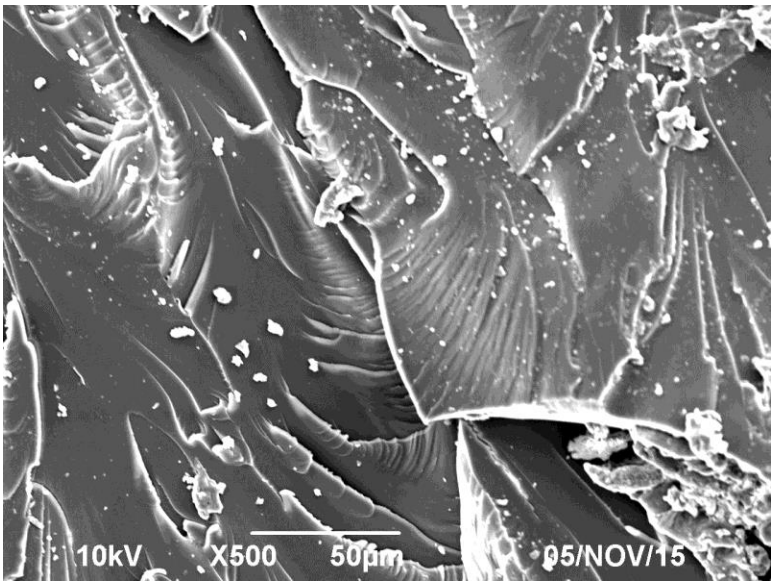

Figure 74: 500x Mag SEM Image of 50:50 AESO/Styrene Copolymer

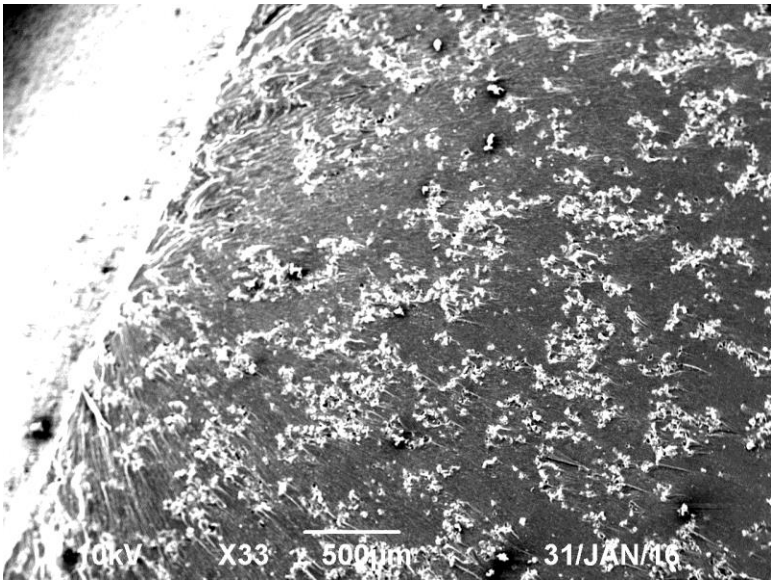

Figure 75: 33x Mag SEM Image of 7 vol% PNSF Filled Composite

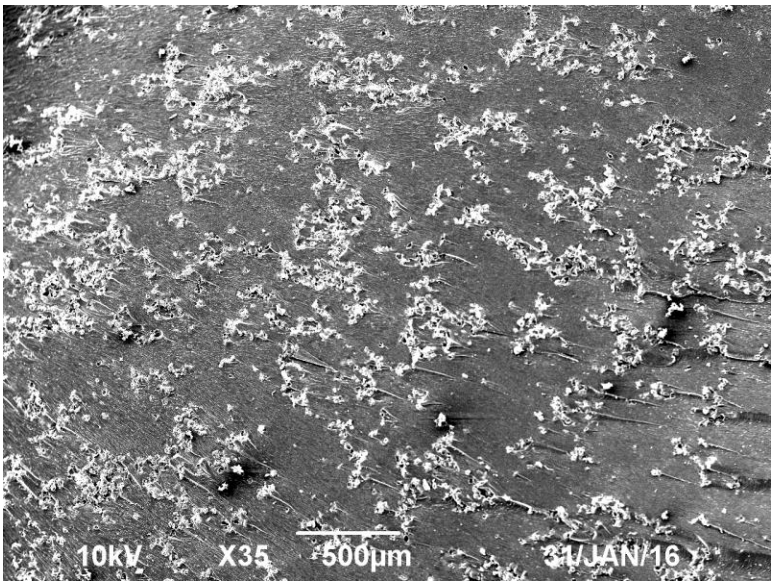

Figure 76: 35x Mag SEM Image of 7 vol% PNSF Filled Composite

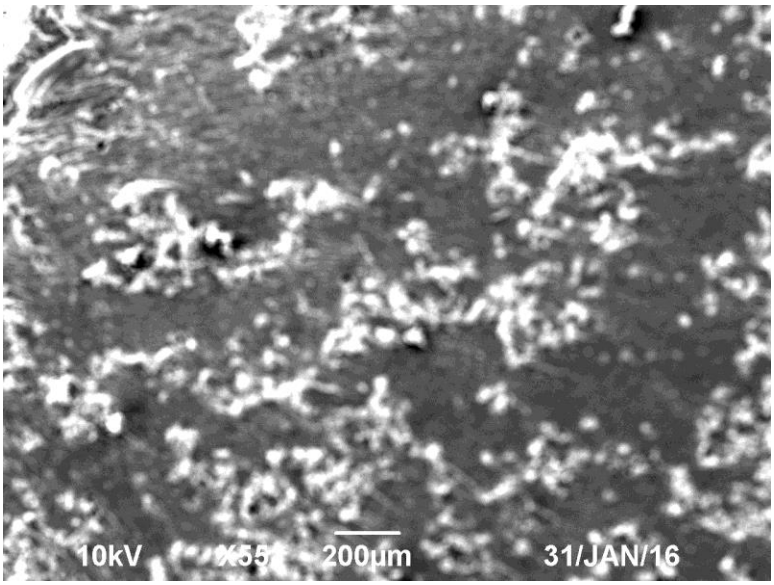

Figure 77: 55x Mag SEM Image of 7 vol% PNSF Filled Composite

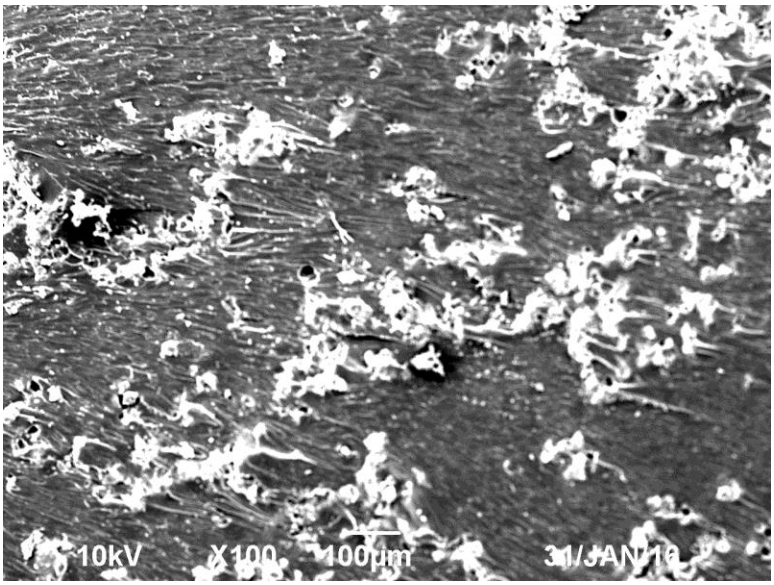

Figure 78: 100x Mag SEM Image of 7 vol% PNSF Filled Composite

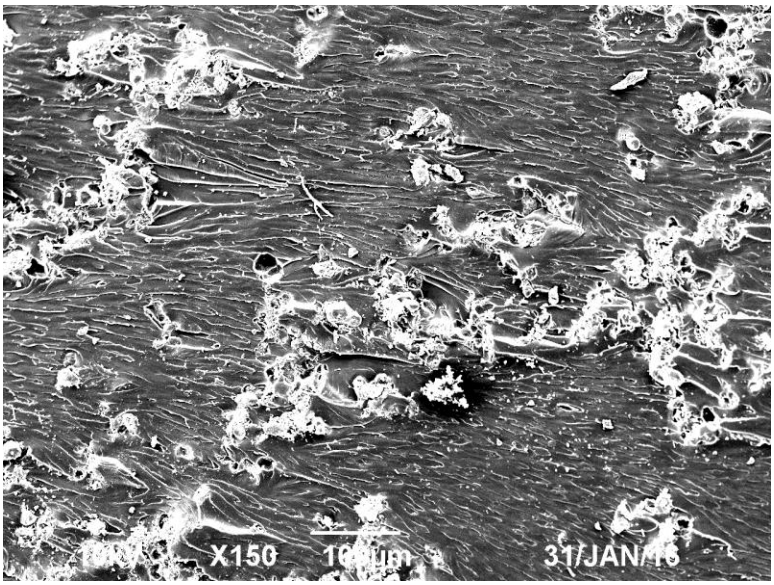

Figure 79: 150x Mag SEM Image of 7 vol% PNSF Filled Composite

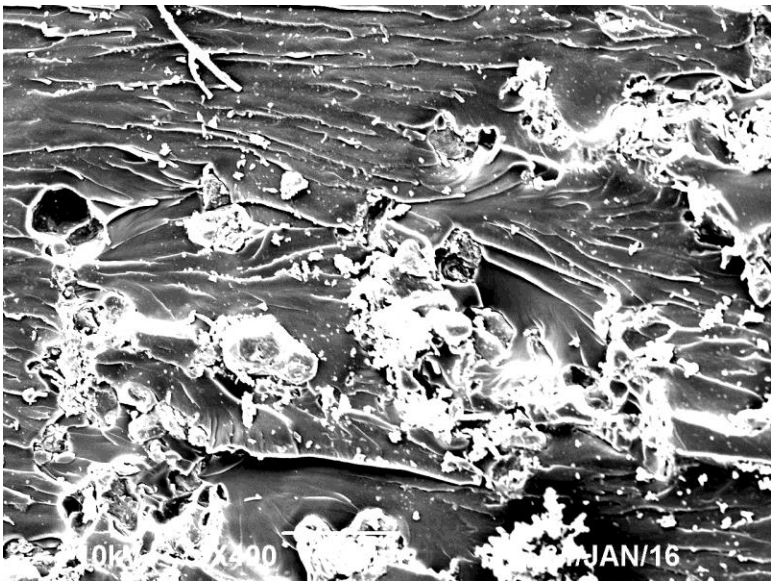

Figure 80: 400x Mag SEM Image of 7 vol% PNSF Filled Composite

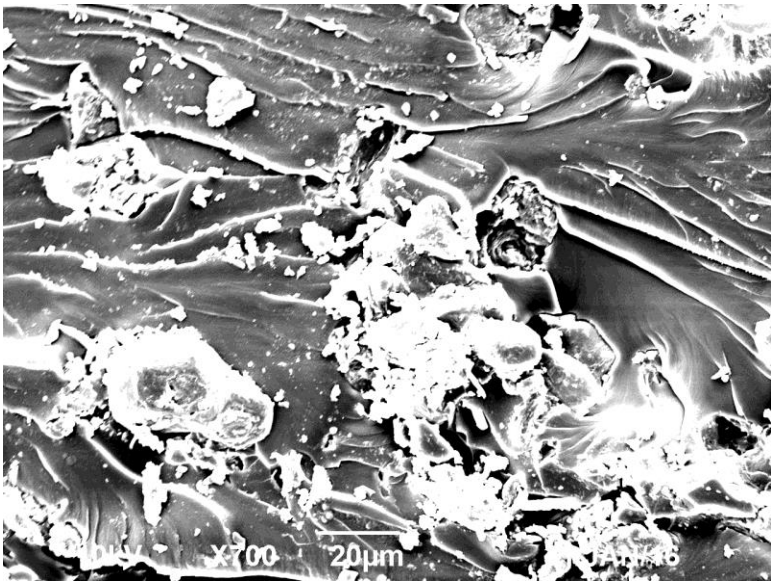

Figure 81: 700x Mag SEM Image of 7 vol% PNSF Filled Composite

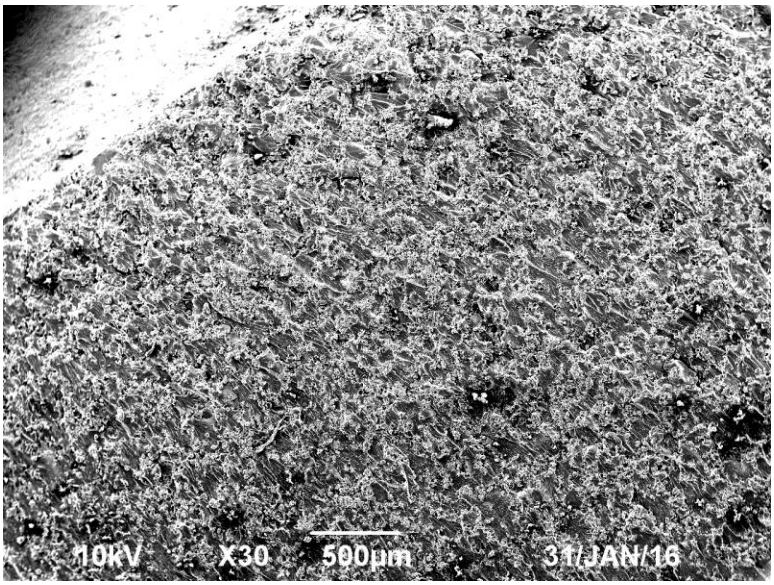

Figure 82: 30x Mag SEM Image of 15 vol% PNSF Filled Composite

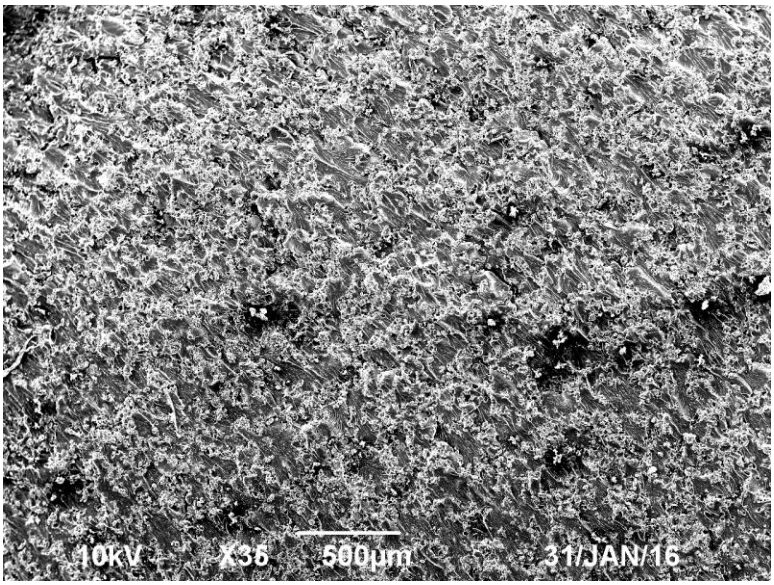

Figure 83: 35x Mag SEM Image of 15 vol% PNSF Filled Composite

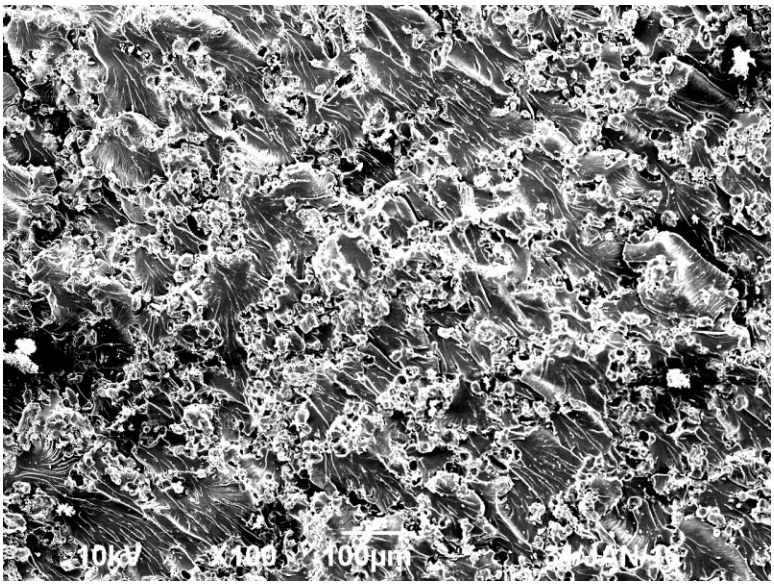

Figure 84: 100x Mag SEM Image of 15 vol% PNSF Filled Composite

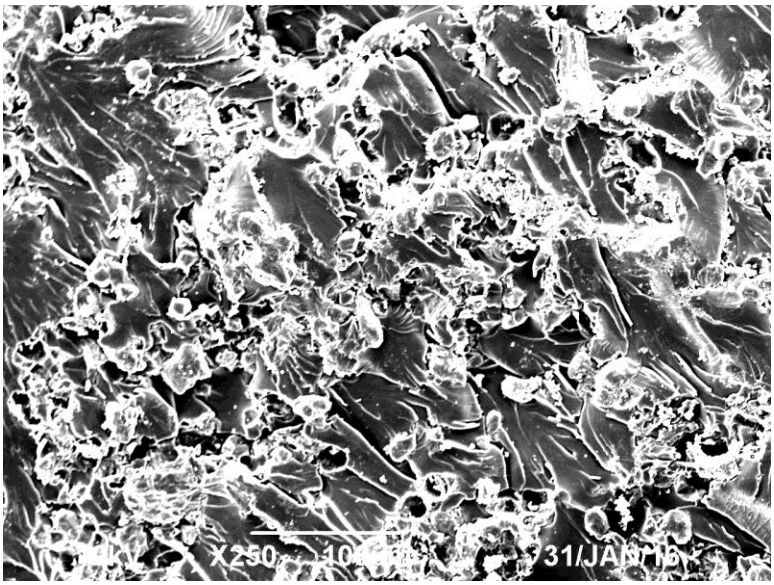

Figure 85: 250x Mag SEM Image of 15 vol% PNSF Filled Composite

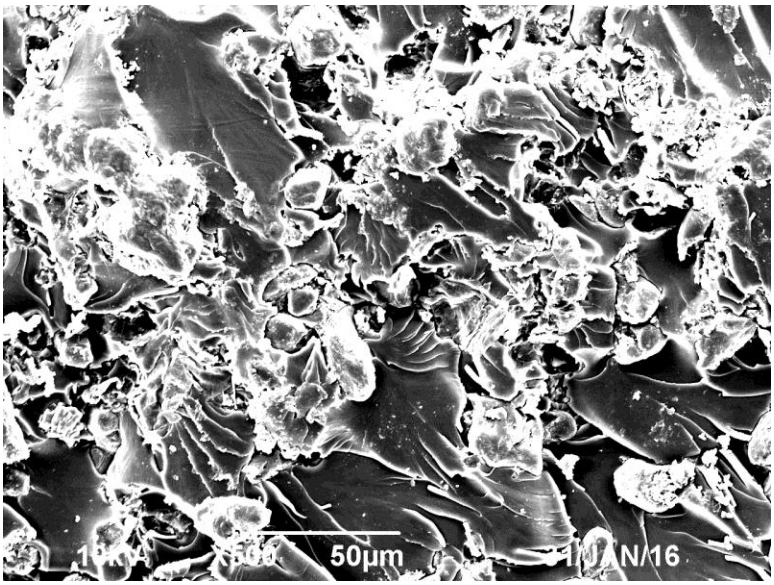

Figure 86: 500x Mag SEM Image of 15 vol% PNSF Filled Composite

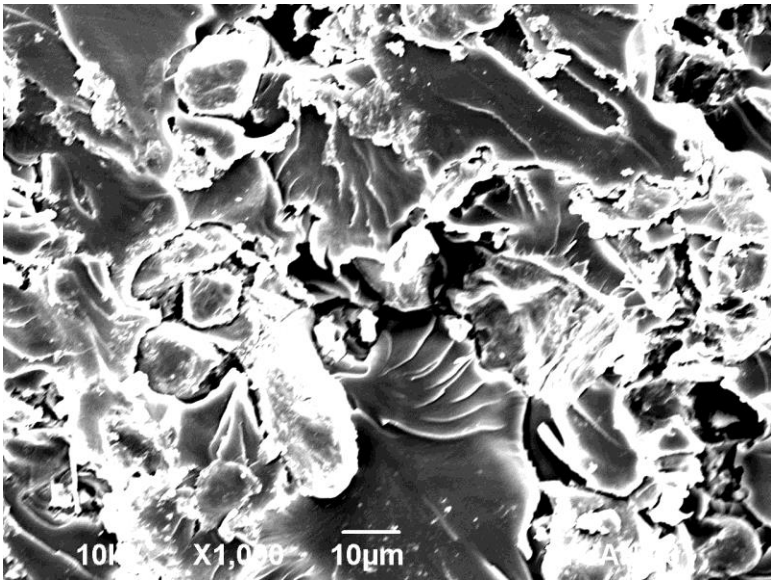

Figure 87: 1000x Mag SEM Image of 15 vol% PNSF Filled Composite

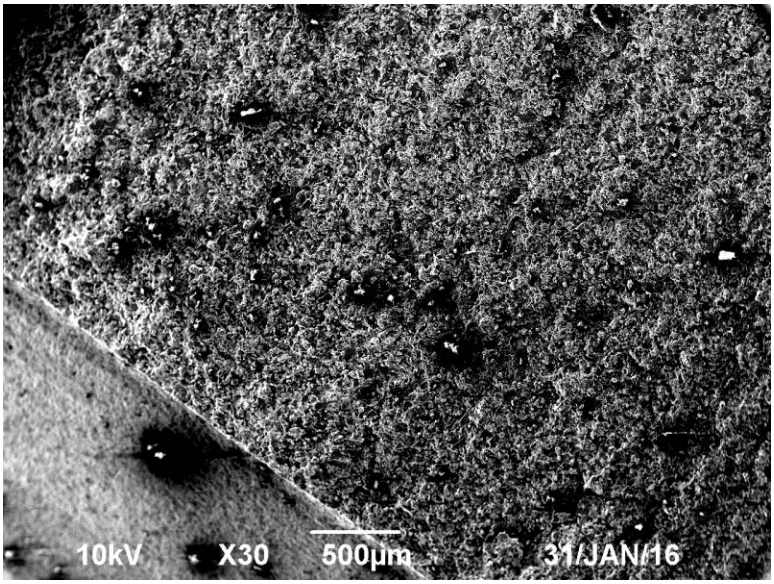

Figure 88: 30x Mag SEM Image of 23 vol% PNSF Filled Composite

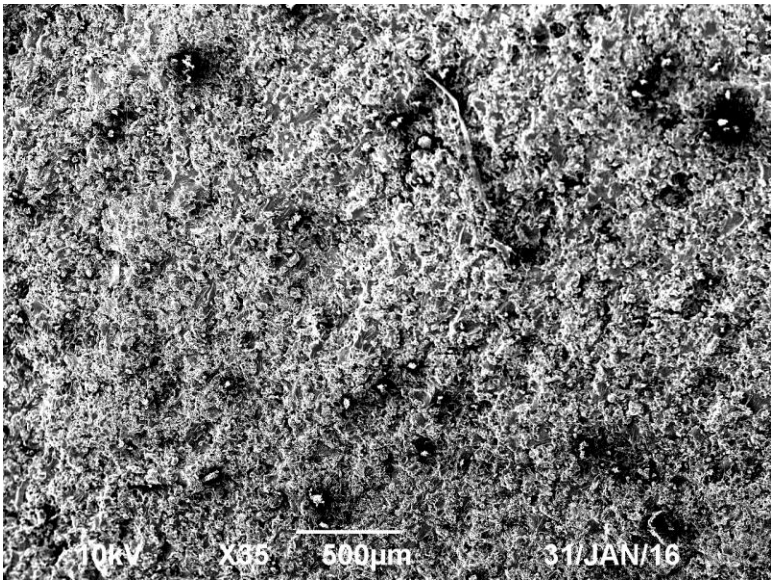

Figure 89: 35x Mag SEM Image of 23 vol% PNSF Filled Composite

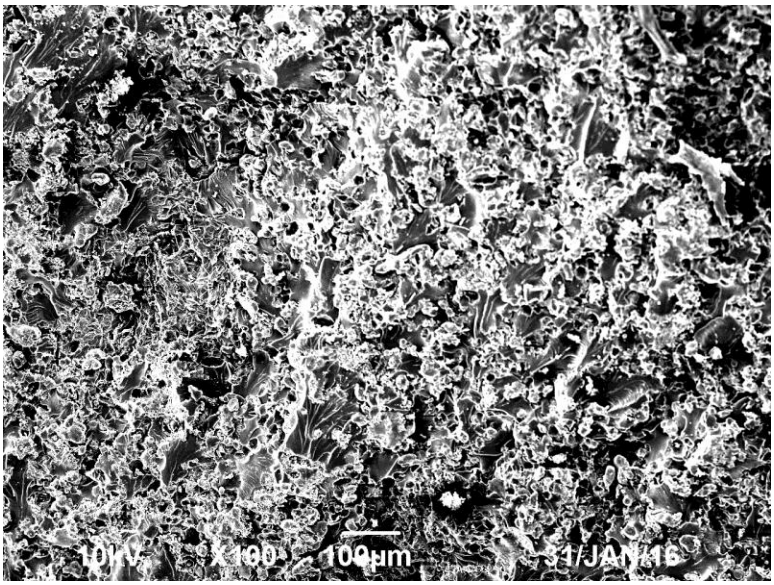

Figure 90: 100x Mag SEM Image of 23 vol% PNSF Filled Composite

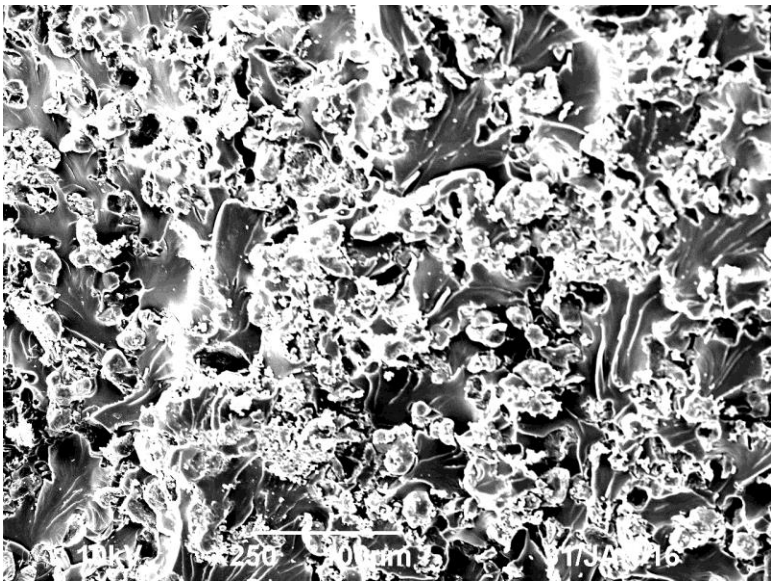

Figure 91: 250x Mag SEM Image of 23 vol% PNSF Filled Composite

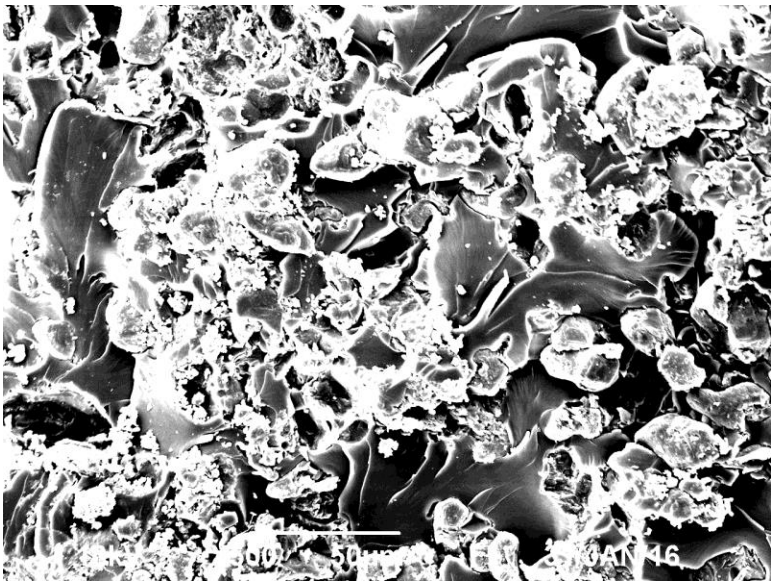

Figure 92: 500x Mag SEM Image of 23 vol% PNSF Filled Composite

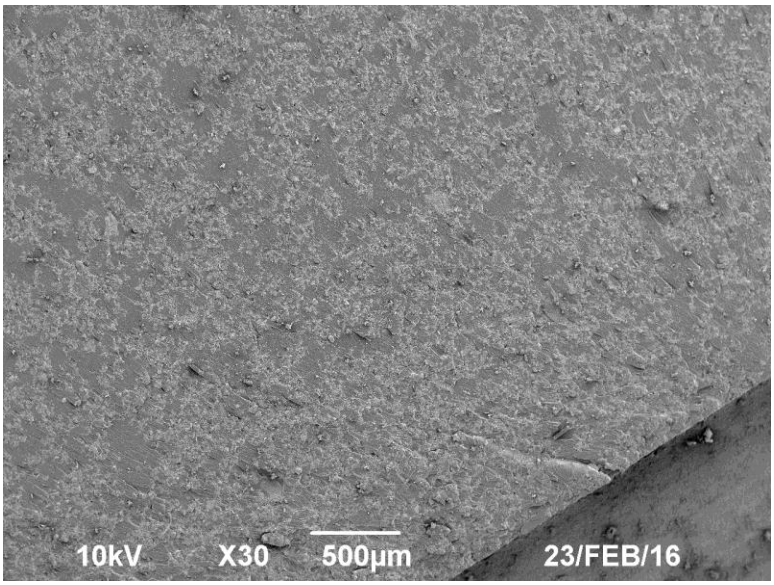

Figure 93: 30x Mag SEM Image of 20 vol% ESC Filled Composite

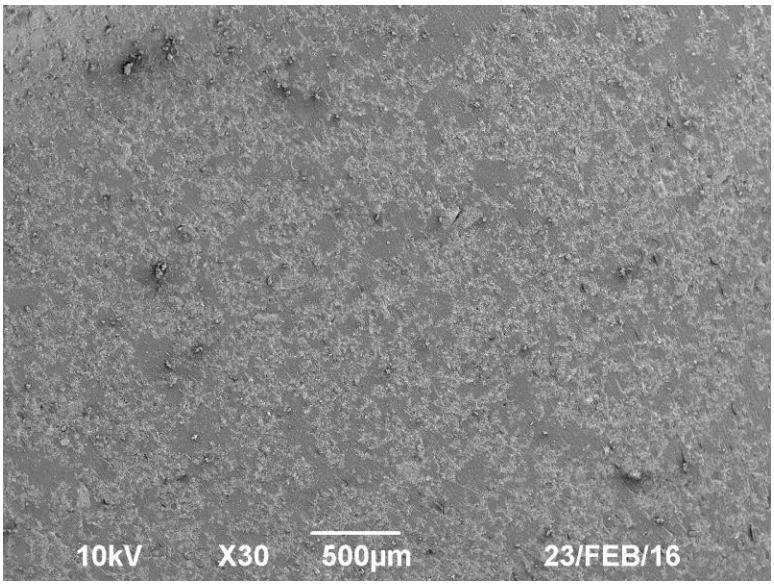

Figure 94: 30x Mag SEM Image of 20 vol% ESC Filled Composite

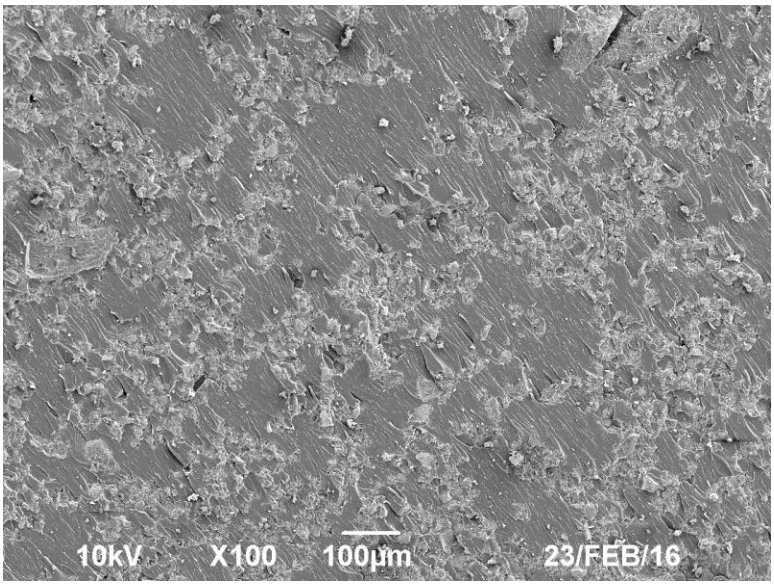

Figure 95: 100x Mag SEM Image of 20 vol% ESC Filled Composite

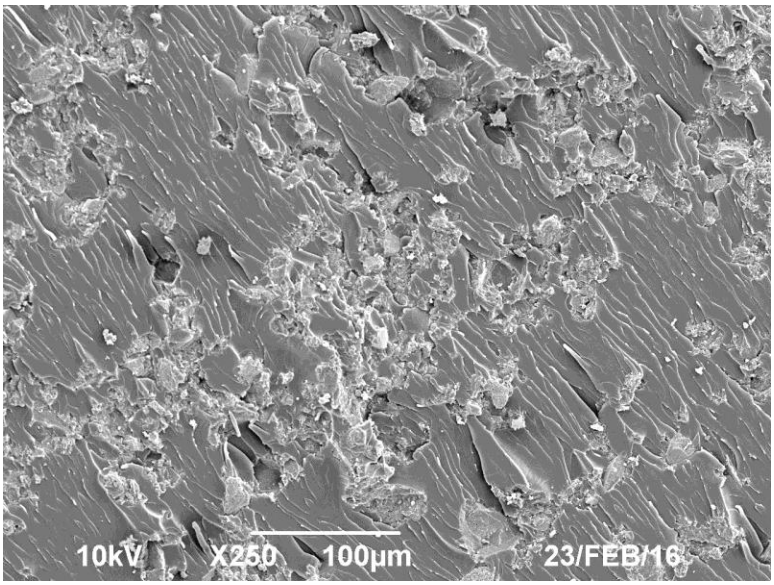

Figure 96: 250x Mag SEM Image of 20 vol% ESC Filled Composite

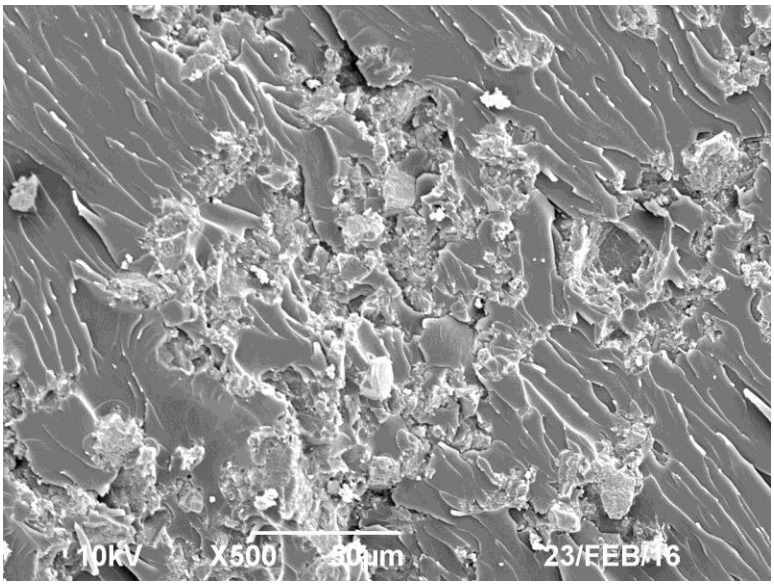

Figure 97: 500x Mag SEM Image of 20 vol% ESC Filled Composite

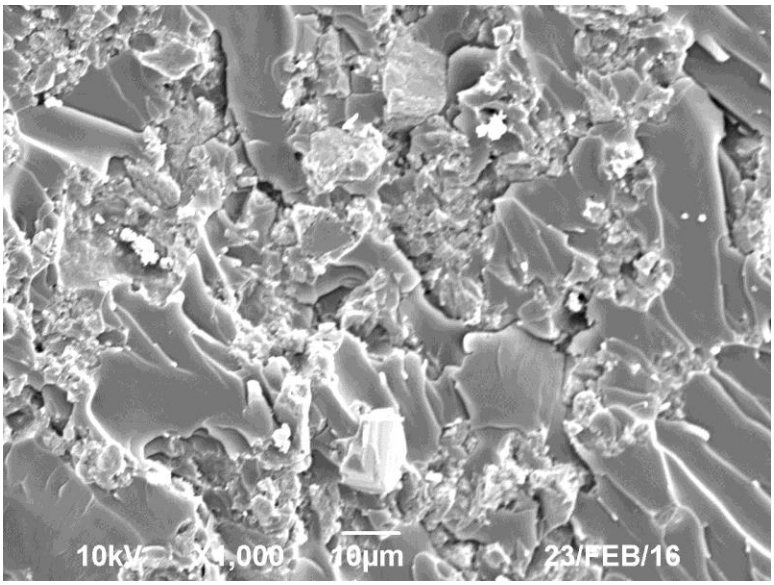

Figure 98: 1000x Mag SEM Image of 20 vol% ESC Filled Composite

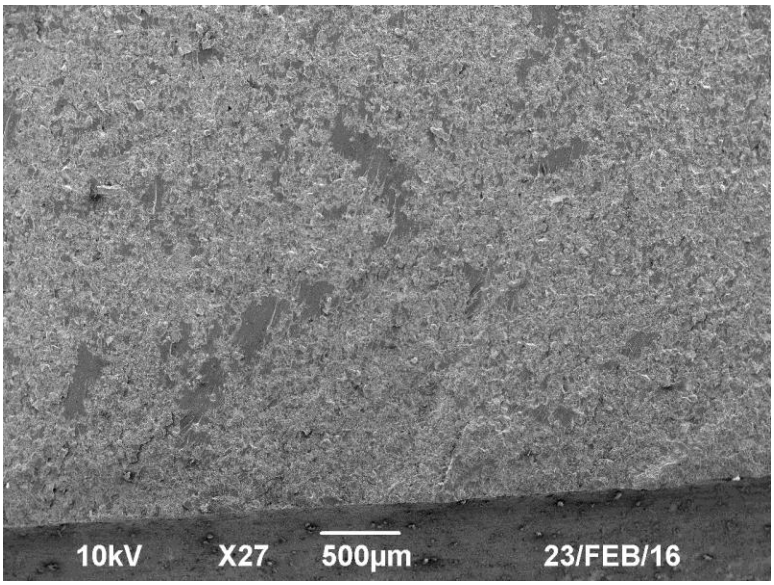

Figure 99: 27x Mag SEM Image of 27 vol% ESC Filled Composite

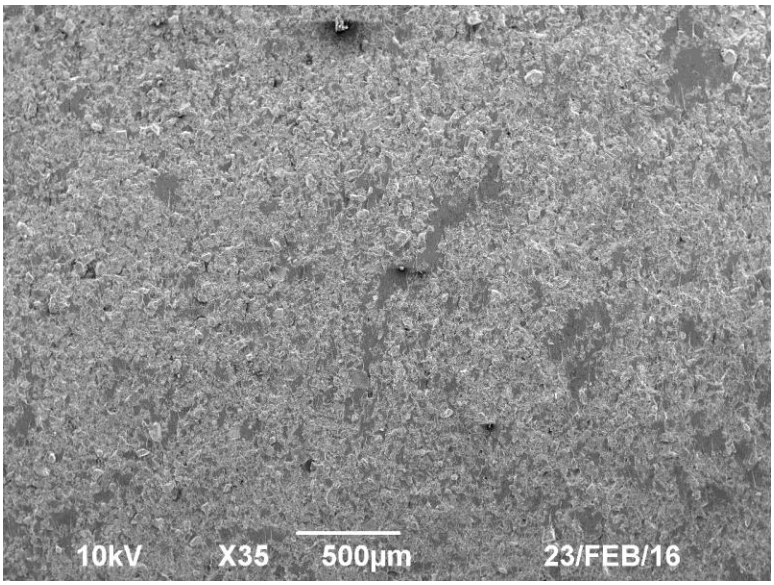

Figure 100: 35x Mag SEM Image of 27 vol% ESC Filled Composite

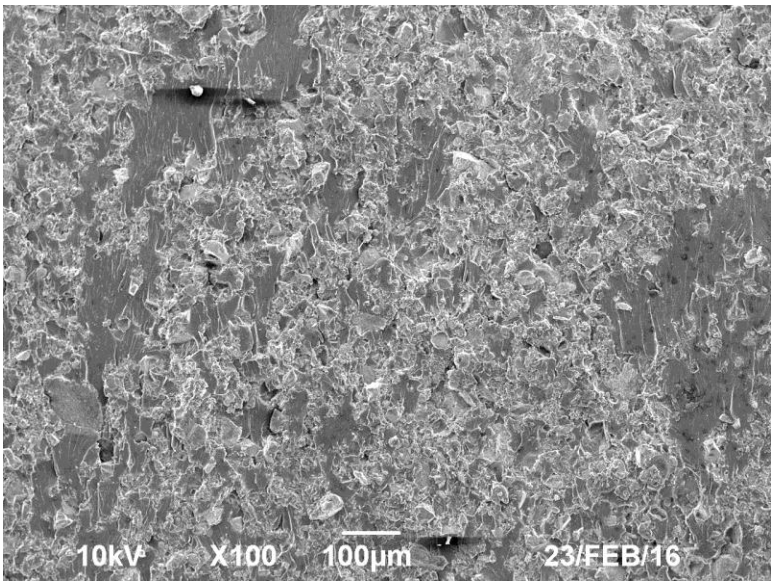

Figure 101: 100x Mag SEM Image of 27 vol% ESC Filled Composite

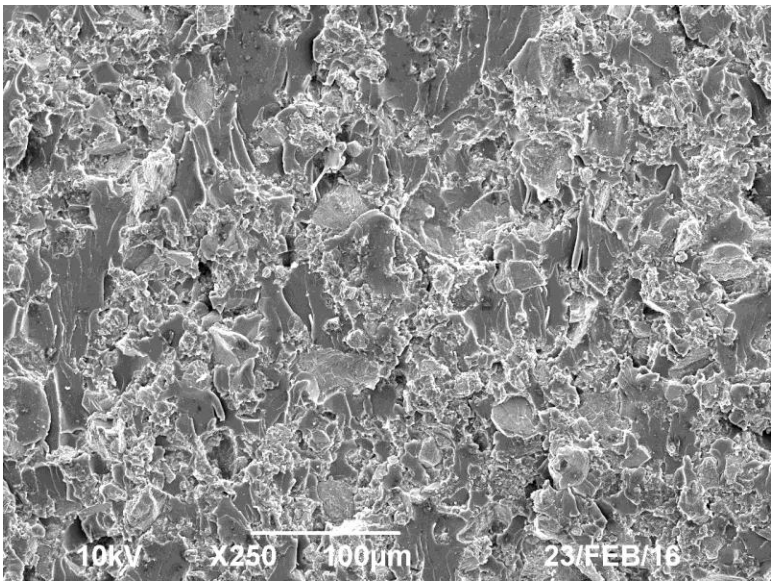

Figure 102: 250x Mag SEM Image of 27 vol% ESC Filled Composite

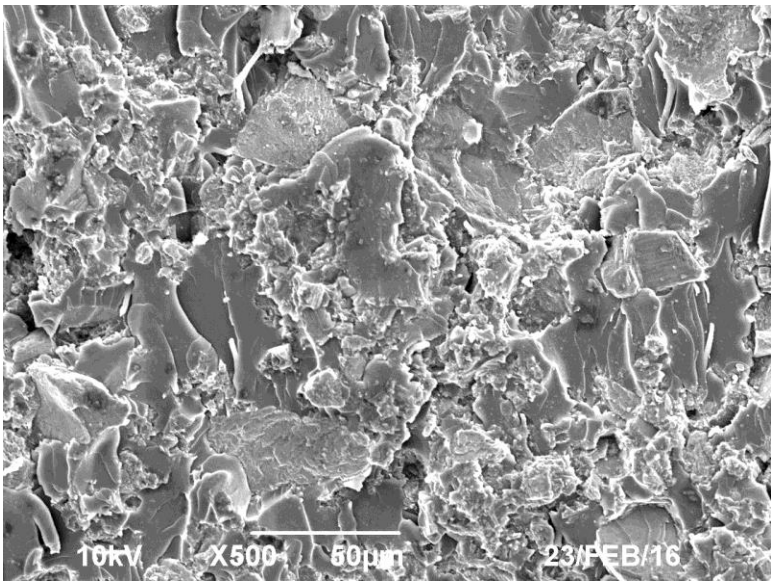

Figure 103: 500x Mag SEM Image of 27 vol% ESC Filled Composite

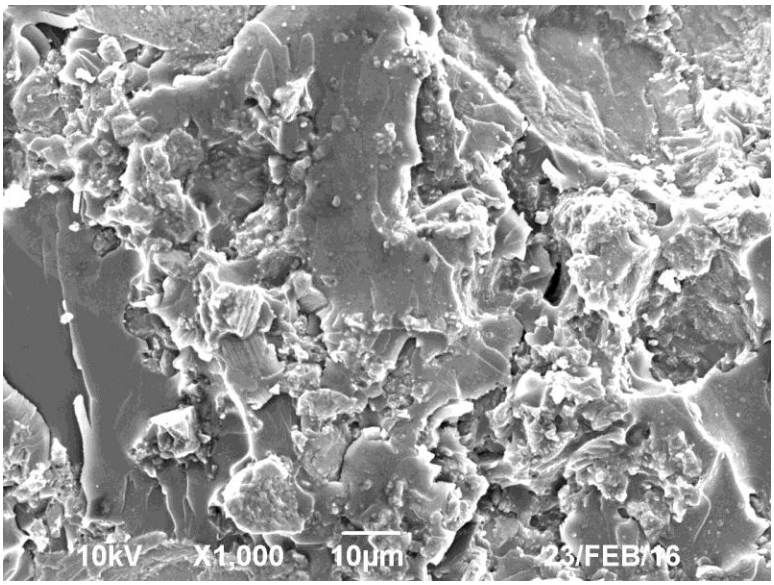

Figure 104: 1000x Mag SEM Image of 27 vol% ESC Filled Composite

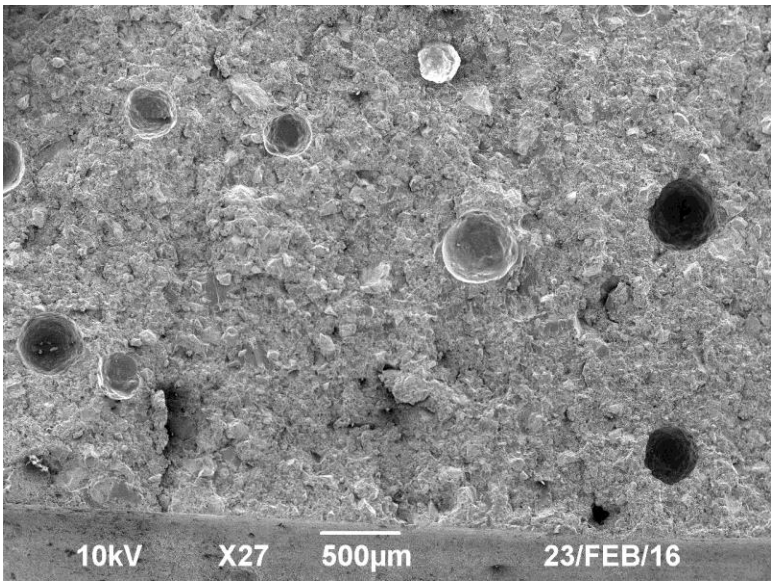

Figure 105: 27x Mag SEM Image of 36 vol% ESC Filled Composite

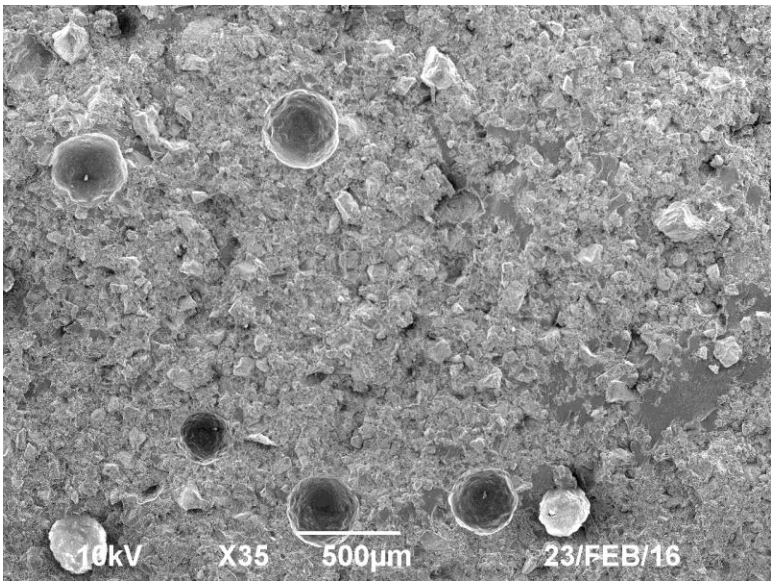

Figure 106: 35x Mag SEM Image of 36 vol% ESC Filled Composite

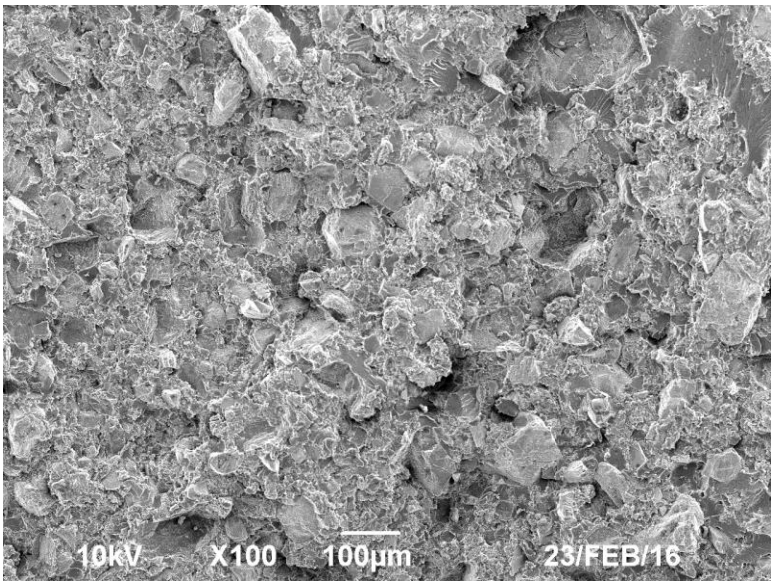

Figure 107: 100x Mag SEM Image of 36 vol% ESC Filled Composite

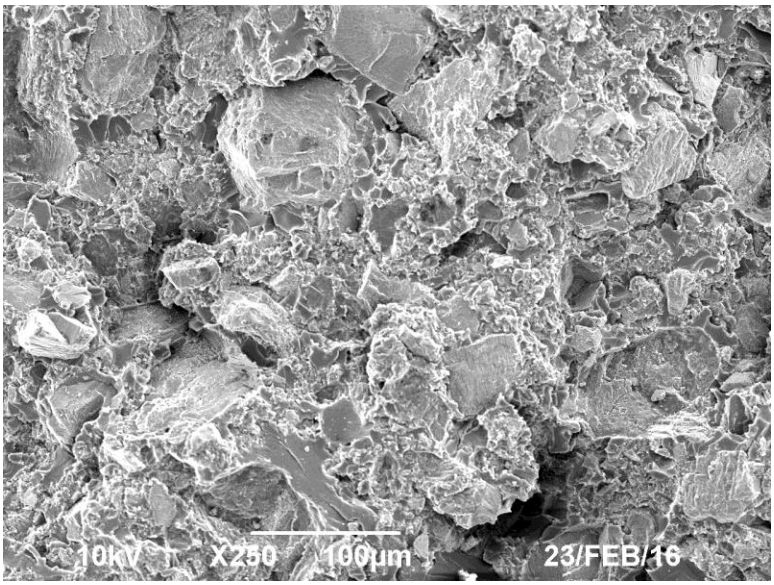

Figure 108: 250x Mag SEM Image of 36 vol% ESC Filled Composite

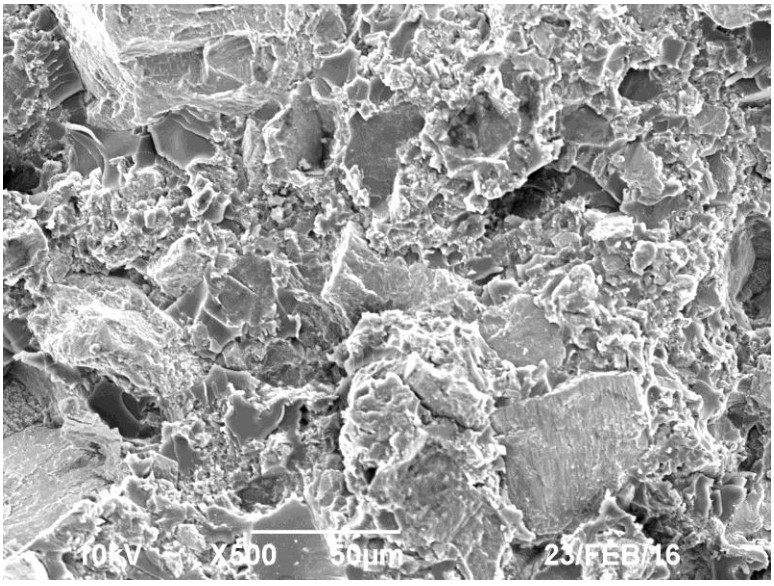

Figure 109: 500x Mag SEM Image of 36 vol% ESC Filled Composite

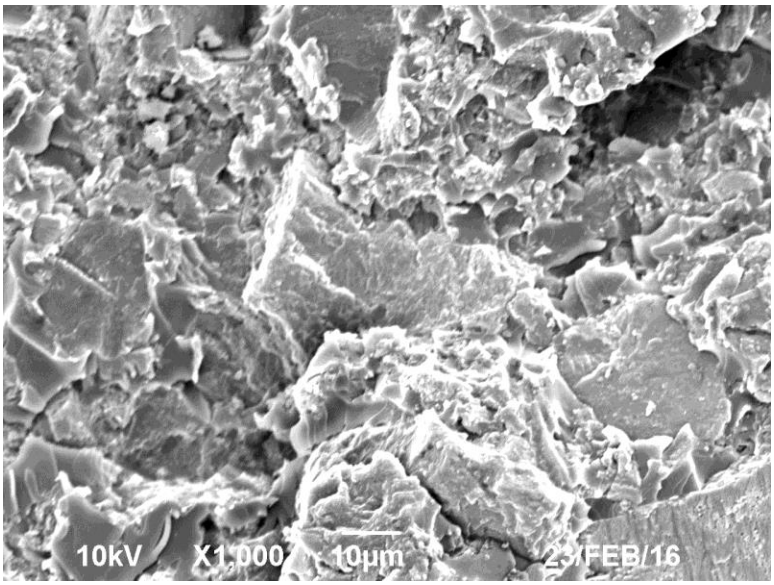

Figure 110: 500x Mag SEM Image of 36 vol% ESC Filled Composite

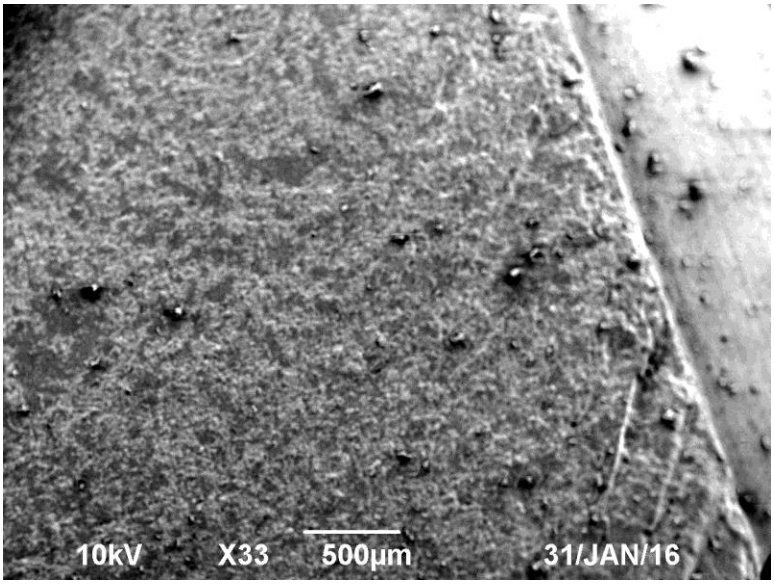

Figure 111: 33x Mag SEM Image of 1 vol% OMC Filled Composite

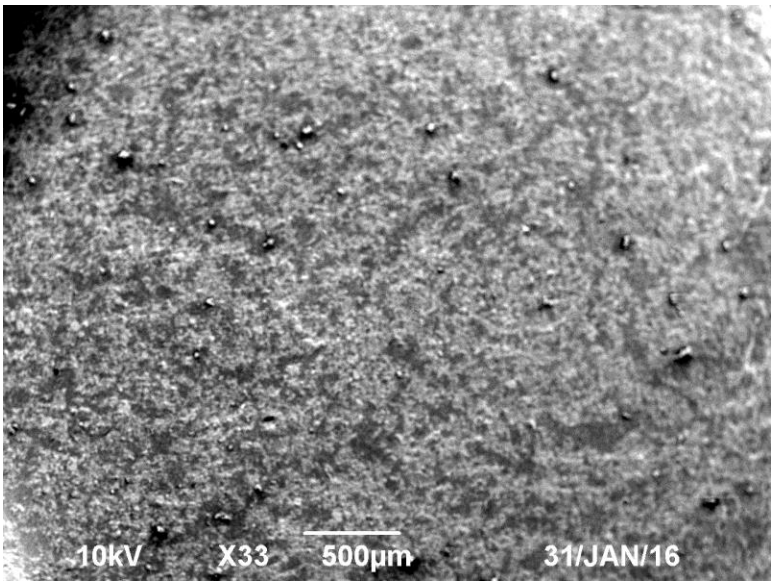

Figure 112: 33x Mag SEM Image of 1 vol% OMC Filled Composite

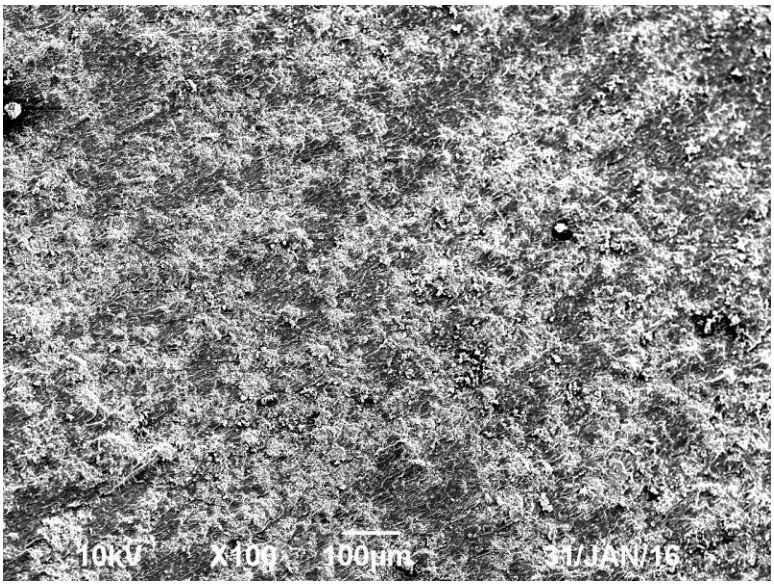

Figure 113: 100x Mag SEM Image of 1 vol% OMC Filled Composite

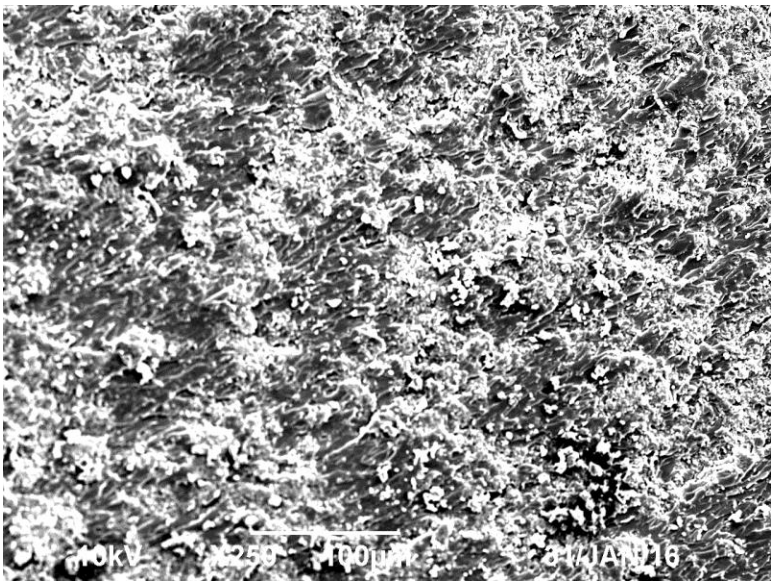

Figure 114: 250x Mag SEM Image of 1 vol% OMC Filled Composite

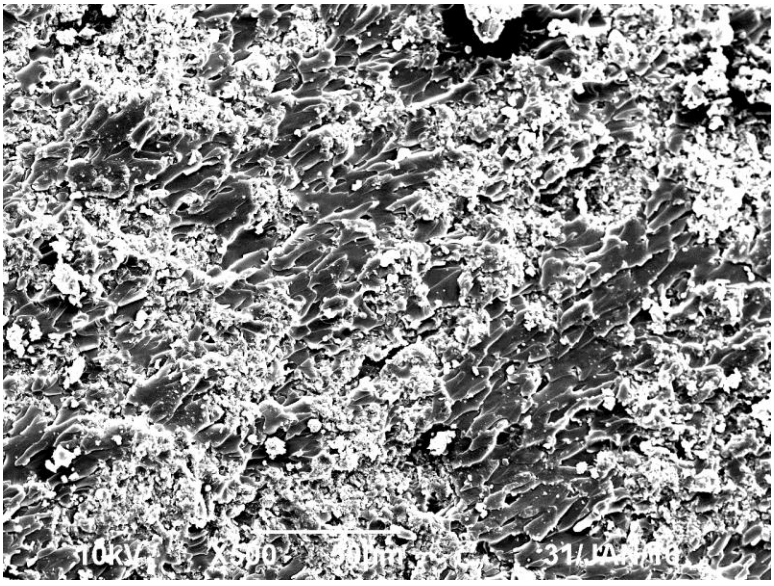

Figure 115: 500x Mag SEM Image of 1 vol% OMC Filled Composite

Figure 116: 1000x Mag SEM Image of 1 vol% OMC Filled Composite

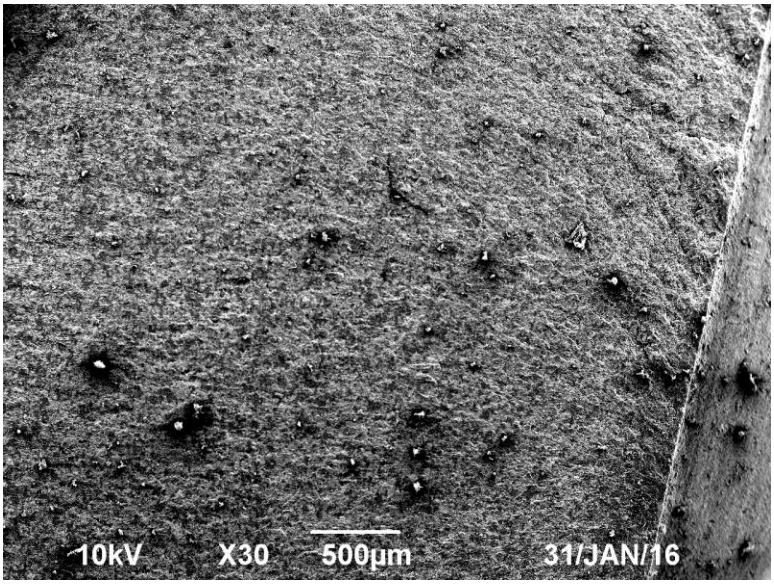

Figure 117: 30x Mag SEM Image of 2 vol% OMC Filled Composite

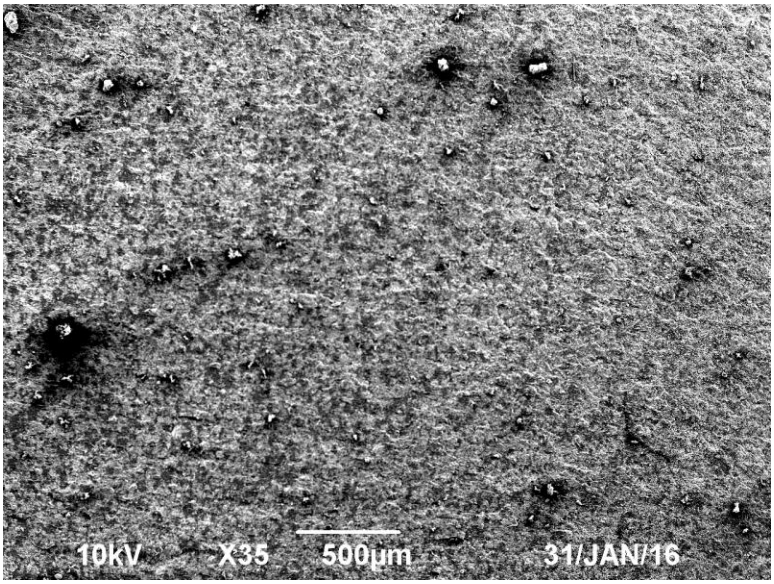

Figure 118: 35x Mag SEM Image of 2 vol% OMC Filled Composite

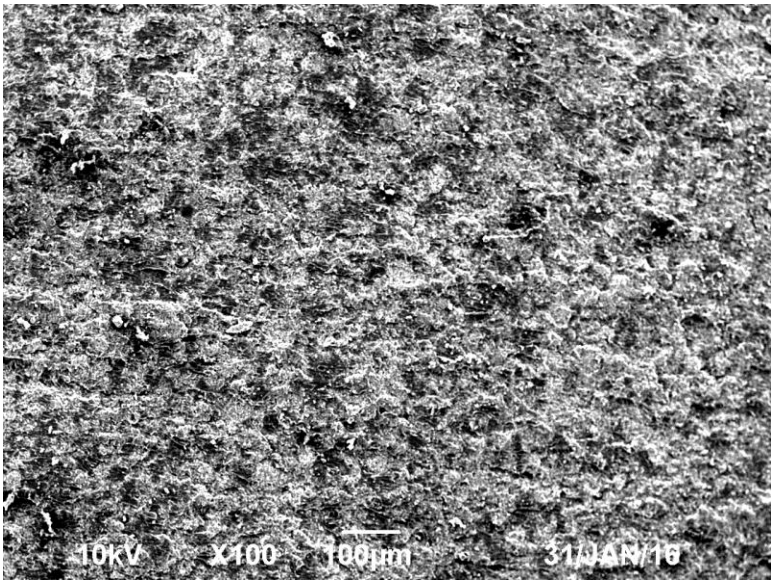

Figure 119: 100x Mag SEM Image of 2 vol% OMC Filled Composite

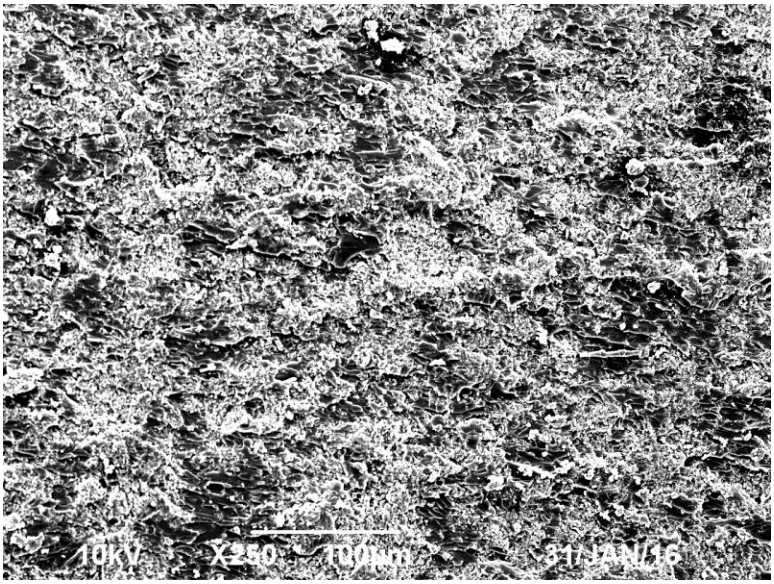

Figure 120: 250x Mag SEM Image of 2 vol% OMC Filled Composite

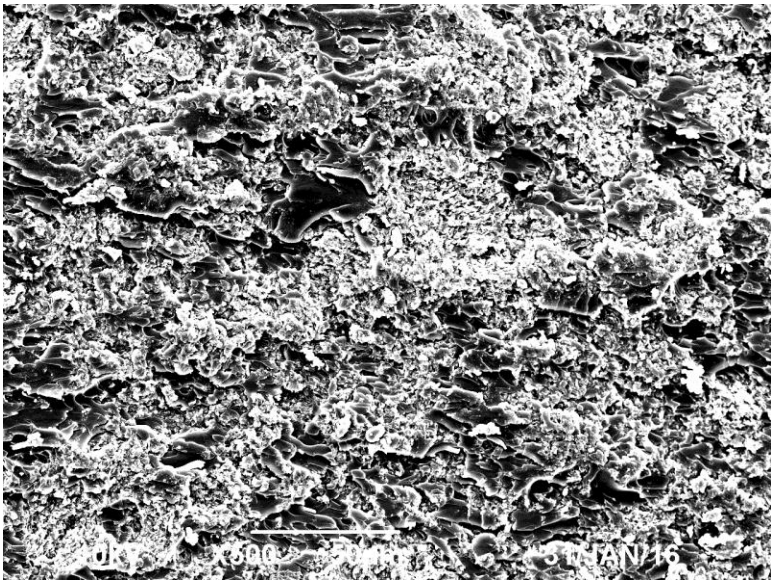

Figure 121: 500x Mag SEM Image of 2 vol% OMC Filled Composite

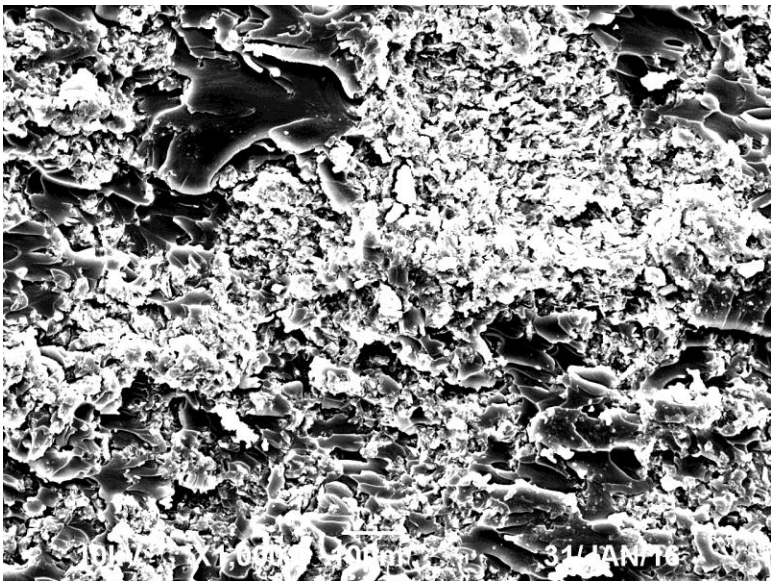

Figure 122: 1000x Mag SEM Image of 2 vol% OMC Filled Composite

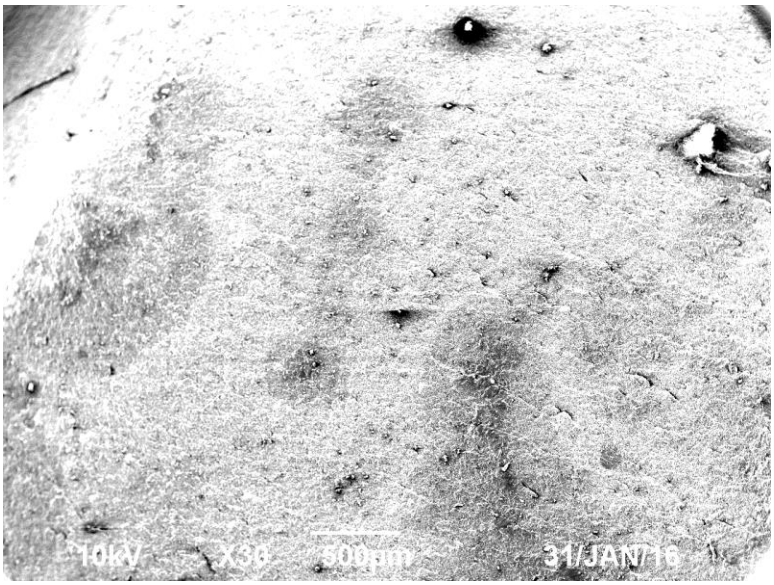

Figure 123: 30x Mag SEM Image of 4 vol% OMC Filled Composite

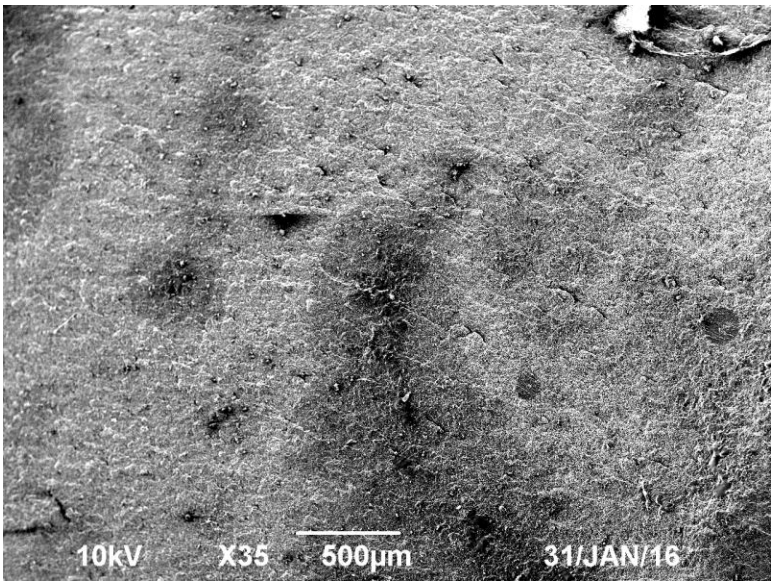

Figure 124: 35x Mag SEM Image of 4 vol% OMC Filled Composite

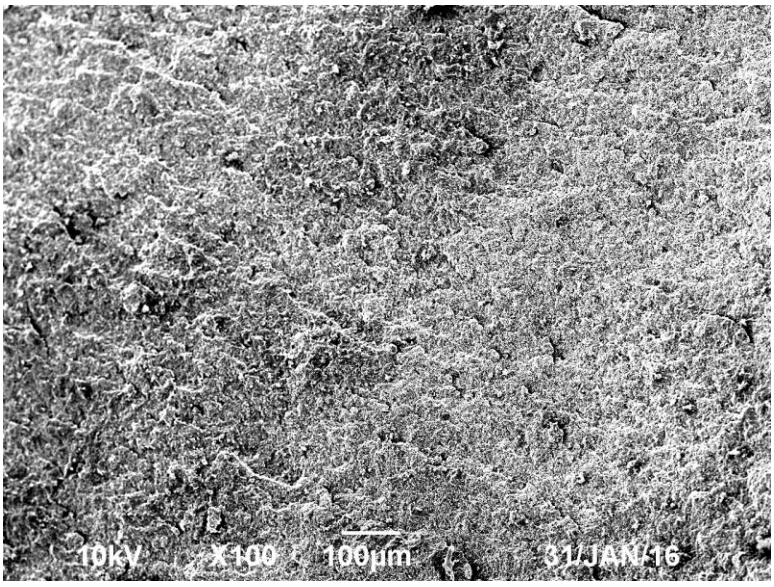

Figure 125: 100x Mag SEM Image of 4 vol% OMC Filled Composite

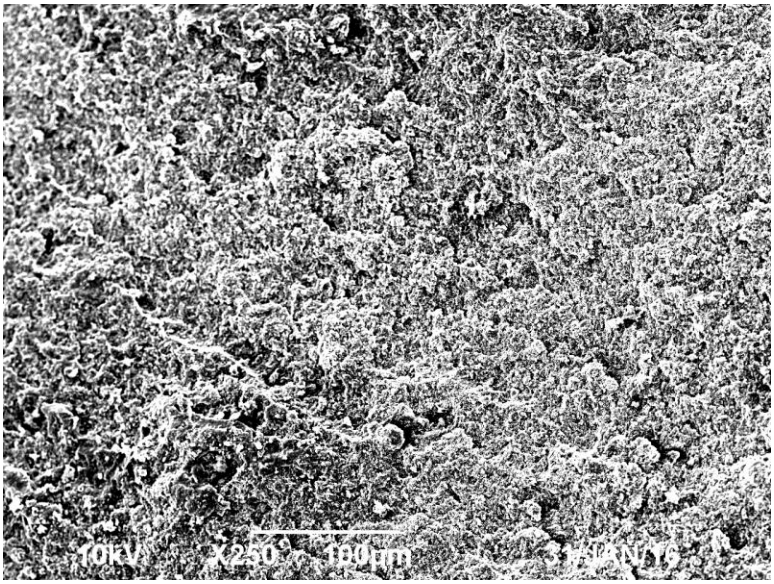

Figure 126: 250x Mag SEM Image of 4 vol% OMC Filled Composite

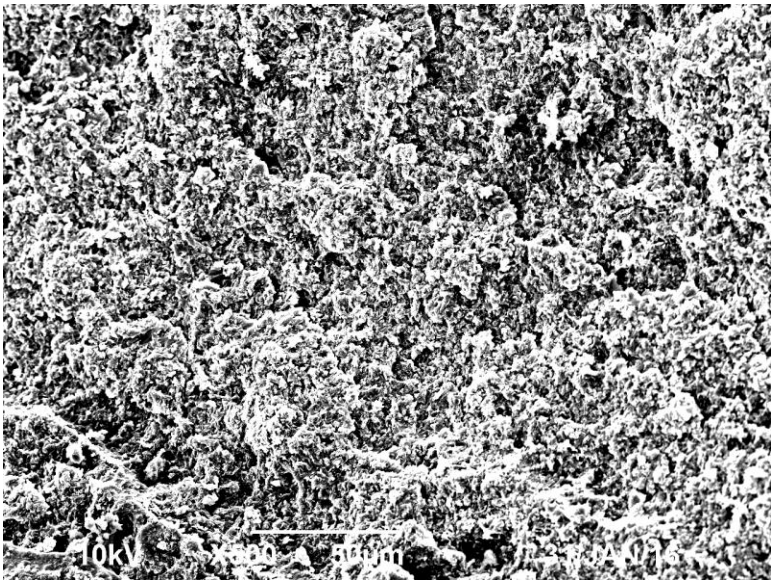

Figure 127: 500x Mag SEM Image of 4 vol% OMC Filled Composite

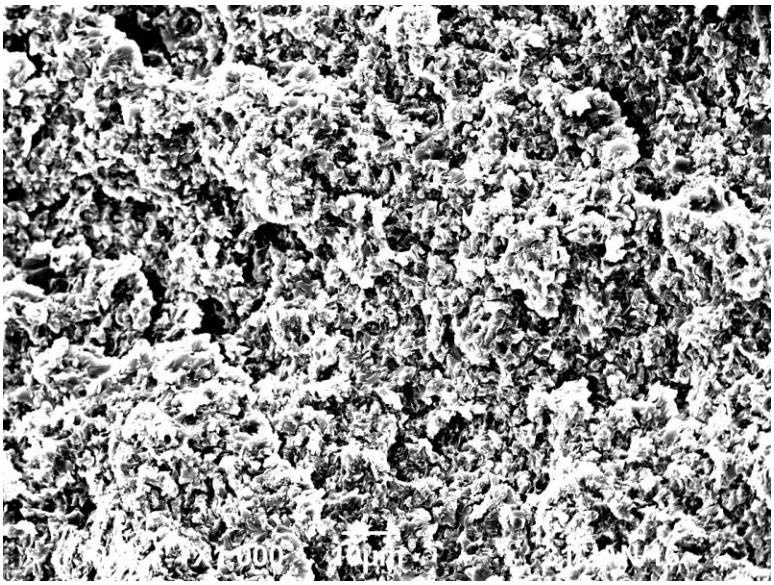

Figure 128: 1000x Mag SEM Image of 4 vol% OMC Filled Composite

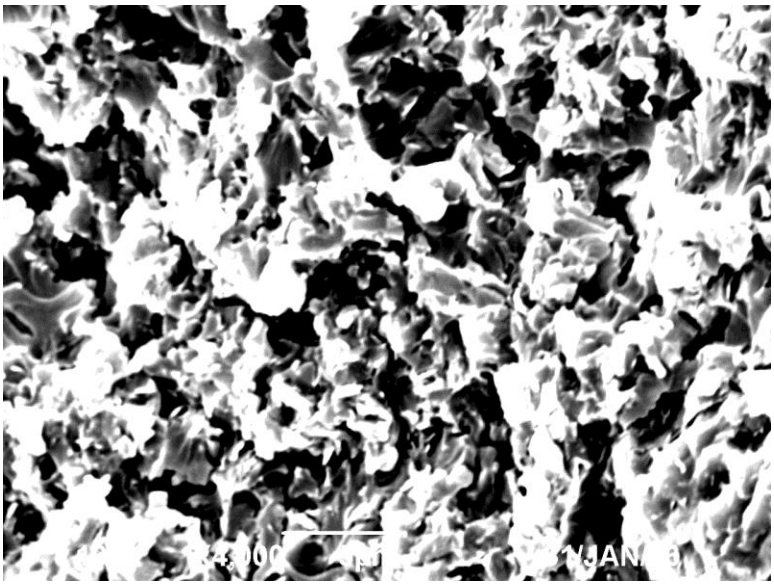

Figure 129: 4000x Mag SEM Image of 4 vol% OMC Filled Composite